Characterization of Inertial Measurement Unit Placement on the Human Body Upon Repeated Donnings

by
Morris Dwight Vanegas
B.S., Massachusetts Institute of Technology (2012)
Submitted to the Department of Aeronautical and Astronautical Engineering and the Department of Mechanical Engineering
in partial fulfillment of the requirements for the degrees of
Masters of Science in Aerospace Engineering
and
Masters of Science in Mechanical Engineering
at the
MASSACHUSETTS INSTITUTE OF TECHNOLOGY
June 2016
© Massachusetts Institute of Technology 2016. All rights reserved.

Author ..... Signature redacted .....
Department of Aeronautical and Astronautical Engineering
Department of Mechanical Engineering
May 19, 2016

Certified by.. Signature redacted .....
Leia Stirling
Assistant Professor
Thesis Supervisor

Accepted by .. Signature redacted .....
Ian Hunter
Professor
Thesis Reader

Accepted by ..... Signature redacted ....
Rohan Abeyaratne
Chair, Mechanical Engineering Graduate Program Committee

Accepted by ..... Signature redacted .....
Paulo C. Lozano
Chair, Aeronautical and Astronautical Engineering Graduate Program Committee

MASSACHUSETTS INSTITUTE OF TECHNOLOGY
JUN 28 2016
LIBRARIES
ARCHIVES

Characterization of Inertial Measurement Unit Placement on the Human Body Upon Repeated Donnings

by

Morris Dwight Vanegas

Submitted to the Department of Aeronautical and Astronautical Engineering and
the Department of Mechanical Engineering
on May 19, 2016, in partial fulfillment of the
requirements for the degrees of
Masters of Science in Aerospace Engineering
and
Masters of Science in Mechanical Engineering

Abstract

Given projections of an increase in the number of consumers wearing sensors in the upcoming years coupled with NASA's technological roadmap for future human space exploration, there is a need to understand and appropriately incorporate the variability of humans during the use of sensors that extract human activity and diagnostics. Accurate estimations of variability in multiple donnings of sensor suites may aid algorithm development for wearable motion capture systems that make use of Inertial Measurement Units (IMUs). The accuracy of any algorithm incorporating these sensors is limited by the accuracy of the sensor to segment calibration. In this study, 22 participants self-placed IMUs on three locations and performed six prescribed motions during each of these five donnings. Placement of the IMU was quantified as distance, orientation, and rotation. For orientation of the sensors at the beginning of the prescribed motions, the bicep orientation mean was less than the forearm, which was less than the chest. No difference in sensor rotation was found between the bicep and forearm, but both locations differed from the chest location. It was found that even with a guide to assist with the starting and ending positions of a motion, the placement of the sensor on the human-body varied at the beginning and end of a motion. This study found no consistent effect of donning on placement, but did find an effect of motion on the measures. Since the placement measures did vary through a motion, the underlying assumptions of a rigid body model used by motion capture algorithms might not be appropriate. Motion capture algorithms need to be careful when using these rigid body assumptions and account for the changes in position and Euler angles due to natural human variability and calibration during multiple donnings of IMUs by non-experts. This study will aid in the development of quick don and doff sensor suites that can be reliably used by a non-expert for real-time decision making.

Thesis Supervisor: Leia Stirling
Title: Assistant Professor

Acknowledgments

I would like to thank Professor Leia Stirling for allowing me to share in the exciting experience of working with the Man-Vehicle Laboratory. Her continued push, communication, and flexibility allowed me to obtain everything I wanted to get out of MIT. This thesis would not exist without her guidance as I dove into research involving human subjects. I hope I was as useful to her as she was to me, and would welcome the opportunity to work with her again. As a guide in research and in my quarter-life crisis (what I dubbed my indecision of what to do next in life), I could not have asked for a better mentor.

A quick thanks to Alan Natapoff for discussions of statistical analysis, and thanks to Jeffrey Hoffman for guidance in determination of relevant motions. I would also like to thank Sarah Schneider for assistance with troubleshooting the Vicon motion capture system.

I would like to acknowledge all the Man-Vehicle Lab graduate students for their willingness to provide help regardless of their workload or the time of day or night, and for also providing me with a work-life balance. Muddy Fridays will forever be engraved in my mind as a place to celebrate and discuss. A special thank you to Jessica Artiles for being someone to bounce ideas off of and continually providing me with user-centered feedback.

And finally, a special thanks to my parents, Rene and Maria Vanegas, and my sister, Pamela Vanegas, for their love, support, and constant facetime messages that kept me sane.

Contents

1 Introduction **19**

1.1 Motivation 19

1.2 Literature Review 20

1.2.1 Motion Capture Systems 20

1.2.2 Implementing IMUs in Human Motion Capture 22

1.2.3 IMU Motion Capture Algorithms 23

1.2.4 Sources of Human Variability 24

1.3 Objective 27

1.4 Thesis Summary 28

2 Experimental Methods **31**

2.1 Participants 31

2.2 Experimental Protocol 32

2.3 Data Acquisition 36

2.3.1 Donning Configuration 36

2.3.2 Motion Capture 37

2.3.3 Motions 39

2.3.4 Target Apparatus 41

2.4 Data Processing 41

2.4.1 Dependent Variable Definitions 42

2.4.2 Segmentation of Motions into Epochs 44

2.5 Statistical Analysis 45

2.5.1 Epoch Table Description 46

3 Results and Discussion **49**

3.1 Strap Mount Configuration 49

3.1.1 Effect of Initial Placement on Distance, Orientation, and Rotation Using a Strap Mount Configuration 49

3.1.2 Epoch Analysis of Strap Configuration 54

3.1.3 Potential Effects on Algorithms 63

3.2 Garment Mount Configuration 69

3.2.1 Effect of Initial Placement on Distance, Orientation, and Rotation 69

3.3 Study Limitations 71

4 Conclusion **73**

4.1 Summary of Contributions 74

4.2 Potential Applications 75

A Recruitment Emails **77**

A.1 Initial Recruitment Email 77

A.2 Reply Email 78

A.3 Confirmation Email 78

B Motion Descriptions for Participants **81**

C Matlab Calculations **83**

C.1 Calculation of Independent Variables 83

C.2 Matlab script to trim motions 87

C.3 Untrimmed and trimmed data comparison 91

D Initial Placement, Strap Configuration Analysis **93**

D.1 Post-hoc Tukey Tests 93

D.2 Post-hoc Student-Newman-Keuls Tests 93

D.3 Levene's test for equality of variances 93

D.4 Levene's test graphs for all location comparisons 93

E Epochs, Strap Configuration Analysis **97**

E.1 Conover-Inman Post-hoc tests for distance, orientation, and rotation for all motions 97

F Effect size **117**

F.1 Dependent variable and IMU individual subject ranges by location . . 117

G Mean and standard deviation Values for Euler Axes **121**

List of Figures

1-1 Shoulder and elbow joints with associated bones. Images taken from Human BioDigital [1]. 26

2-1 Vicon reflective marker with flat base 32

2-2 Opal IMU with three Vicon markers in a triad configuration 33

2-3 Recommended sensor placement (boxes on straps) and researcher placed optical motion capture markers. Sensor placement labeling scheme and IMU reference axes are shown in the bottom of the figure. 34

2-4 Champion compression garments with sewn Velcro for IMU placement 35

2-5 McDavid arm braces placed on the bicep and forearm to prevent subjects from using IMU imprint 35

2-6 Trace of the silhouette of a participant 36

2-7 Predetermined motions showing relevant degrees of freedom (A = elbow flexion and extension; B = forearm pronation and supination; C = wrist ulnar and radial deviation, wrist flexion and extension; D = Lifting arm upwards, which included elbow flexion and extension, shoulder flexion and extension; E = Lifting arm forward and to the side, which included shoulder abduction, flexion and rotation; F = Lifting arm forward from a behind the back starting position, which included wrist, elbow, and shoulder flexion and extension, shoulder abduction, and forearm pronation and supination). Motions have numbered figures to indicate sequence of poses. Subjects performed the sequence in a motion, and then returned to the first pose in the sequence. Target Apparatus only shown in Motion C but was used by four motions (A * indicates the motion used a guide). 37

2-8 Hoop and chest straps for IMUs 38

2-9 Sample of sync in (start) and sync out (stop) signals from IMU access point to Vicon giganet. 38

2-10 Target apparatus stand and hemp loop. Red and purple bands used for targets are not shown. 42

2-11 Definition of the three IMU measurements for each of the three IMUs and associated markers. IMUs had three markers, labeled A, B, and C, used to define the local IMU coordinate system. Each subfigure shows the surrounding markers used in the IMU's measurement calculation. 43

2-12 Example of how rotation is calculated on IMU 2. This view is from the elbow looking towards the shoulder. The rotation angle is the angle between the IMU normal vector and the surrounding body markers' normal vector. From this view, markers IM2A and RSHO are masked. 44

3-1 Shown are the within motion interaction effects between location. Additional significant effects across motions are not shown. Main effect groupings are shown in horizontal bars above graphs in the order of group means from smallest (G1) to largest (G3). Bars show one standard deviation from the mean. Above each graph, asterisks (*) indicate significant difference according to Tukey's Difference Test (p <0.05). . 52

3-2 Side view of motion A at starting point and some angle phi after the elbow has gone through flexion. 57

3-3 Euler axes (Yaw, Pitch, Roll) mean and standard deviations values for IMU 3 for multiple donnings of Motion A. 65

C-1 One subject's RWRB marker z values during multiple repetitions of each motion before (top) and after (bottom) being trimmed. The bottom row axis is in percentage of total motion time, or epoch. 91

D-1 Graphs showing comparisons of two variances for all combinations of IMU locations 96

G-1 Euler axes (Yaw, Pitch, Roll) mean and standard deviation values for IMU 1 for multiple donnings of Motion A. 121

G-2 Euler axes (Yaw, Pitch, Roll) mean and standard deviation values for IMU 2 for multiple donnings of Motion A. 122

G-3 Euler axes (Yaw, Pitch, Roll) mean and standard deviation values for IMU 3 for multiple donnings of Motion A. 122

G-4 Euler axes (Yaw, Pitch, Roll) mean and standard deviation values for IMU 1 for multiple donnings of Motion B. 123

G-5 Euler axes (Yaw, Pitch, Roll) mean and standard deviation values for IMU 2 for multiple donnings of Motion B. 123

G-6 Euler axes (Yaw, Pitch, Roll) mean and standard deviation values for IMU 3 for multiple donnings of Motion B. 124

G-7 Euler axes (Yaw, Pitch, Roll) mean and standard deviation values for IMU 1 for multiple donnings of Motion C. 124
G-8 Euler axes (Yaw, Pitch, Roll) mean and standard deviation values for IMU 2 for multiple donnings of Motion C. 125
G-9 Euler axes (Yaw, Pitch, Roll) mean and standard deviation values for IMU 3 for multiple donnings of Motion C. 125
G-10 Euler axes (Yaw, Pitch, Roll) mean and standard deviation values for IMU 1 for multiple donnings of Motion D. 126
G-11 Euler axes (Yaw, Pitch, Roll) mean and standard deviation values for IMU 2 for multiple donnings of Motion D. 126
G-12 Euler axes (Yaw, Pitch, Roll) mean and standard deviation values for IMU 3 for multiple donnings of Motion D. 127
G-13 Euler axes (Yaw, Pitch, Roll) mean and standard deviation values for IMU 1 for multiple donnings of Motion E. 127
G-14 Euler axes (Yaw, Pitch, Roll) mean and standard deviation values for IMU 2 for multiple donnings of Motion E. 128
G-15 Euler axes (Yaw, Pitch, Roll) mean and standard deviation values for IMU 3 for multiple donnings of Motion E. 128
G-16 Euler axes (Yaw, Pitch, Roll) mean and standard deviation values for IMU 1 for multiple donnings of Motion F. 129
G-17 Euler axes (Yaw, Pitch, Roll) mean and standard deviation values for IMU 2 for multiple donnings of Motion F. 129
G-18 Euler axes (Yaw, Pitch, Roll) mean and standard deviation values for IMU 3 for multiple donnings of Motion F. 130

List of Tables

2.1 Final motions chosen based on Earth-relevance (as defined by Activities of Daily Living) and Space-relevance (as defined by Astronaut Jeffrey Hoffman) 40

2.2 Interpretation of an example summary table of Conover-Inman post-hoc tests on epochs grouped by motion and location. 47

3.1 Main and Interaction effects of Location, Donning, and Motion for initial placement. A p-value of 0 means p <0.0005 50

3.2 Normalized and mean shifted location variances for all dependent variables 53

3.3 Levene's equal variance test of all 11 epochs performed for each combination of motion and location, for each dependent variable. A p-value of p<0.002778 indicates significance, due to the Bonferroni correction. 55

3.4 Kruskal Wallis with Bonferroni correction tests of all 11 epochs for each combination of motion and location, for each dependent variable. A p-value of p<0.002778 indicates significance. 56

3.5 Mean and standard deviation of ranges of values for distance, orientation, and rotation of all subjects within each IMU location grouped by motion 64

3.6 Average range (above) and standard deviation of ranges (below) of Euler angles (in degrees) for all subjects, grouped by IMU location and motion. 67

3.7 Main effects of Location, Donning, and Motion for initial placement of garment configuration. A p-value of $p<0.05$ indicates significance. . . 69
3.8 Normalized and mean shifted location variances for all dependent variables 70

D.1 Tukey Post-hoc pairwise comparison tests for Location, Donning, and Motion during initial placement of IMU 94
D.2 Student-Newman-Keuls Post-hoc tests for Location, Donning, and Motion during initial placement of IMU 95
D.3 Levene's test to determine which IMU Location varied most 96

E.1 Motion A Conover-Inman post-hoc tests for distance. Red indicates p <0.0033 98
E.2 Motion A Conover-Inman post-hoc tests for orientation. Red indicates p <0.0033 99
E.3 Motion A Conover-Inman post-hoc tests for rotation. Red indicates p <0.0033 100
E.4 Motion B Conover-Inman post-hoc tests for distance. Red indicates p <0.0033 101
E.5 Motion B Conover-Inman post-hoc tests for orientation. Red indicates p <0.0033 102
E.6 Motion B Conover-Inman post-hoc tests for rotation. Red indicates p <0.0033 103
E.7 Motion C Conover-Inman post-hoc tests for distance. Red indicates p <0.0033 104
E.8 Motion C Conover-Inman post-hoc tests for orientation. Red indicates p <0.0033 105
E.9 Motion C Conover-Inman post-hoc tests for rotation. Red indicates p <0.0033 106
E.10 Motion D Conover-Inman post-hoc tests for distance. Red indicates p <0.0033 107

E.11 Motion D Conover-Inman post-hoc tests for orientation. Red indicates p <0.0033 108
E.12 Motion D Conover-Inman post-hoc tests for rotation. Red indicates p <0.0033 109
E.13 Motion E Conover-Inman post-hoc tests for distance. Red indicates p <0.0033 110
E.14 Motion E Conover-Inman post-hoc tests for orientation. Red indicates p <0.0033 111
E.15 Motion E Conover-Inman post-hoc tests for rotation. Red indicates p <0.0033 112
E.16 Motion F Conover-Inman post-hoc tests for distance. Red indicates p <0.0033 113
E.17 Motion F Conover-Inman post-hoc tests for orientation. Red indicates p <0.0033 114
E.18 Motion F Conover-Inman post-hoc tests for rotation. Red indicates p <0.0033 115

F.1 Dependent variable individual subject ranges 117
F.2 Euler angle individual subject ranges 118
F.3 Mean and standard deviation of ranges of values for roll, pitch, and yaw of all subjects within each IMU location grouped by motion . . . 119

Chapter 1

Introduction

1.1 Motivation

The ability to use sensors to extract human activity and diagnostics has both Earth and extra-terrestial applications. According to the 2014 IHS MEMS & Sensors for Wearable Report [2], consumers will be wearing close to 500 million sensors by 2019. This estimate includes devices for motion measurement, user interfaces, and health industry products, with an emphasis on personal devices that are used daily by non-experts. Additionally, future space exploration will likely include human crews traveling to other celestial bodies for extended periods of time. NASAs Space Technology Roadmap places human health monitoring as a sub-technology area in one of its fourteen technology areas that must be matured before crews venture out beyond low earth orbit [3]. With increased emphasis on long duration travel beyond Earths gravitational influence, there is a growing need for technologies with improved reliability, self-sufficiency, and minimal-logistical needs. With such small crew sizes proposed for these missions, crew members are likely to find themselves experts in only a few fields. Non-experts, both Earth- and space-bound, in the fields of human motion capture introduce variability during repeated use of these unfamiliar systems.

A necessary requirement to enable such portable and continually-used systems that are reliable, self-sufficient, and require minimal-logistical needs is to understand and appropriately incorporate the variability of humans during repeated use in the

system architecture. This study specifically considers wearable technology systems for estimating human motion. Inertial Measurement Units (IMUs) are small electronic devices that measure acceleration and angular velocity. By quantifying and characterizing the underlying variability in IMU placement on the human body during multiple donnings, we can further understand the effects of calibration poses and natural human variability on the estimated kinematics and associated parameters. This work also provides a database for future algorithm development.

1.2 Literature Review

This section will first describe the benefits and disadvantages of various motion capture systems to support the decision to choose IMUs for this sensor placement study. It will follow this with a detailed description of how IMUs are implemented in human motion capture as well as the type of IMU motion capture algorithms commonly used. Motor control theories describing existing human motion variability and their relation to the rigid body model assumption are presented. To assist in understanding these theories, the associated human limb joints used in this study are presented along with how they are modeled.

1.2.1 Motion Capture Systems

A host of previous research on human motion capture has been conducted in the fields of sport science and medicine. Examples of human motion capture use are to use the human kinematic data to improve motion patterns of athletes and to assist patients in physical rehabilitation. In this section, I provide details on motion capture systems to highlight the decision to select IMUs for this sensor placement study. Although many motion capture technologies have been developed, including optical, image-based, mechanical, and magnetic, these methods do not provide the portability that IMUs offer.

Optical systems are used extensively for motion capture because they offer a reliable and accurate way to record complex motions. Optical systems reconstruct the

locations of 3D markers placed on the body using surrounding cameras and triangulation methods. This method of motion capture is expensive and not portable because it must be used in a structured environment [4].

Image-based solutions, such as Kinect, use computer vision techniques to extract motion parameters from video streams. This method compares the silhouette in the foreground with the silhouette of a synthetic figure and uses a distance-based cost function to determine the subjects pose [5]. This method is limited by the detail of the synthetic figure and has a high computation bandwidth associated with it. Additionally, unlike optical systems, image-based systems must compensate for the loss of 3D information [6].

Exoskeletons are assistive devices currently being researched to augment human motion for rehabilitation, improving strength and motor control, or improving functional performance. Exoskeletons transmit torques to the appropriate human joints using actuators [7]. For example, lower extremity exoskeletons have the potential to assist in load carrying by increasing load capacity and lessening the likelihood of leg or back injury. An upper extremity exoskeleton, Biomimetic Orthosis for the Neurorehabilitation of the Elbow and Shoulder (BONES)[7], generates rotation about the shoulder and elbow to assist with rehabilitation. These stiff mechanical systems can also directly measure joint angles rather than estimating points on the body. However, exoskeletons can be very uncomfortable, increase normal metabolic cost, and limit a users range of motion [8].

Magnetic systems are limited by the fact that they are sensitive to external fields [9]. Although magnetic sensors have the benefit of being portable, they are prone to temporary magnetic disturbances which may affect the reliability of measurements of the earth's magnetic field [10], thus they are only reliable in controlled environments where the surroundings do not alter the local magnetic field.

A common method for estimating rigid body motion is the use of Inertial Measurement Units (IMUs), which are small electronic sensor suites of accelerometers, rate gyros, and magnetometers that measure linear acceleration, angular velocity, and local magnetic field. Compared to other motion capture technologies like optical, image-

based, and magnetic, IMUs provide an inexpensive and portable solution. Recent technological advances have improved the energy consumption, cost, and availability of these sensors [11]. Whereas optical and acoustic devices require a source emission to track objects, IMUs do not, which simplifies system integration and increases portability.

IMUs use this combination of accelerometers, gyroscopes and sometimes magnetometers to estimate the location and orientation of the IMU device in 3D space. The estimation is done by calculating linear displacement (using accelerometer data) and rotational displacement (using gyroscope data) of the object, from a reference point. Although not necessary, a magnetometer can act like a magnetic compass to provide a reference point to north, much like an accelerometer always has a reference point in the direction of gravity [12]. By mapping or calibrating the IMU to a rigid limb on the body, the orientation of body limbs can be estimated from the IMU's output.

1.2.2 Implementing IMUs in Human Motion Capture

A great advantage of IMU systems for motion capture is that they eliminate the restrictions placed on the capture area, that is, they can be as small or big as they need to be for the specific case. IMUs show a very promising approach to motion capture systems that can be used almost anywhere because they are portable and wearable. However, despite these benefits, IMUs have disadvantages.

Accelerometers measure the sum of linear acceleration and gravity. In a quasi-static movement, linear acceleration can be neglected. In a dynamic situation, it is difficult to decouple the two measures and may lead to difficulty calculating attitude accurately [13]. Accelerometer readings start to drift noticeably after a short period due to the long-term noise that causes samples to gradually become further away from their true values. Although less noticeable in applications with constant movement, in applications where values are averaged over longer periods of time, drift can cause severe inaccuracies [14]. Angular velocity measurements by gyroscopes are prone to sensor drift over time and gyroscopes sometimes enter a position called gimbal lock. In control moment gyroscopes, two gimbals can be driven into a configuration where

an estimation of orientation has more than one solution and the gimbals must be reset. Depending on what type of representation is used for IMUs, a similar phenomenon can occur, even with micro-electromechanical system (MEMS) sensors. Magnetometers are susceptible and influenced by electromagnetic interference including ferrous material in the near vicinity. With an estimated orientation for a given IMU, there is still a need to calibrate individual sensors to the global body coordinate system every time the sensor suite is donned.

IMU calibration can be either static or dynamic (e.g. [15], [16], respectively). The most common pose held for a static calibration is a "T" pose in which both arms are held straight out to each side. While the directional acceleration is easily calibrated and initialized on all three arm segments using this pose, the largest error due to this variability was found in the heading estimation (the location of the IMU around an arm segment). Orientation and location are typically not computed by time-integrating the signals from accelerometers and rate gyros, including any sensor drift and noise, because the estimation errors tend to grow unbounded.

Dynamic calibration motions vary but may include simple one degree of freedom motions for relevant segments. Wu et al. [17] developed a self-calibration process incorporating sensor misplacement for in-plane orientation misalignment, but it was not able to aid misalignment in rotations along local body curvature. All these calibrations relate the local coordinate system of the IMU to the global placement of the IMU on the body. Calibration poses increase preparation time for a system and are also only as accurate as the ability of a human to perform a specified motion and place the sensor.

1.2.3 IMU Motion Capture Algorithms

To overcome these individual IMU disadvantages, fusion techniques have been implemented. Starting in 1970, Bortz [18] computed sensor orientation by integrating angular velocity. Since then, others have extended fusion methods and examined Kalman Filter algorithms to obtain dynamic orientations of IMUs by implementing an Euler angle representation [19][20]. To avoid singularities in Euler angles and

to limit the need for linearizing, quaternion-based Extended Kalman Filters (EKF) have been implemented [21][10]. By taking advantage of a stereotypical feature of human locomotion to alternate movements of limb segments, Sabatini [10] updated gyro measurements during zero velocity periods, or rest periods, to try and capture the bias vectors of accelerometers and magnetometers. Sabatini's study showed that the use of an external field to compensate for error drifting decreased error estimation in a controlled environment. However, outside the controlled environment, external magnetic fields vary greatly, and thus this method is limited. Althougth quaternion-based EKF limit the need for linearizing, these methods still require an embedded physical model linearization and is limited to slow motions due to the computation time.

Results of the use of IMUs on robotic hinges rather than on humans [22] show that if accelerometers can be placed exactly on the joint center, simpler algorithms can accurately predict joint-angles without the need for computationally heavy filters. For example, Cheng et al.[22] use variations of a common-mode rejection algorithm to estimate joint angles by using combinations of two accelerometers, one accelerometer and one rate gyro, or two accelerometers on each adjacent limb to the joint angle.

The need for the IMU to be placed exactly on the joint center indicates that the variability of sensor placement by humans during repeated use may be a large cause of motion estimation errors. Although Cheng et al. [22] advise on the use of these methods for experimental setups, they also make the statement that these methods would not work well on humans because these methods require very precise, repeatable motions. As Luinge et al. [23] also conclude, the accuracy of any method is limited by the accuracy of the sensor to segment calibration.

1.2.4 Sources of Human Variability

In order to understand human variability, we must first understand the associated joints of the movements we plan to study. The upper extremities of the human body include the shoulder, elbow, wrist, and finger joints, and the associated muscles crossing these joints. The complex interaction of the bones, muscles, and ligaments

at joints define human movement. One of the most comprehensive musculoskeletal models is the Upper Extremity Kinematic Model by OpenSim [24].

The human shoulder is made up of three bones, including the clavicle (collarbone), the scapula (shoulder blade), and the humerus (upper arm bone) (Fig. 1-1a). The shoulder joint generally refers to the glenohumaral joint (connecting the scapula to the humerus) and the acromioclavicular joint (connecting the clavicle to acromion, the highest point of the shoulder blade) [1]. OpenSim models the articulation between the humerus and scapula as a ball-and-socket joint, but uses a Groot and Brand regression equation [25] to determine the movement of all three bones as a whole [24]. Because of the multiple bones meeting at multiple joints, the shoulder movement is difficult to simulate with just a single ball-and-socket joint or hinge joint.

The elbow joint is also at the intersection of three bones (humerus, ulna, and radius) [1], but two of these bones (ulna, radius) are parallel to each other on the forearm (Fig. 1-1b). OpenSim models the elbow joint with two fixed axis [24]. The first is a hinge-joint to allow for the study of flexion and extention. The second axis runs along the forearm between the radius and ulna to permit pronation and supination.

Because of the complex interaction of all the components of joints, human movement has some associated variability. Stergiou[26] describes human movement variability as the normal variations that occur in motor performance across multiple repetitions of a task. These variations can exist on many levels, from inaccuracies when throwing multiple darts, to stride-to-stride fluctuations in walking [27], to swaying around a central equilibrium point without ever remaining exactly still [28]. For some, movement variability can be attributed to random error or noise. However, there are three theories for the variability in human motion.

The first is the Generalized Motor Program Theory (GMPT) [29]. This theory considers variation in a given movement pattern to be the result of error by the system. In this theory, variation can be considered the result of errors in the ability to predict the necessary parameters for employing the underlying motor program [30]. This is particularly true for novel motions, where corrections of these errors during the

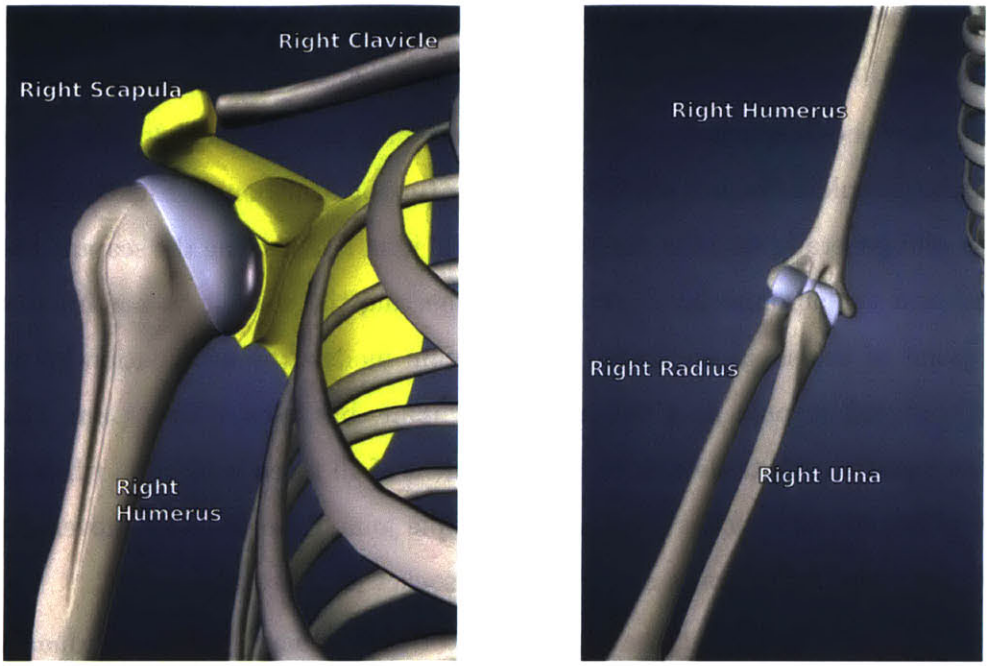

(a) Clavicle, scapula, and humerus bones. (b) Elbow joint and associated bones.

Figure 1-1: Shoulder and elbow joints with associated bones. Images taken from Human BioDigital [1].

motion leads to differences in sequential repetitions of the same motion. Uncontrolled Manifold Theory takes a dynamic systems approach to movements and states that motor variability is associated with the redundancy of elements necessary to solve a task [31]. Having more elements than necessary (multiple muscles fibers) results in the existence of multiple solutions to a motor problem, and thus repeated motions utilize different, albeit very similar, solutions for the same movement [31]. The third theory, the Dynamical Systems Theory, proposes that movement is the result of the interactions of multiple systems within the person, task, and environment [32]. Essentially, all sub-systems self-organize and interact in a specific way, to produce a given movement with the highest efficiency for a specific task [33]. The efficiency, and therefore the movement, changes with changing environments and tasks, and thus the motor system adapts constantly to slightly alter movement to reach higher efficiencies.

All three theories above are similar in the fact that they all agree that decreased

variability results from the efficient execution of a given movement pattern. However, work by Hausdorff has shown that not only do humans always have some natural variability in movement, but this variability is also important for proper movement [34]. Research has shown that increasing gait instability leads to increase likeliness of falling sooner [34] and that after a fall, gait variability increases [35]. Due to loss of strength and flexibility, older adults have greater variability observed in their gait [36]. However, results of looking at the breakdown of the variability through the entropy analysis support a general loss in time series complexity of gait with age [37]. The multi-scale entropy method (MSE) studies a one-dimensional discrete time series by calculating an entropy measure of each consecutive course-grained time series of the original signal, and plotting each time series as a function of a scale factor used to create the course-grained time series [38]. Therefore, even if the magnitude of variability is low, there are still measures in the signals used by entropy analysis to determine complexity, and thus having no variability in movement can be as bad as having a lot of variability. In summary, some variability is needed for efficient execution of a given movement pattern. Therefore, the performance of the prescribed motions in this study have an embedded coupling between the natural human motor variability inherent in humans, and the variability that is due to the rigid body model assumption not being appropriate for motion estimations. As a whole, there is a coupling of operational variability (due to sensor noise and placement) with motor-performance variability (due to the sensorimotor system).

1.3 Objective

The literature suggests that a motion capture system using IMUs where both sensor placement and calibration poses and motions are exact and repeatable provide good estimates of the system state. Motor control, however, is not exact and the theories presented show that variability is inherent in human motion. Despite this underlying human motion variability, measures in this study should remain constant when using a rigid body model. Therefore there is a balance; Not only are sensor placement

(non-expert) and limb motion during calibration (natural human variation) affecting the estimations, but the estimations are also affected by the assumptions in using the rigid body model.

This thesis will first test the hypotheses that initial placement (defined as distance, orientation, and rotation) of IMUs located at the chest, bicep, and forearm by a non-expert are affected by (1) the number of times the sensors are donned, (2) the type of functional motions performed, and (3) the location of the IMU on the body. Next, I will test the hypothesis that placement of IMUs vary throughout a motion to determine whether a rigid-body assumption is still appropriate during functional motions. Finally, given an understanding of the underlying variability, the effect of this variability can be inferred from the calculation of ranges of values commonly used by motion capture algorithms.

1.4 Thesis Summary

Although it is clear that progress is being made to increase accuracy of IMUs as a method for a motion capture system, further investigations need to be made to account for the variability caused by humans. Research has yet to be conducted on how much and in which way users vary in their placement of sensors on the human body. Understanding which type of sensor configurations and sensor mounting options are conducive to less variability provides us with data to assist in designs for housing sensors and allows for the development of quick don and doff sensor suites that can be reliably used by a non-expert for real-time data interpretation.

In this thesis, the uncertainty in IMU placement when donned by a non-expert user is characterized. These data will aid in future algorithm development to minimize and compensate for the donning and doffing variability measured in relevant motions. Chapter 1 provided a background into motion capture systems as well as the advantages, disadvantages, and algorithms used when implementing IMUs in human motion capture. Chapter 2 describes the experimental protocol, data acquisition methods, and statistical analysis methods for this experiment. Chapter 3 presents

results of testing each hypothesis, as well as the limitations of those results. Finally, Chapter 4 describes the application of these results as well as potential future work given this study.

Chapter 2

Experimental Methods

This chapter describes the experiment designed and conducted to study the variability in sensor placement by a non-expert and the natural human variation during limb motion calibration. The first hypothesis studied is that initial placement of IMUs on the body by a non-expert are affected by the number of times the sensors are donned, the type of functional motions performed, and the location of the IMU on the body. Next, the hypothesis of whether a rigid-body assumption is still appropriate during functional motions will be tested by studying how the placement of IMUs vary throughout a motion. Finally, the effect of this variability will be inferred from the calculation of ranges of Euler angles, which are commonly used by motion capture algorithms.

2.1 Participants

The study included 22 participants (6 female) aged 23.3 $\pm$ 3.0 years. The study was carried out in the Man-Vehicle Laboratory within the Department of Aeronautics and Astronautics at the Massachusetts Institute of Technology. Procedures were approved by the MIT Committee on the Use of Humans as Experimental Subjects (COUHES) and participants provided written consent. Participants received a $20 gift card as compensation. Participants were recruited through emails sent out to MIT student groups, the Aeronautical and Astronautical Engineering department,

Figure 2-1: Vicon reflective marker with flat base

and the Mechanical Engineering department at MIT.

2.2 Experimental Protocol

Participants were instructed to self-place four IMUs (APDM, Opal 425 [39]) during the study to analyze the variability in placement on the upper body for two mounting configurations, straps and garment based. These sensors are 48.4 $\times$ 36.1 $\times$ 13.4 mm in size and have a mass of less than 22 grams each. The accelerometer, gyroscope and magnetometer are all three axes and range from $\pm$6g, $\pm$2000 deg/s, and $\pm$0.6 mT, respectively, in each axis.

Prior to data collection, researchers placed 24 passive reflective markers (twelve 9.5 mm diameter markers on the participant and twelve 6.4 mm diameter markers on the IMUs) to permit standard motion capture analysis (Vicon 10-camera Bonita system [40]) (Fig. 2-1). Markers were mounted to the body and to the IMUs using double sided, medical grade tape strips adhered to the bottom side of the marker. All markers were wiped down with alcohol wipes after each subject. On the IMU, the markers were placed in a 90 degree triad (Fig. 2-2).

For data collection, all subjects were asked to perform five donnings and doffings of each of the two IMU configurations. During each donning, one calibration T-pose, in which participants stood still with their arms extended out to their sides to form a "T", and one wall calibration pose, in which participants stood with their arms to their sides and backs on a wall, were performed prior to the six predetermined

Figure 2-2: Opal IMU with three Vicon markers in a triad configuration

motions (see Section 2.3.3) that were performed randomly a total of six times each (total of 36 motions during each donning). The motions were randomized to prevent learning effects.

An instructional donning was performed during the first mounting configuration, in which all straps were adjusted for fit and comfort using the participant's feedback. The instructional donning was also performed for the garment configuration (C9 by Champion Compression Long Sleeve T-shirt). Participants were able to choose from 3 male and 3 female black or dark gray fitted small, medium, and large sizes (Fig. 2-4). Garments available were the same for both males and females. These instructional donnings were purely for fit and none of the predetermined motions were performed. The participants were also fitted for fabric arm braces (McDavid, Elbow support/elastic), placed on the right forearm and bicep, to prevent subjects from using the imprint of the IMU on the skin as a reference for placement during repeated donnings (Fig. 2-5). The braces were not removed during the multiple donnings of the IMUs. During the garment fit, the second configuration, a trace of the silhouette of the participant was created and used as a guide to participants when they repeated the wall calibration pose, limiting variability (Fig. 2-6). The strap and garment configurations were not resized after this instructional donning.

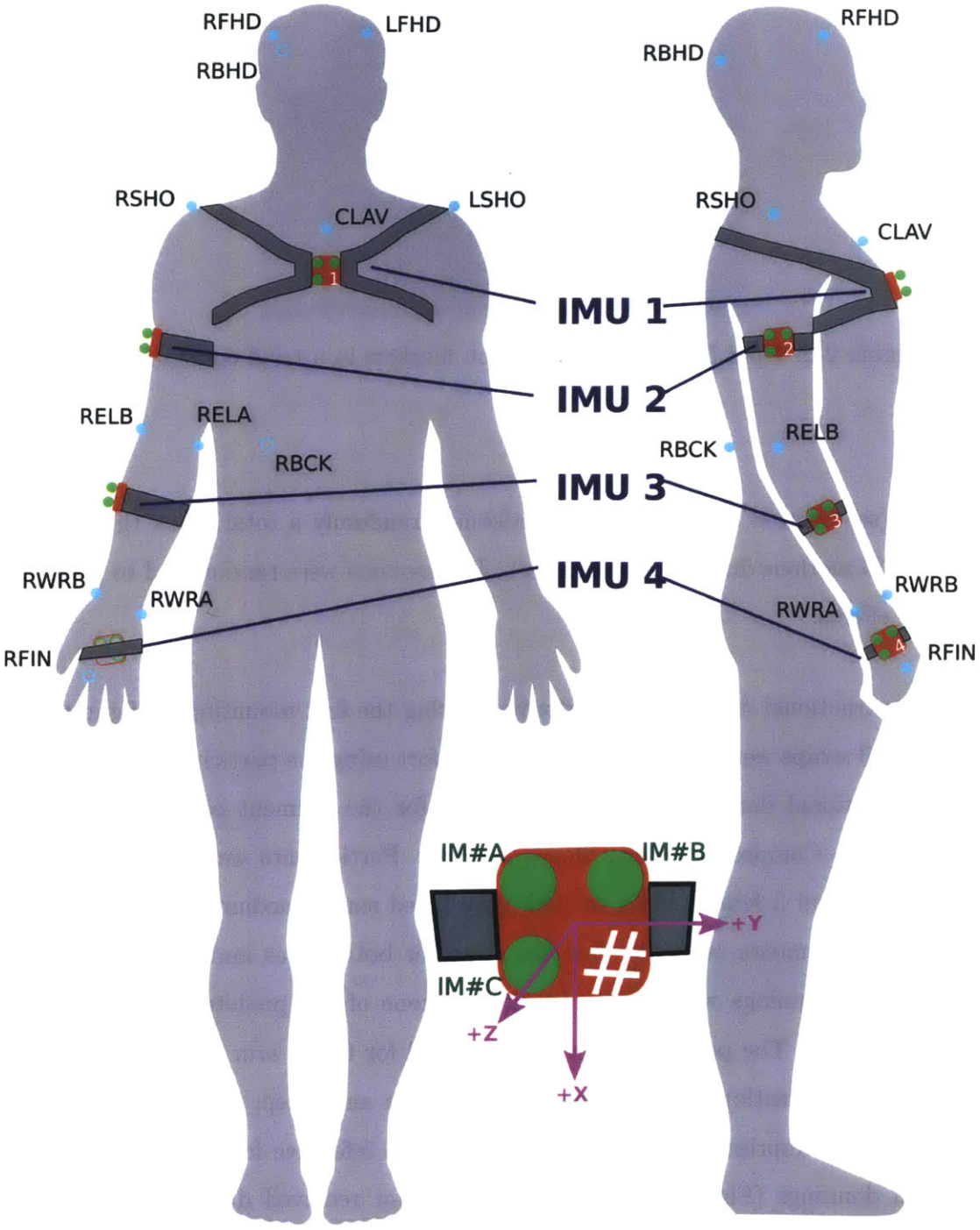

Figure 2-3: Recommended sensor placement (boxes on straps) and researcher placed optical motion capture markers. Sensor placement labeling scheme and IMU reference axes are shown in the bottom of the figure.

Figure 2-4: Champion compression garments with sewn Velcro for IMU placement

Figure 2-5: McDavid arm braces placed on the bicep and forearm to prevent subjects from using IMU imprint

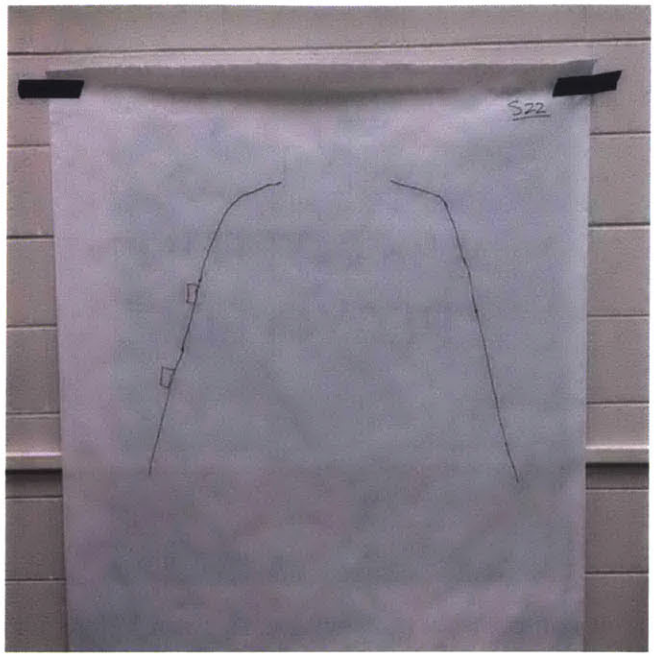

Figure 2-6: Trace of the silhouette of a participant

2.3 Data Acquisition

2.3.1 Donning Configuration

The IMU strap configuration utilized Velcro straps to independently mount the four IMUs (Fig. 2-3). One single hoop strap was used for each IMU placed on the hand, forearm, and bicep (Fig. 2-8a). A chest strap with two connection points, two snap buttons on one side of the IMU, and hoops for each arm was used to secure an IMU to the chest (Fig. 2-8b). Velcro strips were sewn onto the garments to allow the easy and quick placement of IMUs on the garment. One IMU was placed on chest, right bicep, and right forearm after the participant had chosen a size, to ensure proper location placement (Fig. 2-4). The fourth IMU placed on the hand always used a strap configuration.

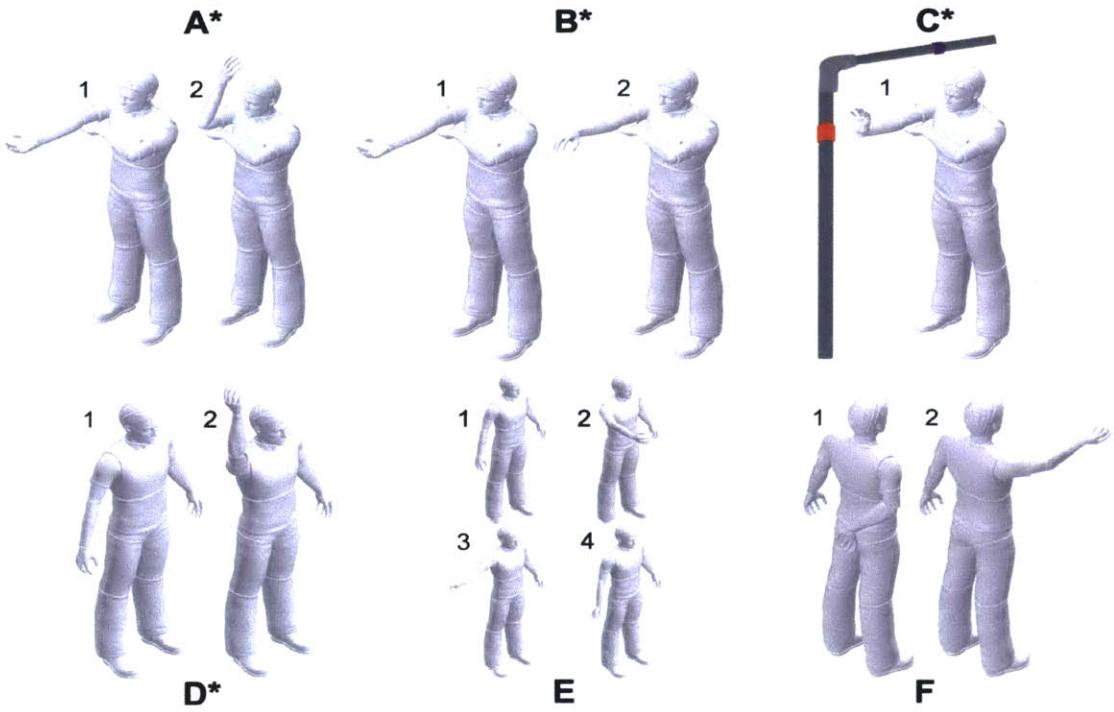

Figure 2-7: Predetermined motions showing relevant degrees of freedom (A = elbow flexion and extension; B = forearm pronation and supination; C = wrist ulnar and radial deviation, wrist flexion and extension; D = Lifting arm upwards, which included elbow flexion and extension, shoulder flexion and extension; E = Lifting arm forward and to the side, which included shoulder abduction, flexion and rotation; F = Lifting arm forward from a behind the back starting position, which included wrist, elbow, and shoulder flexion and extension, shoulder abduction, and forearm pronation and supination). Motions have numbered figures to indicate sequence of poses. Subjects performed the sequence in a motion, and then returned to the first pose in the sequence. Target Apparatus only shown in Motion C but was used by four motions (A * indicates the motion used a guide).

2.3.2 Motion Capture

Vicon data were sampled at 120 Hz. The IMU data were sampled at 128 Hz and wirelessly logged in real-time and synchronized to enable comparison of the optical and inertial data. In addition, all participants were video recorded during the trials. Motion Studio software by APDM was used to capture data from the IMUs. A 9 pin axial cable connected the IMU wireless access point to the Vicon motion capture giganet to allow synchronization between the two systems. A 3.3 volt signal from the access point to the Vicon giganet indicated a sync in command (Fig. 2-9). The

(a) IMU in single hoop strap mount

(b) IMU in chest strap mount

Figure 2-8: Hoop and chest straps for IMUs

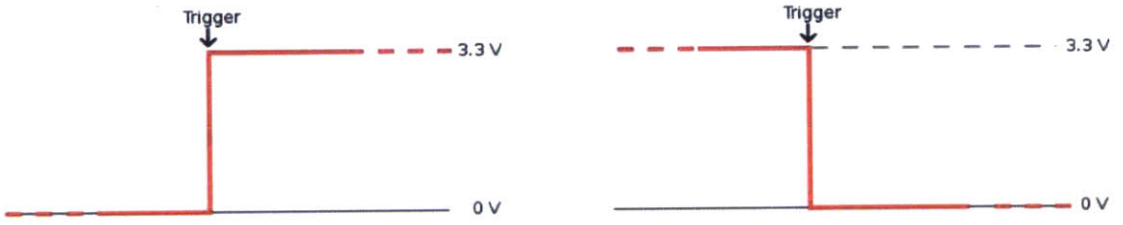

Figure 2-9: Sample of sync in (start) and sync out (stop) signals from IMU access point to Vicon giganet.

Vicon system was configured to start and stop on these remote signals. To ensure the entire motion was captured, each trial captured data a few frames before and after the motion was performed.

The Opal IMUs utilize docking ports to charge and sync. When programming a new session of multiple IMUs, the IMUs must all be plugged into the daisy-chained docking ports. The IMUs are configured through the Motion Studio Software by inputting sample rates, IMU locations, and external signals to sync the IMU and Vicon systems. When the configuration is uploaded, the IMUs are removed from the docking ports and given a few seconds to sync, as indicated by all IMUs flashing a blue LED synchronously. The IMUs then wirelessly transmit their data to the access point, which parses multiple signals and communicates with the computer running the Motion Studio software.

2.3.3 Motions

Six predetermined motions were described to the participants prior to data collection through text and visual descriptions. The visual descriptions posted on the wall during the experiment for reference are shows in Fig. 2-7 while the text description provided to the participants prior to data collection can be found in Appendix B. The motions were chosen to include a range of single and multiple (more than one) degrees of freedom. Motions included elbow, wrist, and shoulder flexion and extension; forearm pronation and supination; wrist ulnar and radial deviation; and shoulder abduction and rotation. The visual descriptions of the motions were within eye sight of the participants during data gathering for reference. During 4 of the 6 motions, a target apparatus was used to determine the starting and ending positions (Fig. 2-7).

Motions were chosen to have both Earth and Space relevance, so results of this study could be applied to both fields. Activities of Daily Living (ADL) is a term used in the healthcare industry since 1950's and was used by this study to define an Earth relevance. ADL refers to people's daily self care activities, and is regularly used to define a person's functional status. Basic activities include functional mobility, bathing, dressing, self-feeding, and personal and toilet hygiene. Space relevance of motions was determined through informal discussions with a former shuttle astronaut in which he was asked to act out activities he would perform in one work day while in space. Motions chosen for this study encompassed both Earth and Space applications (Table 2.1).

Fig. 2-7 describes in detail how to perform each motion. Table 2.1 provides the rational, through examples, for why the motions chosen have both an Earth and space relevance. Eating with a spoon in space is very similar to that on Earth [41], therefore motion A was chosen. Motion B was also chosen not only because it provided a different degree of freedom of the elbow joint, but also because it is a common way to lock drawers on the Space Shuttle [41]. Motion C provided a full degree of freedom characterization of the wrist. Motion D replicates a common way to move around inside the Space Shuttle to prevent bumping your head [41]. Although a very robotic

Table 2.1: Final motions chosen based on Earth-relevance (as defined by Activities of Daily Living) and Space-relevance (as defined by Astronaut Jeffrey Hoffman)

Motion	Potential Motion	Relevant DoF	ADL / Activities	Earth Relevance Example	Space Relevance Example
A	Flexion and extension of the elbow joint	Elbow flexion; Elbow extension	Eating	Cleaning face with napkin; Exercise	Cleaning face with a napkin or moist wipes
B	Pronation and supination of arm/wrist	Pronation; Supination	Bathing	Managing faucets	Managing controls; Locking/unlocking drawers.
C	Wrist circles, starting with wrist extended	Wrist ulner and radial deviation; Wrist flexion and extension	Eating	Cleaning; Eating; Reaching	Managing controls
D	Elbow extension to reach above you.	Elbow extension; Elbow flexion; Shoulder flexion; Shoulder extension	Organization; Reaching	Placing items on top shelf	Reaching buttons; Opening drawers "above" you
E	Shoulder range of motion	Shoulder abduction; Shoulder flexion; Shoulder rotation	Reaching	Reaching; Placement of dinner table	Reorientation
F	Wallet motion	Wrist flexion and extension; Wrist radial deviation; Forearm pronation and supination; Elbow flexion, extension; Shoulder abduction; Shoulder Extension	N/A	Self defense; Toileting	N/A

movement, motion E a way to characterize the shoulder joint by using all of its degrees of freedom. And finally, motion F, although lacking a space relevance example, was chosen because it coupled many of the degrees of freedom in motions A through E.

2.3.4 Target Apparatus

The apparatus was created out of 19.05 mm [3/4 inch] PVC pipe and consisted of two poles at 90 degrees, one vertical at arms reach of the participant and one horizontal above the head of the participant (Fig. 2-10a). The vertical bar had a red target placed at shoulder height. The horizontal bar had a purple target placed above the participant, at a height just above the reach of the participant. The apparatus was adjusted to the height of each participant and was not adjusted during data collection. The adjustment was made using a tight fit between concentric PVC pipes. Two screw holes 304.8 mm [12 inches] apart along the length of the pipe were milled into the larger of the two pipes. Hemp string was looped repeatedly between the two holes, exposing half of the loop to the outside of the pipe. This pipe was then fitted over the smaller pipe. The number of loops of hemp directly correlated with the stiffness of the coupling between the two pipes. This method allowed for a continuous range of height to better tailor towards all subjects (Fig. 2-10b).

2.4 Data Processing

Vicon Nexus software was used to reconstruct, label markers, fill in gaps, and export the optical data. A Biomechanical Toolkit was used to import these data to Matlab [42]. In-house code was used to calculate IMU position, orientation, and rotation. Here, data for IMUs 1, 2, and 3 are presented. IMU 4, located at the top of the hand, was not included in the analysis because the location of the triad markers on the IMU was not continually observable by the Vicon motion capture system.

(a) Target apparatus stand (b) Hemp loop for continuous height changes

Figure 2-10: Target apparatus stand and hemp loop. Red and purple bands used for targets are not shown.

2.4.1 Dependent Variable Definitions

As shown in Fig. 2-3, each IMU had a triad of markers labeled A, B, and C corresponding to the top left, top right, and bottom left markers, respectively. The centroid of each IMU was defined as the midpoint between markers B and C. IMU position was defined as the distance between the IMU's centroid and a pre-specified body-fixed marker for each IMU (Fig. 2-11). IMU orientation was defined as the angle (in degrees) the IMU had rotated along the plane of initial placement. A vector from the IMU centroid to the pre-specified body-fixed marker defined zero degrees. The angle between this vector, and a vector created from marker C to A on each IMU, defined the IMU orientation (Fig. 2-11).

IMU rotation was defined as the angle about the local body curvature (Torso, bicep, and forearm for IMU 1, 2, and 3, respectively). IMU rotation was calculated as the dot product of a normal vector to the IMU plane and a normal vector created from surrounding body-fixed markers (Fig. 2-11). An example of IMU 2 rotation

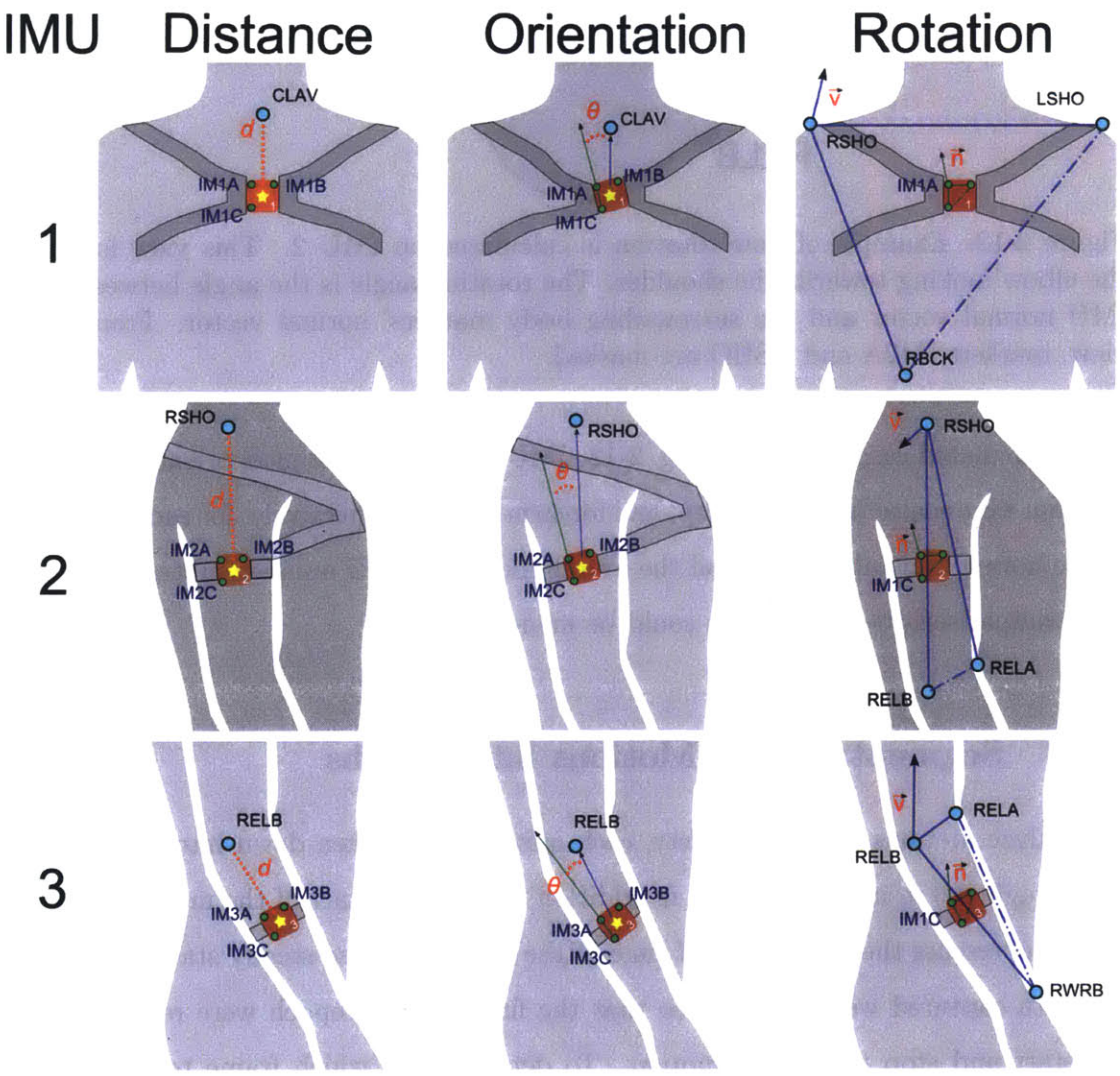

Figure 2-11: Definition of the three IMU measurements for each of the three IMUs and associated markers. IMUs had three markers, labeled A, B, and C, used to define the local IMU coordinate system. Each subfigure shows the surrounding markers used in the IMU's measurement calculation.

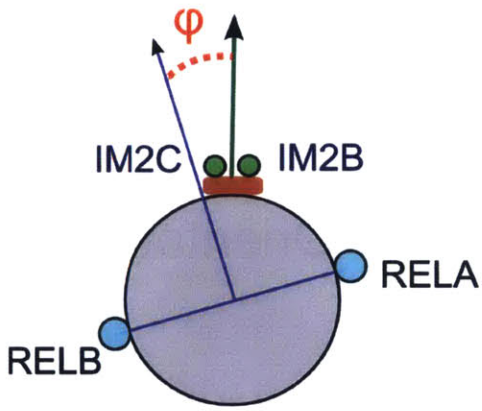

Figure 2-12: Example of how rotation is calculated on IMU 2. This view is from the elbow looking towards the shoulder. The rotation angle is the angle between the IMU normal vector and the surrounding body markers' normal vector. From this view, markers IM2A and RSHO are masked.

being calculated can be found in Fig. 2-12. IMU 1, 2, and 3 distance, orientation, and rotation were scaled by torso, bicep, and forearm length, respectively, for each subject. These normalized values then had the overall means by IMU number subtracted such that comparisons between IMUs could be made.

2.4.2 Segmentation of Motions into Epochs

To analyze motions in their entirety, each motion was broken down into 11 epochs, 10 through 100 in multiples of 10, in addition to epoch 0 (start of the motion). Each epoch represents the percentage of time of the motion. These steady state frames of the data captured were trimmed so that the first and last epoch were representing the start and stop times of a motion. To determine at which frame to cutoff, 20 frames from the beginning and end of the captured motion were used to determine a mean and standard deviation of the z-axis value of a marker RWRB (located at the wrist). The RWRB marker was chosen because it swept through a large range once the motion started. The z-value was easy to distinguish when the motion started.

Progressing from the start of the captured motion forward, the first frame with a value that was greater than the mean of the sampled frames plus three standard deviations was considered the start of the motion. Three standard deviations from

the mean was chosen as the criteria because it would encompass 99% of the normally distributed data with that particular mean. The end of the motion was determined in a similar way, except that a new mean and standard deviation were calculated from frames sampled from the end of the captured motion. The length of frames used for determining the mean and standard deviation at the beginning and end of a motion was set to 20 (160 ms) and 36 (300 ms), respectively. Appendix C.3 shows the differences between the raw and trimmed data. Appendix C.2 shows the Matlab code used to trim the data.

2.5 Statistical Analysis

The first objective was to test the hypothesis that initial placement of IMUs is affected by the number of donnings, types of motions performed, and the location of the IMU on the body. This was done by performing ANOVAs to examine the main and interaction effects of the independent variables (location, donning, and motion) at the first frame of a motion. A p value <0.05 was used to indicate statistical significance. The Tukey Difference test and the Student-Newman-Keuls test were used for post-hoc comparisons. Levene's test was used to assess the equality of variances. To test the second objective of determining whether a rigid-body assumption is still appropriate, a non-parameteric epoch analysis, which studies the motions at eleven evenly spaced normalized points in time, was performed. Kruskal-Wallis with Bonferroni corrections was used to examine differences in epochs for each motion at specific IMU locations. A Bonferroni corrected value of 0.002778 was used to counteract the effect of multiple comparisons. The value was determined by dividing the original $p = 0.05$ significance value by 18, the number of motion (6) and location (3) combinations. Conover-Inman was used for post-hoc comparisons and described further in section 2.5.1. SYSTAT statistical software was used for all calculations.

2.5.1 Epoch Table Description

Conover-Inman post-hoc statistical tests for all epochs were grouped into tables of combinations of motions and locations. An example of such a table can be found in Table 2.2.

The tables show epochs of a particular motion and IMU along the top and left sides. The table is populated with the Conover-Inman post-hoc significance value comparing two epochs within a given motion and location. Only half the table is populated because a Conover-Inman test of two epochs is the same regardless of which epoch was used first. A red color indicates significance because the test revealed a value below the significance value located at the top left of the table (Labeled A in Table 2.2). From this table, five trends of epochs for a particular motion and IMU can be deduced.

The first trend is the trend of initial epochs (Labeled B in Table 2.2). This group of values on the top left of the table shows differences between the first few epochs. If these values are mostly black, it means the first few epochs were not significantly different from each other. This trend is more often present in IMUs with small ranges of motion, such as IMU 2 (bicep) during motion A. Similarly, a trend of final motion epochs (Labeled F in Table 2.2) signifies no difference between the final seconds of a motion. Again, this trend is present most often in IMUs with small ranges of motions, either due to the small range of the motion itself, or because the IMU location isolates the IMU from the dynamics of the motion occurring a few degrees of freedom away.

The third trend, trends in apex epochs (Labeled D in Table 2.2), reveals similarities in epochs during the middle of a motion. Initial and final epoch trends are caused by the acceleration and deceleration of the limbs at the beginning and end of a motion, thus small changes in the position of the IMU can occur. Similarly, apex epochs are similar when an IMU is decelerating to a stop, and accelerating in the opposite direction. During this change in direction, the position of the IMU may not change significantly, and thus more black values are seen in the center of the table. Symmetrical epochs (Labeled E in Table 2.2) are an extension of apex epochs. A

Table 2.2: Interpretation of an example summary table of Conover-Inman post-hoc tests on epochs grouped by motion and location.

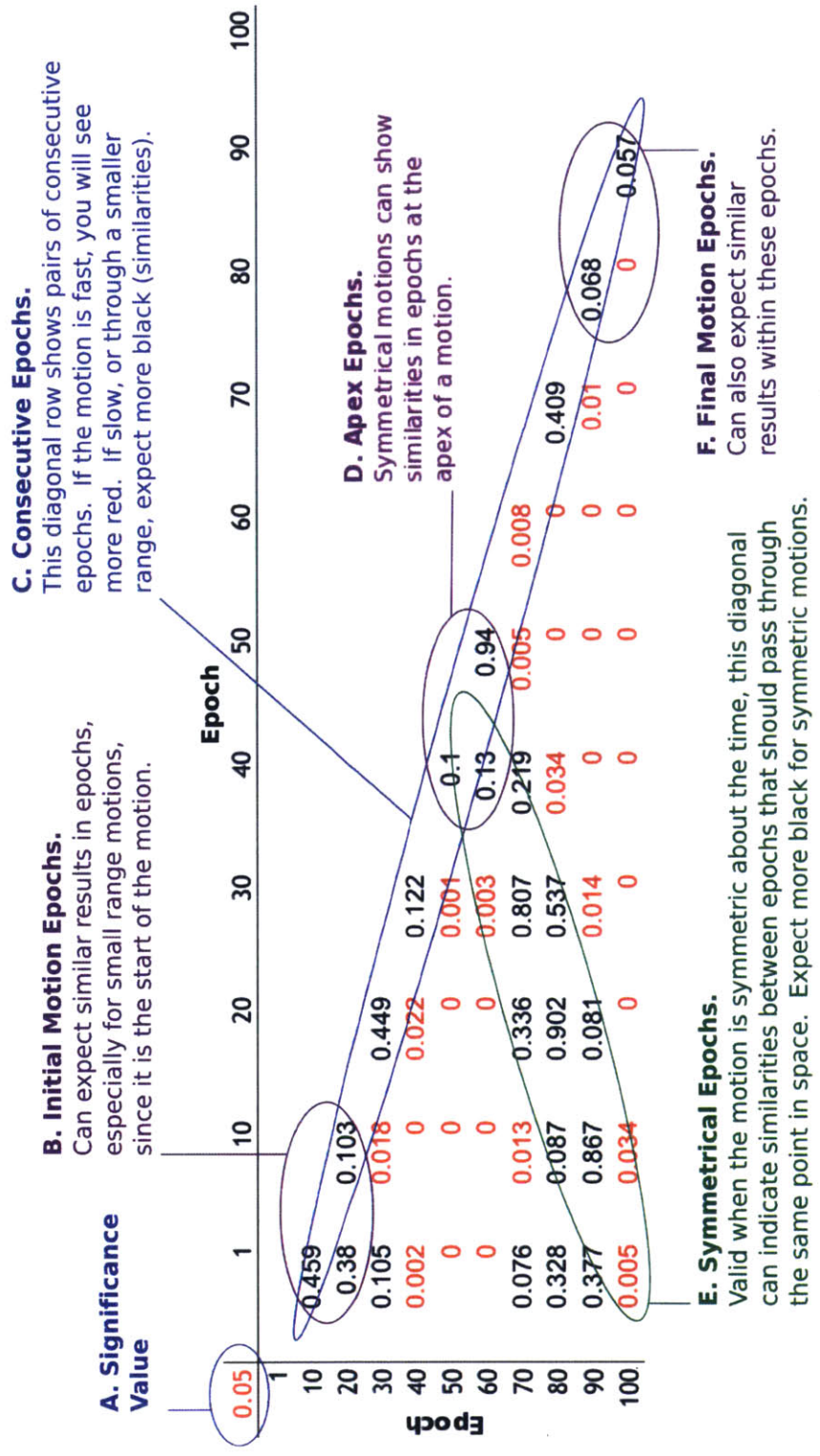

trend of black values from the bottom left to the center of the table can reveal similarities between symmetric epochs, or epochs that are the same distance from the end or beginning of a motion. For example, a symmetric motion like Motion D, where the second half of the motion is the first half done in reverse, would likely show no differences between epochs 1 and 100, 10 and 90, 20 and 80, etc. because the IMU is passing through the same position in space during these two different epochs. A motion like Motion E, however, is not likely to have symmetrical or apex epoch trends since the first half is the not the same as the second half of the motion.

The last epoch trend is trends in consecutive epochs (Labeled C in Table 2.2). On the example table in Table 2.2, a significant difference between epochs 1 and 40 is present. However, there are no significant differences between epochs 1 and 10, 10 and 20, 20 and 30, and 30 and 40. This could be explained by one of two things: either the change happened slowly enough to not be apparent in a small time frame, but is large enough to be significantly different on a larger time frame, or the epoch intervals are too small for the variability present, allowing for overlap of the distribution of dependent variables of consecutive epochs. IMU 1 (torso) tends to have this trend because, although a motion requires the torso to stay still, the IMU may shift slowly during a motion.

Chapter 3

Results and Discussion

As stated in Section 1.3, the specific aims are to characterize the uncertainty in IMU distance, orientation, and rotation during donning by a non-expert. Participants performed five donnings of self-placed IMUs on the chest, bicep, and forearm. Within each donning, participants performed six repetitions each of six prescribed motions.

3.1 Strap Mount Configuration

3.1.1 Effect of Initial Placement on Distance, Orientation, and Rotation Using a Strap Mount Configuration

The first specific aim tested the hypotheses that initial distance, orientation, and rotation of IMUs are affected by (1) the number of times the sensors are donned, (2) the type of functional motions performed, and (3) the location of the IMU.

3.1.1.1 Effect of Location, Donning, and Motion

A three-factor ANOVA was conducted for each dependent variable (distance, orientation, and rotation) to test for main and interaction effects of location, donning, and motion. Significant effects were found for all main effects, two-way, and three-way interactions (p <0.0005) for all three IMU dependent measurements (Table 3.1).

As expected, post-hoc pairwise comparisons of the IMU location main effect using

Table 3.1: Main and Interaction effects of Location, Donning, and Motion for initial placement. A p-value of 0 means p <0.0005

	Distance		Orientation		Rotation	
Source	F-Ratio	p-Value	F-Ratio	p-Value	F-Ratio	p-Value
LOCATION	826.892	0	650.955	0	81.374	0
DONNING	108.384	0	159.805	0	122.235	0
MOTION	111.501	0	267.452	0	355.272	0
LOCATION*DONNING	35.208	0	91.874	0	168.646	0
LOCATION*MOTION	43.733	0	84.86	0	555.957	0
DONNING*MOTION	6.868	0	9.013	0	12.566	0
LOCATION*DONNING*MOTION	5.774	0	9.89	0	9.512	0

Tukey's Difference Test showed significant differences between all three locations for IMU distance (p <0.0005), which is consistent with different reference markers being used for each IMU (Table D.1). For IMU orientation, significant differences were found between locations 1 and 2 (p <0.0005), and locations 1 and 3 (p <0.0005), but not between locations 2 and 3 (p = 0.554). Similarly, for IMU rotation, significant differences were found between locations 1 and 2 (p <0.0005), and locations 1 and 3 (p <0.0005), but not for locations 2 and 3 (p = 0.837). This is likely due to IMUs 2 and 3 having the same single hoop strap type, while IMU 1 at the chest had a more complicated strap with four attachment points and was therefore different than either of the other two IMUs. Also, the bicep and forearm are closer in shape than the torso is to either.

Pairwise comparisons for donning main effect showed no significant difference between donnings 1 and 3 (p = 0.225), 1 and 5 (p = 0.485), and 3 and 5 (p = 0.995). Donnings 2 and 4 were significantly different from the other donnings (p <0.0005). This confirms hypothesis 1, that there are significant main effects of donning. However, no consistent trend in any dependent variable with consecutive donnings was found. This implies that multiple donnings do not show learning effects. For initial placement, multiple donnings did not lead to more or less accurate placement.

Student-Newman-Keuls post-hoc tests were used to group similar motions (Table D.2). For IMU distance and orientation, there were 3 groupings: (1) motion A, (2) motions B and C, and (3) motions D, E, and F. For IMU rotation, the only

groupings were motions A and C, while all other motions were grouped into their own sub-group. For distance and orientation, motions B and C were consistently grouped together because they had the same starting position, thus if we are looking at IMU placement only at the start of a motion, it is expected to see no significant differences in placement between these similar motions when scaled by anthropometry because their starting positions are the same during every trial.

3.1.1.2 Interaction Effects of Location and Motion

Since no consistent trend in any dependent variable was found with consecutive donnings, the donnings were pooled and interaction effects of motion with location were analyzed. Fig. 3-1 shows the significant differences within motions for all IMUs. Dependent variables were normalized by anthropometry to compare between subjects and mean shifted to compare between IMU locations. Hypothesis 2 suggested that prescribed motions may affect the dependent measurements. IMU 1 showed the largest variance in orientation. This may be due to the complexity of the shoulder joint. Although motions A, B, and C had similar starting position, the focus of the participants was on lining up their hand with the target. This aligning does not constrain the height of the shoulder. Changes in shoulder height directly correspond to orientation changes of IMU 1. This effect with shoulder height would not be seen in distance or rotation of IMU 1 because a change in shoulder height would move both IMU 1 and the marker at the clavicle up or down (so distance would stay the same) and a change in shoulder height is orthogonal to plane in which rotation of IMU 1 is defined (independent of rotation). As seen in the three plots in Fig. 3-1, motions D, E, and F were consistently grouped together for distance and orientation. These three motions had different starting positions than motions A, B, and C, but similar starting positions to each other. Even though we observe embedded groupings such as motions B and C, as well as grouping of motions D, E, and F in two of the three independent variables, the groupings are not consistent, which indicates that the starting orientation has an effect on the dependent variables. Relative placements are important because the relationship between the local and global coordinate system is

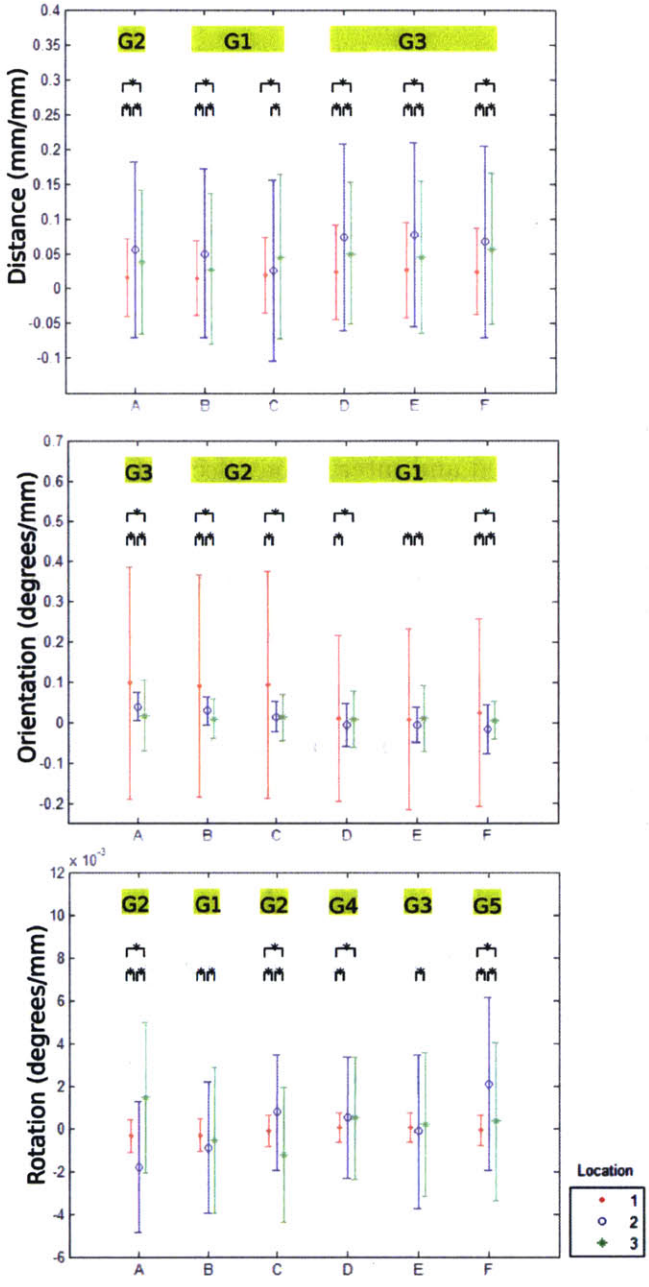

Figure 3-1: Shown are the within motion interaction effects between location. Additional significant effects across motions are not shown. Main effect groupings are shown in horizontal bars above graphs in the order of group means from smallest (G1) to largest (G3). Bars show one standard deviation from the mean. Above each graph, asterisks (*) indicate significant difference according to Tukey's Difference Test (p <0.05).

Table 3.2: Normalized and mean shifted location variances for all dependent variables

Variable	Variance		
	IMU 1	IMU 2	IMU 3
Distance (mm/mm)	0.0038 $\star\diamond$	0.0172 $\star\triangleleft$	0.0119 $\diamond\triangleleft$
Orientation (degrees/mm)	0.0646 $\star\diamond$	0.0024 $\star\triangleleft$	0.0044 $\diamond\triangleleft$
Rotation (degrees/mm)	5.5×10^{-7} $\star\diamond$	1.24×10^{-5} $\star$	1.21×10^{-5} $\diamond$

$\star$, $\diamond$, and $\triangleleft$ indicate significance (p <0.0005) between IMUs 1 and 2, 1 and 3, and 2 and 3, respectively.

defined in the calibration pose.

Hypothesis 3 suggests that location of IMU may affect the dependent variables. IMU distance showed significant differences across all locations, with the group mean lowest for location 1. This is consistent as the torso enabled the most precise placement of the IMU centroid due to having more constraints than the straps on IMUs 2 and 3 (Fig. 2-3). IMU 1 orientation was also found to be significantly different from IMUs 2 and 3. The similarity in orientation between IMUs 2 and 3 is consistent with the strap configurations. For the strap configuration evaluated, the location of the IMU had an effect on IMU placement. There is a component of IMU placement that may be due to the user's natural placement variability, but there is also a portion that can be influenced by the strap type.

3.1.1.3 Variance of IMU Distance, Orientation, and Rotation During Initial Placement

To compare variances, dependent variables were normalized and mean shifted for all dependent variables. Levene's test showed significant differences in the variances for the distance (p <0.0005) and orientation (p <0.0005) for all three IMU locations (Table 3.2). For distance, location 2 was the most variable and location 1 was the least variable. For orientation, location 1 was the most variable while location 2 was the least variable. There was no significant difference in rotation variance between locations 2 and 3 (Table D.3).

As a component of this variance may be attributed to strap type, it is important to consider how the straps were implemented. The straps associated with IMU 1 were constrained by four incoming straps with two connection points while IMUs 2 and 3 had two incoming straps and two connection points (Fig. 2-8). The loop on IMUs 2 and 3 that secured the IMU to the bicep and forearm allowed for more freedom of movement along the limb as well as movement along the local body curvature. In order to don these straps, the Velcro was looped through a buckle that was the same width as the IMU. This fixture limited changes in orientation of the IMU because the Velcro was as wide as the buckle, causing the IMU to align with the strap more consistently. The strap on IMU 1 was donned by looping each arm (much like a sweater is put on) and then snapping two buttons on one side of the IMU. Since the strap lengths were not changed, the chest strap was expected to provide consistent placement of the IMU centroid and to limit rotation about the torso. However, each of the two buttons had snaps that allowed some pivot, and thus small changes in strap location on the shoulder and under the armpit induced changes in IMU orientation. The data were consistent with these strap types and showed IMU 1 variance to be highest for orientation, but lowest for distance and rotation as compared to the other two IMUs. Comparisons of two variances for all combinations of IMU locations can be found in Appendix D.4.

3.1.2 Epoch Analysis of Strap Configuration

Specific Aim 2 tests the hypothesis that distance, orientation, and rotation vary throughout a motion. To test this hypothesis, an epoch analysis was conducted, as described in Section 3.1.2.3.

3.1.2.1 Testing Equality of Variances

Levene's test was initially used to test if the variances of all eleven epochs were equal for all three dependent variables. To do this, the data was grouped by motion and location (Table 3.3). Given the multiple comparisons, a Bonferroni correction was

Table 3.3: Levene's equal variance test of all 11 epochs performed for each combination of motion and location, for each dependent variable. A p-value of $p<0.002778$ indicates significance, due to the Bonferroni correction.

	Distance			Orientation			Rotation		
Motion	IMU 1	IMU 2	IMU 3	IMU 1	IMU 2	IMU 3	IMU 1	IMU 2	IMU 3
A	0	0.017	0	0.001	0.011	0	0	0	0
B	0.904	0	0	0.028	0.055	0	0	0.86	0
C	0.016	0	0	0.005	0	0.028	0	0.597	0
D	0	0.031	0	0.007	0.011	0	0	0	0
E	0	0.019	0.034	0	0	0	0	0	0
F	0	0	0	0	0	0	0	0	0

implemented, as described in section 2.5. Levene's test revealed that variances in epochs were not equal (p <0.05) for all but four combinations of motion and location for distance, orientation, and rotation. The four combinations that did not reveal significant results were distance for motion B at IMU 1 (p = 0.904), orientation for motion B at IMU 2 (p = 0.055), and rotation for both motion B at IMU 2 (p = 0.86) and motion C for IMU 2 (p = 0.597). Since this test of variance homogeneity revealed that there is sufficient evidence to claim that the variances are not equal, non-parametric tests were used to analyze the epoch data.

3.1.2.2 Non-Parametric Analysis of Epochs within Motion and Location Combinations

A Kruskal-Wallis non-parametric analysis was conducted on all epochs of a dependent variable with data grouped by motion and location (Table 3.4). Once again, a Bonferroni corrected value of 0.002778 was used to counteract the effect of multiple comparisons. The value was determined by dividing the original p = 0.05 significance value by 18, the number of motion (6) and location (3) combinations. The non-parametric analysis revealed a main effect of epoch for all but 3 combinations of motion and location for distance, orientation, and rotation. The three combinations that did not reveal significant results were distance for motion B at IMU 1 (p = 0.687), distance for motion C at IMU 1 (p = 0.071), and rotation for motion B

Table 3.4: Kruskal Wallis with Bonferroni correction tests of all 11 epochs for each combination of motion and location, for each dependent variable. A p-value of $p<0.002778$ indicates significance.

	Distance			Orientation			Rotation		
Motion	IMU 1	IMU 2	IMU 3	IMU 1	IMU 2	IMU 3	IMU 1	IMU 2	IMU 3
A	0.001	0	0	0	0	0	0	0	0
B	0.687	0	0	0	0	0	0.484	0	0
C	0.071	0	0	0	0	0	0.002	0	0
D	0	0	0	0	0	0	0	0	0
E	0	0	0	0	0	0	0	0	0
F	0	0	0	0	0	0	0	0	0

at IMU 1 ($p = 0.484$). IMU 1 did not show significance for distance and rotation for motion B because motion B was pronation and supination of the wrist with the arm extended in front, and thus the torso was isolated during the motion. Motion C explored the range of motion of the wrist, and thus the torso and IMU 1 was also isolated.

3.1.2.3 Pairwise Comparisons Between All Epochs within Motion and Location Combinations

This section summarizes the results of all pairwise comparisons between epochs for all combinations of motion and location. First, examples of rigid body dependent measurement outcome are presented to gain an intuition for expectations given a rigid body model. Variability in the three dependent measures is confounded by variability due to donning position, motor position errors, joint complexity, effects of posture, and the underlying discretization of time. The results, grouped by motion, are then presented in the context of the rigid body assumptions and the sources of variability.

Results of all Conover-Inman test can be found in Appendices E.1-20. As shown in Table 2.2, summary tables were interpreted through five regions: initial motion epochs, final motion epochs, apex epochs, consecutive epochs, and symmetrical epochs.

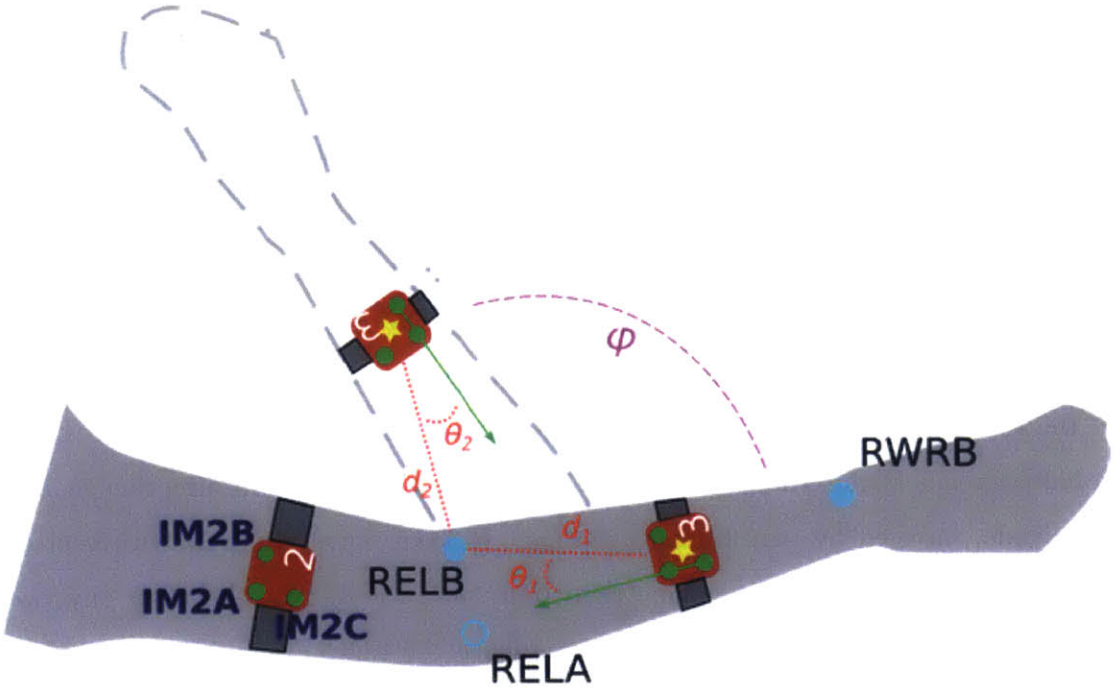

Figure 3-2: Side view of motion A at starting point and some angle phi after the elbow has gone through flexion.

3.1.2.3.1 Dependent Variable Expectations for a Prescribed Motion given Rigid Body Model

Prior to discussing the results of the pairwise comparisons between all epochs, we must first develop an intuition for expected results given (1) a rigid body model and (2) how the dependent variables in this study were defined (Fig. 2-11). We will use motion A as an example of a pure motion that can be coupled with other degrees of freedom, but the logic can be applied to any prescribed motion in this study. Figure 3-2 shows the location of the forearm at the beginning of the motion and at some flexion angle ϕ after the forearm has rotated about the elbow.

Distance for IMU 3 (forearm) was defined as the distance between the centroid of IMU 3 and marker RELB located on the outside of the elbow.

Since distance was defined to be a straight line between two points on the same rigid body (RELB and the centroid of IMU 3), the distances d_1 and d_2 should be equal (Fig. 3-2). Given a rigid body model, we should expect the distance value of

the IMUs to not change throughout motions.

Orientation was defined as the angle (in degrees) the IMU had rotated along the plane of initial placement. It was defined by two vectors. The first vector points in the direction of the length of distance defined for IMU 3 (from the centroid of IMU 3 to RELB). The second vector is a vector created from marker C to A on IMU 3. If we assume a rigid body model, the first vector would not change during motions, similar to how distance did not change. The second vector, defined by two markers on the IMU, would not change in magnitude either because the IMU is rigid. On a global reference frame, these two vectors will experience changes in direction, not in magnitude, induced by performing a motion. However, given that the two vectors are defined by markers on the same rigid body, and the distance between any two markers is not changing, both vectors experience the same exact rotations due to the motions, and the angle between the two vectors remains constant ($\theta 1 = \theta 2$ in Fig. 3-2). Given a rigid body model, we should expect the orientation value of the IMUs to not change throughout motions.

Finally, IMU rotation was defined as the angle about the local body curvature. It was calculated using the dot product between the normal vectors of two planes (Fig. 2-11). The first plane is made from three markers (RELB, RELA, and RWRB) on the same rigid body. The three markers uniquely define a plane on the rigid body segment. The second plane is defined by the triad of markers on IMU 3. Given that the IMU is one solid piece, the configuration of these three markers on each IMU will not change during motions. If we assume a rigid body model, then the relative distance between any two markers and the angles at marker points in either plane would not change during motions. The two normal vectors are on the same rigid body segment, so from a global reference frame, a change in direction of one normal vector due to a motion will be the exact same change experienced by the second normal vector. The distributive property of the dot product tells us that any transformation applied to both unit vectors will result in the same dot product. Therefore, given a rigid body model, we should expect the rotation value of the IMUs to not change throughout motions.

There are limitations to the expectations given above due to the definition of the dependent variables themselves. The first is that the definition of the dependent variables assumes single axis motion, which is not typically observed in the naturalistic motions performed. Trends found with these definitions do not inform how many axes were used during specific motions. Therefore, conclusions on changes in dependent variables can be attributed to coupling of motion or joint complexity that is not modeled in the rigid body assumptions. Second, postural changes such as arching your back or slouching your shoulders can cause shifting of the IMUs, the mounts, or the body markers. For example, there are many positions the shoulder joint can be in while still leaving the rest of the arm parallel to the ground and in front of the participant, as they were instructed to do for some motions. Dependent measures of IMU placement, more so in those that use multiple body markers such as rotation, can change due to these postural shifts. With single axis motion, we would not expect these measurements to change, however, coupled motions and postural changes confound our ability to assess the rigid body model with these metrics.

3.1.2.3.2 Relating Pairwise Comparisons Between All Epochs to Rigid Body Model Expectations

The Conover-Inman pairwise comparisons of all epochs within groupings of IMUs and motions reveal that significant differences in the distance measurement of IMUs are present at different epochs of a motion. Even a single degree of freedom motion like motion A showed significant differences between initial and final epochs for distance for the IMUs on the forearm and bicep.

Motion A required participants to begin with their right arm completely extended in front of them pointing at a target, and then flex and extend their elbow while keeping their bicep parallel to the ground. Because motion A is a symmetric motion, as expected, no consistent significant differences between symmetric and apex epochs were found for IMU 1 for all three measures. IMU 3 showed significant differences in final epochs for distance and orientation, but not for rotation, showing that although a guide was provided, variability in final hand positioning was still present.

Orientation showed significant differences in final epochs for all three IMUs. These final epoch trends in distance and orientation for all three IMUs may be caused by the shifting in height of the shoulder (IMU 1), not keeping their bicep parallel to the ground (IMU 2), and coupling forearm pronation with elbow flexion (IMU 3). We cannot decouple what is responsible for the differences seen using our current definition of the dependent variables since they could be due to the rigid body model not being appropriate or postural changes by the participants. Although Motion A showed significant differences between different epochs for all three IMUs for rotation, no consistent significant epoch trends defined earlier were found. These embedded differences may be due to the postural changes that affect the shoulder joint. However, since we do see significant differences, it is important to take these into account when interpreting IMU data.

Motion B required the participant to pronate and supinate their hand from a palm facing the ceiling position, to a palm facing the ground, and back, all while maintaining their arm extended directly in front of them. For the Conover-Inman epoch post-hoc tests, IMU 1 did not have many significant differences between all epochs for all three independent variables. This is likely because IMU 1 is located on the chest and motion B required movement of the wrist. IMU 2 showed differences between consecutive epochs for rotation, likely due to the complexity of the shoulder joint which could have also rotated when the forearm pronated. All other differences between consecutive epochs were sporadic and showed no consistency in the five epoch trends defined earlier. As expected from a symmetric motion where the second half is the first half of the motion in reverse, IMU 3 showed no significant differences between epochs in symmetric, apex, initial, or final areas for distance, meaning the distances calculated in the first half were similar to the distances calculated in the second half. While the distance measure showed these trends, all three measures for IMU 3 did show significant differences in epoch areas not defined in Table 2.2. These inconsistent significant differences in IMU 3 outside of the defined areas signify relative motion between the fixed markers on the body and the markers on the IMU, which are assumed to be on the same rigid body, and thus should show no significant

differences at all.

Motion C explored the degrees of freedom in the wrist. Kruskal-Wallis analysis did not show significant differences for IMU 1 for distance, but did show significant differences for all other combinations of IMU and dependent measures (Table 3.4). Due to the triad of markers on IMU 4 on the hand not being continually observable by the Vicon motion capture system, IMU 4 was not analyzed. Given a rigid body model, the isolated movement of motion C about the wrist should lead to no significant differences in any measure for IMUs 1, 2, and 3. However, in practice, these motions were not isolated to the wrist and differences were found for all IMUs for all measures.

Motion D was a more complex (more degrees of freedom) motion than motions A, B, and C, requiring the participant to move their arm through 180 degrees of shoulder flexion and extension. IMU 1 showed no significant differences in initial epochs, final epochs, or apex epochs for distance, but did show significant differences for epochs outside of the epoch trends defined earlier. Given the large angles of flexion and extension of motion D, these differences may be attributed to the complexity of the shoulder joint. This complexity may alter the plane created by the shoulder and clavicle markers and may cause measurements to vary, even for IMU 1. As expected for a symmetric motion, IMU 2 for distance and IMU 3 for rotation showed no significant differences for symmetric epochs. However, all three measures showed significant differences in asymmetric portions of motion D for all IMUs. With a rigid body model, only shoulder and elbow flexion and extension are assumed for this motion. Small changes in pronation and supination and small changes in shoulder rotation during the motion cause changes in all three measures. The kinematic chain coupling joints is more apparent in this motion since multiple joints are used. Although symmetric epoch trends exist, the significant differences in asymmetric epochs for this complex motion means that further disambiguation of actual body motion and model assumption is required.

Motion E required the participant to move their shoulder through three different planes while maintaining their arm straight. Post-hoc tests revealed that IMU 1 showed no significant differences for distance and orientation in the final three epochs

of the motion. This is consistent with the large movements of the arm in the first three parts of the motion that, due to the center of mass of the subject changing, induce a torque that may cause the torso to shift, while a rotation about the axis of the arm in the last quarter of the motion will not. This final rotation about the shoulder also explains why IMU 2 showed no significant differences in the final epochs for orientation. Rotation of IMU 2, which was about the same axis as the final quarter of the motion, did show significant differences in final epoch trends because the reference markers for IMU 2 from which rotation was calculated (two on the elbow joint, one on the acromion) shifted with this motion due to the complexity of the shoulder joint. During the final quarter of the motion, IMU 3 showed a higher number of significant comparisons than IMU 2 for orientation. This could be due to subjects focusing on their hand orientation and pronating their forearm to face the palm of their hand to their thigh. Additionally, significant differences are seen outside of the trends defined earlier for all IMUs. Given that the motion was selected to only explore the three degrees of freedom of the shoulder, we expected no differences in measures between IMUs 2 and 3. Because we do see these differences, they are likely do to the confounding factors discussed earlier and should be further explored.

Motion F was the most fluid of all the motions, but its symmetry leads one to expect to still see no significant differences between symmetric epochs. This is true for IMUs 1 and 2 for distance but not for any other measures. Motion F also shows an inconsistent significance in initial and final epoch trends for all IMUs. Because there was no guide behind the participant to assist in making the motion symmetrical, we are seeing an effect of posture (unintentionally slouching, for example) of the participant playing a role since they lack a visual feedback to adjust for variations in limb positions. Significant differences are seen between beginning and middle epochs, and middle and final epochs for all IMU and dependent measure combinations. This means that the distances between body markers and markers on the IMUs are changing because of the complexity of the shoulder, elbow, and wrist joints.

It would be possible to differentiate pronation, supination, and other degrees of freedom with marker data from that trial. Similarly, posture during the experiment

could defined and determined given the arrangement of markers. However, this disambiguation was not studied in the scope of this experiment but is future work.

3.1.3 Potential Effects on Algorithms

Given an understanding of the underlying variability of IMU placement on the human body, the next steps are to understand how placement variations affect Euler angles, which are commonly used in current motion estimations algorithms. Interpretation of Euler angles should consider how estimating these parameters can be confounded with the variability in IMU placement. Essentially, IMUs are in a kinematic chain and the relative orientations between joint angles are dependent on placement and calibration.

As an example, the mean Euler angles and standard deviations for IMU 3 for motion A are shown in Figure 3-3. The solid line shows the average Euler angles for IMU 3 for all five donnings for all participants. The shaded areas represent the standard deviation calculated from the repetitions of motion A for each donning. For example, the red line in the top graph of Figure 3-3 represents the average yaw of IMU 3 for all repetitions within the second donning of each participant. The pink shaded region represents the standard deviation across all subjects. Euler axes means and standard deviations for all motions can be found in Appendix G. Although the graphs in Appendix G show mean and standard deviation values for the entirety of the motions, this section will only study the ranges of position measures and Euler angles for the first epoch (initial placement).

3.1.3.1 Range of Placement Parameters During Initial Placement

First, the ranges of the dependent variables (distance, orientation, and rotation) were calculated. The range was defined as the difference between the maximum and minimum variable values for a particular IMU, for all motions and donnings for each subject. A table of the ranges of each dependent variable for each subject, grouped by IMU location, can be found in Appendix F.1. Table 3.5 shows the mean and

Table 3.5: Mean and standard deviation of ranges of values for distance, orientation, and rotation of all subjects within each IMU location grouped by motion

Motion	IMU	Distance (mm)		Orientation (deg)		Rotation (deg)	
		Mean	SD	Mean	SD	Mean	SD
A	1	12.01	17.94	9.61	14.20	38.16	28.72
	2	44.91	38.95	11.51	7.64	30.78	22.30
	3	27.95	27.72	5.12	10.38	13.68	24.31
B	1	12.94	16.59	10.21	13.69	35.24	33.67
	2	43.87	41.04	9.15	8.15	21.74	26.25
	3	22.70	35.04	3.17	6.80	20.05	29.76
C	1	13.21	15.37	10.07	12.41	10.07	12.41
	2	35.50	44.72	6.11	8.40	17.86	21.65
	3	27.29	35.95	3.55	7.53	24.07	22.28
D	1	12.12	20.61	4.75	11.50	19.94	39.42
	2	45.45	49.09	3.89	9.42	17.61	28.09
	3	24.34	39.06	2.31	8.04	10.64	29.48
E	1	15.92	18.45	5.25	10.09	27.49	27.66
	2	51.89	43.35	3.77	8.50	25.38	24.80
	3	30.63	27.16	3.60	7.38	14.62	24.08
F	1	15.45	17.30	6.42	10.75	30.77	29.91
	2	48.53	45.97	1.40	11.53	13.33	26.29
	3	18.05	26.91	3.01	6.70	14.06	25.78

Figure 3-3: Euler axes (Yaw, Pitch, Roll) mean and standard deviations values for IMU 3 for multiple donnings of Motion A.

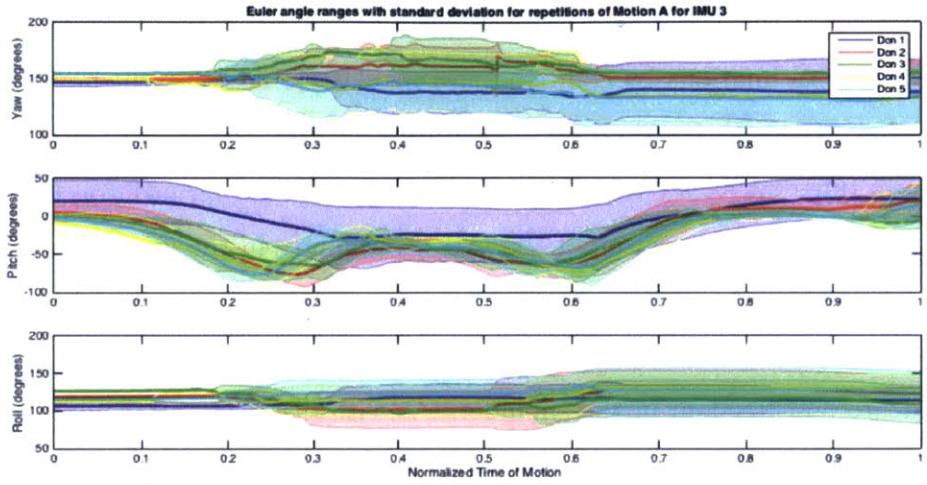

standard deviation of all 22 subject ranges, grouped by IMU location and motion. These numbers represent the average range you can expect from a subject during a given motion for all three dependent variables for all three IMUs.

Distance for IMU 1 was defined as the distance between the centroid of IMU 1 and a marker on the center of the clavicle. Since the distance between these two points is small when the strap is worn correctly, it can be expected that the average range when pooling all subjects would also be small. The distance variable for IMU 2 corresponds to the distance of the centroid of IMU 2 to a marker on the shoulder of the participant. The shoulder is the most complex joint of all joints in this study. The distance between an IMU on the bicep and a marker on the acromion can vary depending on the starting position of a motion and the location of the hoop strap on the bicep, which varies more than the strap used for IMU 1. The distance between the centroid of IMU 3 and a marker on the outside of the elbow joint define the distance variable for IMU 3. Variation in distance of IMU 3 can be attributed to pronation and supination of the forearm, where the total distance parameter would change because the elbow joint would pronate relatively less than the forearm.

Orientation of all IMUs was defined as the angle between two vectors. The first

vector was from the centroid of the IMU to the associated body marker used for the distance measurement. The second vector was a vector from marker C to marker A on the triad of the IMU, as seen in Figure 2-11. Orientation of IMU 1 could affect algorithm estimations by confounding torso lateral flexion into the variability in orientation of the IMU. Similarly, orientation of IMU 2 can couple movement variability in different axes (which axis depends on the starting position of IMU 2) with variability in the orientation of the IMU. Variability in the orientation of IMU 2 may be affected by shoulder posture since the marker on the acromion defines one of the vectors for the calculation of orientation. These orientation changes confound all three degrees of freedom in the shoulder. As with distance, differences in angles rotated of the forearm and elbow during pronation and supination may lead to changes in the orientation of IMU 3, counfounding elbow flexion and extention and elbow pronation and supination.

Rotation was defined as the deviation, in degrees, about the local body curvature. The chest is the least uniform local body curvature (as compared to the bicep and forearm). Although participants were sized for the straps, muscle and bone movement on the chest and back of a participant during different starting positions, as well as the increased curvature on female participant's chests, could also lead to rotation of the chest strap during initial placement. This large range of rotation could couple variations in the torso rotation with variations in IMU rotation, especially when studying small torso movements. Similarly, the use of the bicep and forearm muscles during motions can cause tilts in IMUs 2 and 3 that confound estimations of rotation.

3.1.3.2 Range of Euler Angles During Initial Placement

Given that many algorithms use Euler angles of IMUs to estimate orientation, a better method of determining the effect of IMU placement variability on algorithms is to study the range of Euler angles experienced by the IMUs during repeated use. Table 3.6 shows the average range of all three Euler angles at the first epoch for each IMU location, grouped by motion. The Euler axes on the IMUs are shown in Fig. 2-3. When determining ranges of Euler angles for different IMUs results have to

Table 3.6: Average range (above) and standard deviation of ranges (below) of Euler angles (in degrees) for all subjects, grouped by IMU location and motion.

IMU	Euler Axis	A	B	C	D	E	F
1	Roll (X)	9.08	8.29	7.68	13.38	10.35	30.07
		7.13	2.97	1.87	13.73	8.31	33.78
	Pitch (Y)	5.40	5.82	8.15	6.36	6.17	9.30
		3.29	1.36	4.59	6.16	5.60	2.42
	Yaw (Z)	48.55	32.04	14.33	24.09	21.97	44.19
		41.31	17.41	16.98	25.14	18.17	29.78
2	Roll (X)	29.06	20.02	20.40	43.34	98.64	23.52
		35.44	22.31	26.35	7.60	45.11	13.64
	Pitch (Y)	12.18	10.26	9.20	26.61	28.35	16.67
		6.23	6.63	6.68	21.28	29.74	8.59
	Yaw (Z)	22.28	25.29	13.73	7.49	99.66	6.27
		17.66	23.78	6.34	4.55	25.72	8.19
3	Roll (X)	4.36	20.69	21.79	55.70	20.53	29.51
		7.04	23.48	23.92	41.67	13.01	20.60
	Pitch (Y)	29.98	19.24	8.86	26.55	30.86	29.02
		28.56	24.86	4.27	36.15	30.80	25.20
	Yaw (Z)	3.89	21.64	13.73	26.35	15.64	63.63
		3.81	13.96	10.66	15.26	24.07	40.66

be grouped by motion because the starting positions can be rotated by as much as 90 degrees and would incorrectly show a large range for an IMU Euler angle if grouped together.

To obtain the values in Table 3.6, all trials in all donnings for each subject were grouped by motion and the Euler angles for each IMU at the first epoch was obtained. The range was defined as the difference between the largest and smallest Euler angle for a specific motion and IMU. The ranges shown in Table 3.6 are the averages of the ranges and the standard deviation of all 22 subjects.

As can be seen in Fig. 2-3, the yaw axis of IMU 1 points in front of the participant. Any deviation in this axis would be a result of the participant rotating in the coronal plane (torso lateral flexion). This means that motion estimation algorithms with inappropriate or incomplete calibrations couple deviations in posture with variability of IMUs. This can affect both standing (torso lateral flexion) and walking (determinants of gait) estimations. The roll axis of IMU 1 represents deviations in the transverse plane (torso rotation) and the yaw axis of IMU 1 represents deviations in the sagittal plane (torso tilt). The large ranges for these axes will be affected by the participant's posture.

The pitch axis (y-axis) of IMU 2 points in the same direction as the yaw axis of IMU 1 when the arms are at the side. In that configuration, deviations about the pitch axis of IMU 2 would be a result of torso lateral flexion of the participant. However, the pitch axis of IMU 2 can also indicate torso rotation when the participant's arm is held in front of them, and can indicate torso tilt when the participant's arm is held in front of them and the shoulder is rotated. Similar to IMU 2, IMU 3 can indicate different movements depending the starting position. The roll axis of IMU 3 can indicate elbow pronation and supination at all times, but the same axes give insight into torso lateral flexion when the arm is held out in front.

Table 3.6 shows that, even within the same IMU, the ranges of Euler angles vary between different motions that have the same starting positions. The starting position, as well as the location of the IMU on the body, have an effect on the Euler angles of the IMU. Thus orientation estimations algorithms need to account for the

Table 3.7: Main effects of Location, Donning, and Motion for initial placement of garment configuration. A p-value of $p<0.05$ indicates significance.

	Distance		Orientation		Rotation	
Source	F-Ratio	p-Value	F-Ratio	p-Value	F-Ratio	p-Value
LOCATION	0.634	0.439	0.551	0.701	0.351	0.741
DONNING	1.451	0.256	0.954	0.495	0.329	0.898
MOTION	1.318	0.263	0.089	0.772	0.202	0.933

location on the body of the IMU as well as the functional motions performed.

3.2 Garment Mount Configuration

3.2.1 Effect of Initial Placement on Distance, Orientation, and Rotation

The first specific aim tested the hypotheses that initial distance, orientation, and rotation of IMUs are affected by (1) the number of times the sensors are donned, (2) the type of functional motions performed, and (3) the location of the IMU. Participants performed five donnings of the garment configuration, but within each donning, only performed one repetition of one motion (either motion A or B) for this portion of the study. Thirteen participants performed motion A.

A three-factor ANOVA was conducted for each dependent variable to test for effects of location, donning, and motion. No significant main effects were found using the garment mount configuration. This can be attributed to the garment mount, which has fewer attachment points than the strap mount configuration. Since the garments have less embedded structure, it was expected to see increased placement variability as compared to the strap configuration, and perhaps a garment worn system with increased variability will not be able to distinguish differences based on the effect size of the placement variability.

To compare variances, dependent variables were normalized and mean shifted for

Table 3.8: Normalized and mean shifted location variances for all dependent variables

Variable	Variance		
	IMU 1	IMU 2	IMU 3
Distance (mm/mm)	0.0019 $\star\diamond$	0.0277 $\star\triangleleft$	0.02595 $\diamond\triangleleft$
Orientation (degrees/mm)	0.0304 $\star\diamond$	0.0541 $\star\triangleleft$	0.0472 $\diamond\triangleleft$
Rotation (degrees/mm)	0.0433 $\star\diamond$	0.0868 $\star\triangleleft$	0.0781 $\diamond\triangleleft$

$\star$, $\diamond$, and $\triangleleft$ indicate significance (p <0.0005) between IMUs 1 and 2, 1 and 3, and 2 and 3, respectively.

all dependent variables. Levene's test showed significant differences in the variances for all variables (p <0.0005) for all three IMU locations (Table 3.8). For distance, location 2 was the most variable and location 1 was the least variable. For orientation, location 2 was the most variable while location 1 was the least variable. For rotation, location 2 was the most variable and location 1 was the least variable. Again, a component of this variance may be attributed to mount type so it is important to consider how the garment was implemented. IMUs 1, 2, and 3 were mounted onto the garment using Velcro prior to data collection. The IMUs were not removed from this position during all donnings. Because the garment was a long sleeve garment, the two markers at the elbow and the marker on the shoulder were placed on top of the garment, not on the participant's skin. The garments had a "V" neck and the sleeves were short enough that the markers on the wrist and the clavicle were not affected. Participants were instructed to pick a garment that was comfortable yet snug enough for them to have confidence in placing the IMU in the same location.

Distance had consistently low variability for all IMUs, which could potentially be explained by the markers being on the garment. If the garment was fitting enough, the distance measurement would be less variable. A tight fitting garment would also explain why orientation varied less than rotation. Although there was no strap to help the IMU align, the IMU was still constrained to the garment, and if the garment was tight enough to remain straightened along the length of the arm, IMUs 2 and 3 would have less range through which to vary in orientation. A similar explanation can be used for IMU 1. A snug garment would prevent wrinkles when donned, ensuring

the location between two IMUs is at a maximum limit. As for rotation, similar to the straps, the garments allowed freedom of movement along the local body curvature for IMUs 2 and 3, as evidence by the highest variability in the garment configuration being IMU 2 for rotation.

3.3 Study Limitations

This study made use of strap and garment mounting configurations for the IMUs and understands that not all sensors are mounted in this manner. These results, however, can inform sensor attachment design. While an arm brace was used to limit the imprint on the skin, participants still had proprioceptive feedback which could aid in re-alignment of the IMU. Additionally, the age of the subjects was based on volunteers and availability. Care must be taken when applying these results to other age ranges. IMU 4 was removed from the analysis due to dropped markers, limiting where we can state if the rigid body model assumptions apply to the hand. The garment configuration had limited motions performed, so currently, comparisons between garments can only be made between elbow flexion and extension, and elbow pronation and supination. Finally, variability in the three dependent measures is confounded by variability due to donning position, motor position errors, joint complexity, effects of posture, and the underlying discretization of time and therefore we cannot decouple the expectations of these measurements given a rigid body model and the expectations of these measurements due to someone coupling a motion that was not intended.

Chapter 4

Conclusion

The accuracy of rigid body motion estimation is dependent on sensor placement and calibration. Therefore, characterization of sensor placement is needed to aid in development of algorithms and sensor attachment design for wearable motion capture systems. This thesis first tested the hypotheses that initial placement (defined as distance, orientation, and rotation) of IMUs located at the chest, bicep, and forearm by a non-expert is affected by (1) the number of times the sensors are donned, (2) the type of functional motions performed, and (3) the location of the IMU on the body. Next, it tested the hypothesis that placement of IMUs varied throughout a motion to determine whether a rigid-body assumption is still appropriate during functional motions. Finally, given an understanding of the underlying variability, the effect of this variability was inferred from the calculation of ranges of values commonly used by motion capture algorithms.

This study made use of off-the-shelf strap mounting configurations for the IMUs and found that the chest mount varied the least in initial placement in terms of distance and rotation, but its orientation varied more than when the IMUs were placed on the bicep and forearm. Although significant differences in IMU placement were found between donnings, no consecutive effects were found, showing that repeated donnings of a sensor suite do not lead to decreased variability in placement. It also found that the lack of a guide to assist with starting and ending positions of a motion results in significant differences in placement at the beginning and end

of motions. The placement of the sensor on the human-body varies throughout a motion, and cannot be expected to be the same even within a single donning due to confounding variations in donning position, motor position errors, posture effects, and the complexity of the joints studied, and thus the underlying assumption of a rigid-body model used by motion capture algorithms might not be appropriate. Motion capture algorithms need to account for the changes in position and Euler angles due to natural human variability and calibration during multiple donnings of IMUs by non-experts.

4.1 Summary of Contributions

The results presented in this study examined the effects of self-donning on IMU distance, orientation, and rotation at the chest, bicep, and forearm, both on initial placement and during motions. It also studied the potential effects of variable ranges on orientation estimation algorithms. The list of contributions from this study include:

- Developed a comprehensive database of both IMU data as well as external Vicon motion capture data, that encompasses motions, locations, and donnings, for use in future algorithm development.

- Determined that, given the variation in the placement measures of IMUs throughout a motion, the rigid-body model used by motion capture algorithms might not be appropriate.

- Quantified variances of IMU distance, orientation, and rotation at 3 locations on the body to assist with future sensor mount designs.

- Determined that for strap configurations, orientation of the IMU at the chest varies the most as compared to bicep and forearm IMU orientations. Thus, algorithms that use chest mounts couple rotations in the coronal plane with deviations of the IMU itself.

4.2 Potential Applications

This research was the first to characterize the way users vary placement of sensors on the human body. Relating mounting locations, motions, and number of donnings to IMU placement provides data to assist in designs for housing sensors and can aid the development of quick don and doff sensor suites that can be reliably used by a non-expert for real-time decision making. This study made use of IMUs but the results can be applied to any sensor that uses the same size sensor suite and mounting configurations and any wearable sensor should consider using these results to guide the design of their sensors and interpret their data.

For example, let's say a designer wants to use a sensor to measure overall fatigue of an athlete. The longitudinal axis of the electrode of an electromyography (EMG) sensor should be aligned parallel to the length of the muscle fibers to obtain the best readings [43]. In this case, an EMG mount design would want to limit the orientation of the sensor. According to this study, orientation varies less for the bicep than for the forearm. If the EMG is used as a measure for overall fatigue, a designer can now make a quantitative decision on where to place an EMG sensor depending on the functional motions likely to be performed and muscle groups likely to be activated. If the designer is only interested in the forearm muscles in particular, then a different mount should be considered if the Euler angle ranges at the forearm make the EMG signals to small for the motions performed. Alternatively, they can consider different motions that use larger ranges of the forearm muscles so the Euler angle ranges affaect the EMG readings less.

Similarly, future algorithms can benefit from these results. By specifying the location of the IMU on the body, algorithms can adapt thresholds for Euler angle estimations to try and remove any confounding human movements. For example, if studying small changes in human motion (like the tilt of a tight-rope walker during a performance), estimations of Euler angle changes of an IMU on the chest (IMU 1) will combine torso lateral tilt with the variability in placement of the IMU, especially during small angle changes. Below a certain threshold, a future algorithm might weigh

the values of an IMU located on the forearm of the performer (IMU 3) higher than the values of IMU 1 located at the chest, since the forearms may also provide an indication of how much the performer is adjusting their balance. Above that threshold, which is based on the Euler angle ranges determined in this study, there is increased confidence that changes in Euler angles of the IMU on the chest are representative of the lateral tilt of the performer, and not just variations in the placement of the IMU at the beginning of the study, or variations that the rigid body model is not capturing.

Appendix A

Recruitment Emails

All emails were approved by the MIT Committee on the Use of Humans as Experimental Subject (COUHES) and sent to MIT student groups, the Aeronautical and Astronautical Engineering department, and the Mechanical Engineering department at MIT.

A.1 Initial Recruitment Email

MITs Man Vehicle Laboratory is looking for volunteers to participate in a research experiment studying the variability in placement of inertial measurement units (IMUs) on the human body. This study involves donning IMUs and performing a set of predetermined motions inside a motion capture room. No experience with IMUs or motion capture systems is necessary.

All participants will receive a $20 Amazon gift card for completing the experiment. The study will take approximately 1.5 hours of your time. Participants must be over the age of 18 and possess no limited range of motion, pain, or discomfort when performing everyday tasks.

To participate in the study, send an email to Morris Vanegas at mvanegas [at] mit [dot] edu with the subject "Human Variability Subject: [Your name]"

Thank you!

A.2 Reply Email

Hi! Thank you for volunteering to participate in this study!

Please choose and reply with the best day that fits your schedule from the following link to participate in this study: Human Variability Experiment Available Time Slots. Although the experiment is only expected to last 1.5 hours, we encourage a 2-hour block to be able to handle unexpected delays.

A confirmation email will follow your date submission with further details about the day of the experiment.

Once again, if you have any questions, please contact Morris Vanegas at mvanegas@mit.edu.

A.3 Confirmation Email

Hello!

We have confirmed your slot as a participant in this study on [Date inserted].

Details about the experiment are below. Once again, send any questions Morris Vanegas at mvanegas@mit.edu.

Attire

Upper Body

Small Inertial Measurement Units (IMU) will be strapped on directly onto your skin, therefore tight-fitting clothing that leaves your arms exposed are best. Examples include undershirts, sleeveless shirts, and tank tops. You will be donning and doffing garments with sensors attached, therefore a tight fitting shirt is preferred.

Lower Body

No IMUs will be placed on your lower body, but baggy clothing can interfere with the motion capture data. For the lower body, please wear comfortable shorts or bottoms that are not too loose. Minimizing the movement of your clothes is best.

Head

You will wear a cap during the experiment. Please plan your hair style for the day accordingly. Wearing contacts for your vision is recommended.

Motion Capture

The Vicon motion capture system uses reflective markers to determine motion. Therefore, do not bring clothing with reflective strips, patches, logos, or designs to the experiment. Darker colored clothes are preferred. You will be provided with a location to safely store any jewelry. No reflective clothing. The markers (blue) and IMUs (red) will be placed on your body as described in the bottom image. If possible, limit skin care lotion immediately before the study to allow marker adhesive to work well.

Location

The experiment will take place in room 37-127. Please meet your experimenter in the Man-Vehicle Laboratory waiting area in 37-144 at your confirmed time slot (the room with a refrigerator). A locked room will be available to house your possessions. Time has been allocated for changing into your clothes, so do not feel obligated to walk around campus in your experiment attire.

Appendix B

Motion Descriptions for Participants

Motion A:

Begin with your right arm completely extended directly in front of you with your palm up. Place your left hand under your right tricep to maintain it level to the ground. Bend at your right elbow to completely flex your bicep while maintaining your forearm and hand in a straight line. Hold for 1 second. Extend your right elbow to return to a position where your right arm is completely extended in front of you with your palm up.

Motion B:

Begin with your right arm completely extended directly in front of you with your palm up. Place your left hand under your right tricep to maintain it level to the ground and to keep it from rotating. Rotate your wrist, forearm and hand until your palm is facing the ground. Rotate your wrist, forearm and hand until your palm is facing the ceiling.

Motion C:

Begin with your right arm completely extended directly in front of you, with your palm facing forward and fingers pointed up. Place your left hand under

your right forearm to maintain it level to the ground and to keep it from rotating. Using only your wrist, rotate your hand in a complete circle once starting clockwise.

Motion D:

Begin with your right arm completely extended at your side with your palm facing your thigh. Reach for the target above you and touch it with your fingertips. Return to fully extended arm at your side with your palm facing your thigh.

Motion E:

Begin this multi-step motion with your right arm completely extended at your side with your palm facing your thigh. Keep your arm completely extended during this entire motion. 1. Lift your arm 90 degrees until your arm is completely extended in front of you, level to the ground, palm facing to your left. 2. Move your arm 90 degrees to the right until your arm is completely extended to the right, level to the ground, palm facing in front of you. 3. Lower your arm 90 degrees downward until your arm is completely extended at your side and your palm is facing in front of you. 4. Rotate your entire arm at the shoulder to the starting position where your arm is completely extended at your side and your palm is facing your thigh.

Motion F:

Begin as if you were grabbing your wallet from your right back pocket with your palm facing the back of the room. Move your hand in front of you with your palm facing the ceiling as if you are handing your wallet over to the target.

Appendix C

Matlab Calculations

C.1 Calculation of Independent Variables

The following is the matlab function getDistance.m, which calculates the distance of each IMU centroid to the associated marker. Similar functions getOrientation.m and getRotation.m were created and used in the processing of data.

```
function [ output ] = getDistance( markers, location, epoch, subject )

% markers = acq to specific trial
% location = 1,2 or 3, for a specific IMU
% epoch = 1, 10, 20, 30 etc. as a percentage of where in the motion to
% get the data

% global variable to use specific subject anthropometry
global anthropometry;

% Get the range of useful data, without the steady state
ind1 = find(~isnan(markers.RWRB(:,3)),1,'first');
ind2 = find(~isnan(markers.RWRB(:,3)),1,'last');
range = ind2-ind1;      % new range with steady state value omitted

% Define the frame you are using, for this particular epoch
```

```
if epoch == 1
        frame = ind1;       % just use this new range
else
        try
            % epoch percent of the range, plus the start index
            frame = ind1 + floor(range*epoch/100);
        catch
            frame = 0;
        end
end

if frame==0
    output = NaN;
else

if location == 1
    try
        % IMU centroid
        centroid = [(markers.IM1B(frame,1)+markers.IM1C(frame,1))/2,...
                    (markers.IM1B(frame,2)+markers.IM1C(frame,2))/2,...
                    (markers.IM1B(frame,3)+markers.IM1C(frame,3))/2];

        % IMU distance to associated marker
        distance = sqrt((centroid(1,1)-markers.CLAV(frame,1)).^2 + ...
                        (centroid(1,2)-markers.CLAV(frame,2)).^2 + ...
                        (centroid(1,3)-markers.CLAV(frame,3)).^2 );

        % Scaling factor with associated body measure
        scale = anthropometry(subject, 1);

        % Check for zeros
        if (markers.IM1B(frame,1)==0 || markers.IM1B(frame,2)==0 || ...
                markers.IM1B(frame,3)==0 ||...
                markers.IM1C(frame,1)==0 ||...
                markers.IM1C(frame,2)==0 ||...
                markers.IM1C(frame,3)==0 ||...
```

```
                markers.CLAV(frame,1)==0 ||...
                markers.CLAV(frame,2)==0 || ...
                markers.CLAV(frame,3)==0)
            output = NaN;
        else
        % Scale
            output = distance/scale;
        end
    catch
        output = NaN;
    end

elseif location == 2
    try
        % IMU centroid
        centroid = [(markers.IM2B(frame,1)+markers.IM2C(frame,1))/2,...
                    (markers.IM2B(frame,2)+markers.IM2C(frame,2))/2,...
                    (markers.IM2B(frame,3)+markers.IM2C(frame,3))/2];

        % IMU distance to associated marker
        distance = sqrt((centroid(1,1)-markers.RSHO(frame,1)).^2 + ...
                        (centroid(1,2)-markers.RSHO(frame,2)).^2 + ...
                        (centroid(1,3)-markers.RSHO(frame,3)).^2 );

        % Scaling factor with associated body measure
        scale = anthropometry(subject, 2);

        % Check for zeros
        if (markers.RSHO(frame,1)==0 || markers.RSHO(frame,2)==0 || ...
                markers.RSHO(frame,3)==0 ||...
                markers.IM2B(frame,1)==0 ||...
                markers.IM2B(frame,2)==0 ||...
                markers.IM2B(frame,3)==0 ||...
                markers.IM2C(frame,1)==0 ||...
                markers.IM2C(frame,2)==0 ||...
                markers.IM2C(frame,3)==0)
```

```
            output = NaN;
        else
        % Scale
            output = distance/scale;
        end


    catch
        output = NaN;
    end

elseif location == 3
    try
        % IMU centroid
        centroid = [(markers.IM3B(frame,1)+markers.IM3C(frame,1))/2,...
                    (markers.IM3B(frame,2)+markers.IM3C(frame,2))/2,...
                    (markers.IM3B(frame,3)+markers.IM3C(frame,3))/2];

        % IMU distance to associated marker
        distance = sqrt((centroid(1,1)-markers.RELB(frame,1)).^2 + ...
                        (centroid(1,2)-markers.RELB(frame,2)).^2 + ...
                        (centroid(1,3)-markers.RELB(frame,3)).^2 );

        % Scaling factor with associated body measure
        scale = anthropometry(subject, 3);

        % Check for zeros
        if (markers.RELB(frame,1)==0 || markers.RELB(frame,2)==0 || ...
                markers.RELB(frame,3)==0 ||...
                markers.IM3B(frame,1)==0 ||...
                markers.IM3B(frame,2)==0 ||...
                markers.IM3B(frame,3)==0 ||...
                markers.IM3C(frame,1)==0 ||...
                markers.IM3C(frame,2)==0 ||...
                markers.IM3C(frame,3)==0)
```

```
            output = NaN;
        else
        % Scale
            output = distance/scale;
        end

    catch
        output = NaN;
    end
end % IMU location

end  % frame = 0

end
```

C.2 Matlab script to trim motions

```
function [ output ] = plotMarkers( markers, motion )

markers.RWRB(markers.RWRB == 0) = NaN;
markers2 = markers;
hold on
figure(1)
loc=1;
if motion=='A'
    loc=1;
elseif motion=='B'
    loc=2;
elseif motion=='C'
    loc=3;
elseif motion=='D'
    loc=4;
elseif motion=='E'
```

```
    loc=5;
elseif motion=='F'
    loc=6;
end
subplot(2,6,loc);
%x = linspace(0,1,length(markers.RWRB));
%original = length(markers.RWRB);
plot(markers.RWRB(:,3));


% WITH 3 SD CUTOFF
% 120 hz.  250ms = .25 of second = .25 of 120 = 30 length
framesbeg = 20; framesend = 36;
if motion=='A'
    framesbeg = 20; framesend = 36;
elseif motion=='B'
    framesbeg = 20; framesend = 36;
elseif motion=='C'
    framesbeg = 20; framesend = 36;
elseif motion=='D'
    framesbeg = 35; framesend = 36;
elseif motion=='E'
    framesbeg = 35; framesend = 36;
elseif motion=='F'
    framesbeg = 20; framesend = 36;
end


cutoff = 3;  cutoffend = 3;
ind1 = find(~isnan(markers2.RWRB(:,3)),1,'first');
ind2 = find(~isnan(markers2.RWRB(:,3)),1,'last');
last = length(markers2.RWRB(:,3));
start = [nanmean(markers2.RWRB(ind1:ind1+framesbeg,3)),...
    nanstd(markers2.RWRB(ind1:ind1+framesbeg,3))];
stop  = [nanmean(markers2.RWRB(ind2-framesend:ind2,3)),...
    nanstd(markers2.RWRB(ind2-framesend:ind2,3))];
```

```
a=1;
b=2;

for i = 1:last
    diff = markers2.RWRB(i,3);
    if (diff > (start(1) + cutoff*start(2)) ||...
            diff < (start(1)-cutoff*start(2)))
        markers2.RWRB(1:i,3) = NaN;
        a = i;
        break
    end
end
for i = last:-1:1
    diff = markers2.RWRB(i,3);
    if (diff > (stop(1) + cutoffend*stop(2)))
        markers2.RWRB(i:last,3) = NaN;
        b = i;
        break
    end
end
markers2.RWRB(~any(isnan(markers2.RWRB),2),:);

hold on
figure(1)
loc = 9;
if motion=='A'
    loc=7;
elseif motion=='B'
    loc=8;
elseif motion=='C'
    loc=9;
elseif motion=='D'
    loc=10;
elseif motion=='E'
    loc=11;
elseif motion=='F'
```

```
    loc=12;
end
subplot(2,6,loc)
x2 = linspace(0,100,b-a+1);
plot(x2,markers2.RWRB(a:b,3))
set(gca,'xtick',0:10:100)

output = markers2;

end
```

C.3 Untrimmed and trimmed data comparison

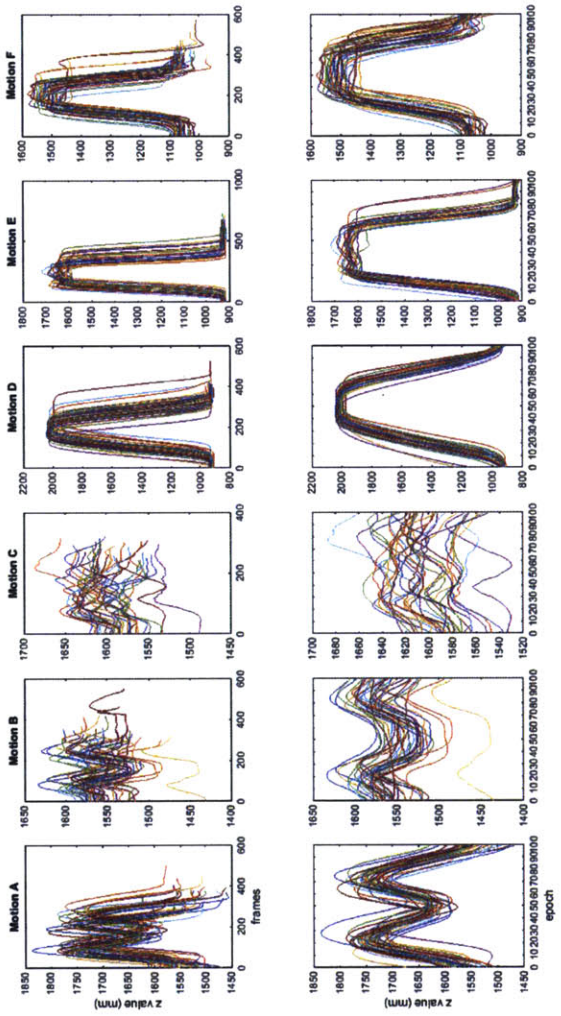

Figure C-1: One subject's RWRB marker z values during multiple repetitions of each motion before (top) and after (bottom) being trimmed. The bottom row axis is in percentage of total motion time, or epoch.

Appendix D

Initial Placement, Strap Configuration Analysis

D.1 Post-hoc Tukey Tests

D.2 Post-hoc Student-Newman-Keuls Tests

D.3 Levene's test for equality of variances

D.4 Levene's test graphs for all location comparisons

Table D.1: Tukey Post-hoc pairwise comparison tests for Location, Donning, and Motion during initial placement of IMU

		Distance		Orientation		Rotation	
Location(i)	Location(j)	Difference	p-Value	Difference	p-Value	Difference	p-Value
1	2	-0.037	0	0.044	0	0	0
1	3	-0.023	0	0.043	0	0	0
2	3	0.014	0	-0.001	0.837	0	0.554
Donning(i)	Donning(j)	Difference	p-Value	Difference	p-Value	Difference	p-Value
1	2	-0.007	0	-0.031	0	0	0
1	3	0.002	0.225	-0.025	0	-0.001	0
1	4	0.017	0	0.005	0.065	-0.001	0
1	5	0.002	0.458	-0.002	0.696	-0.001	0
2	3	0.01	0	0.006	0.007	0	0
2	4	0.024	0	0.036	0	0	0
2	5	0.009	0	0.028	0	0	0
3	4	0.014	0	0.029	0	0	0.984
3	5	0	0.995	0.022	0	0	1
4	5	-0.015	0	-0.007	0.002	0	0.984
Motion(i)	Motion(j)	Difference	p-Value	Difference	p-Value	Difference	p-Value
A	B	0.005	0	0.01	0	0	0
A	C	0.007	0	0.012	0	0	0.979
A	D	-0.012	0	0.049	0	-0.001	0
A	E	-0.013	0	0.048	0	0	0
A	F	-0.013	0	0.05	0	-0.001	0
B	C	0.001	0.94	0.003	0.675	0	0
B	D	-0.017	0	0.039	0	-0.001	0
B	E	-0.019	0	0.039	0	-0.001	0
B	F	-0.019	0	0.04	0	-0.001	0
C	D	-0.019	0	0.037	0	-0.001	0
C	E	-0.02	0	0.036	0	0	0
C	F	-0.02	0	0.037	0	-0.001	0
D	E	-0.001	0.933	-0.001	1	0	0
D	F	-0.001	0.941	0.001	1	0	0
E	F	0	1	0.001	0.99	-0.001	0

Table D.2: Student-Newman-Keuls Post-hoc tests for Location, Donning, and Motion during initial placement of IMU

Distance					Orientation					Rotation				
Sub-Group	LOCATION	Group Mean	Group Size	p-Value	Sub-Group	LOCATION	Group Mean	Group Size	p-Value	Sub-Group	LOCATION	Group Mean	Group Size	p-Value
1	1	0.021	26,427.00	1	1	2	0.008	25,286.00		1	1	0	22,824.00	1
2	3	0.044	26,619.00	1		3	0.009	22,215.00	0.559	2	2	0	21,564.00	
3	2	0.058	28,915.00	1	2	1	0.052	23,869.00	1		3	0	19,040.00	0.269
Sub-Group	DONNING	Group Mean	Group Size	p-Value	Sub-Group	DONNING	Group Mean	Group Size	p-Value	Sub-Group	DONNING	Group Mean	Group Size	p-Value
1	4	0.027	14,827.00	1	1	4	0.008	12,666.00	1	1	1	0	15,201.00	1
2	3	0.041	15,724.00		2	1	0.013	16,665.00		2	2	0	14,518.00	1
	5	0.042	15,050.00			5	0.015	12,598.00	0.193	3	5	0	10,828.00	
	1	0.044	18,167.00	0.095	3	3	0.037	13,466.00	1		3	0	11,854.00	
3	2	0.051	18,193.00	1	4	2	0.043	15,975.00	1		4	0	11,027.00	0.825
Sub-Group	MOTION	Group Mean	Group Size	p-Value	Sub-Group	MOTION	Group Mean	Group Size	p-Value	Sub-Group	MOTION	Group Mean	Group Size	p-Value
1	3	0.03	14,938.00		1	6	0.002	11,702.00		1	2	-0.001	11,830.00	1
	2	0.031	14,655.00	0.371		4	0.002	10,518.00		2	1	0	11,262.00	
2	1	0.036	13,380.00	1		5	0.003	10,823.00	0.8		3	0	11,779.00	0.483
3	4	0.048	12,264.00		2	3	0.039	13,514.00		3	5	0	9,358.00	1
	6	0.05	14,051.00			2	0.042	13,174.00	0.159	4	4	0	8,546.00	1
	5	0.05	12,673.00	0.57	3	1	0.051	11,639.00	1	5	6	0.001	10,653.00	1

Table D.3: Levene's test to determine which IMU Location varied most

	Distance			Orientation			Rotation		
LOCATION	Mean	Variance	p-Value	Mean	Variance	p-Value	Mean	Variance	p-Value
1	0.022	0.004	0	0.051	0.065	0	0	0	0
2	0.056	0.017		0.011	0.002		0	0	
1	0.022	0.004	0	0.051	0.065	0	0	0	0
3	0.044	0.012		0.009	0.004		0	0	
2	0.056	0.017	0	0.011	0.002	0	0	0	0.205
3	0.044	0.012		0.009	0.004		0	0	

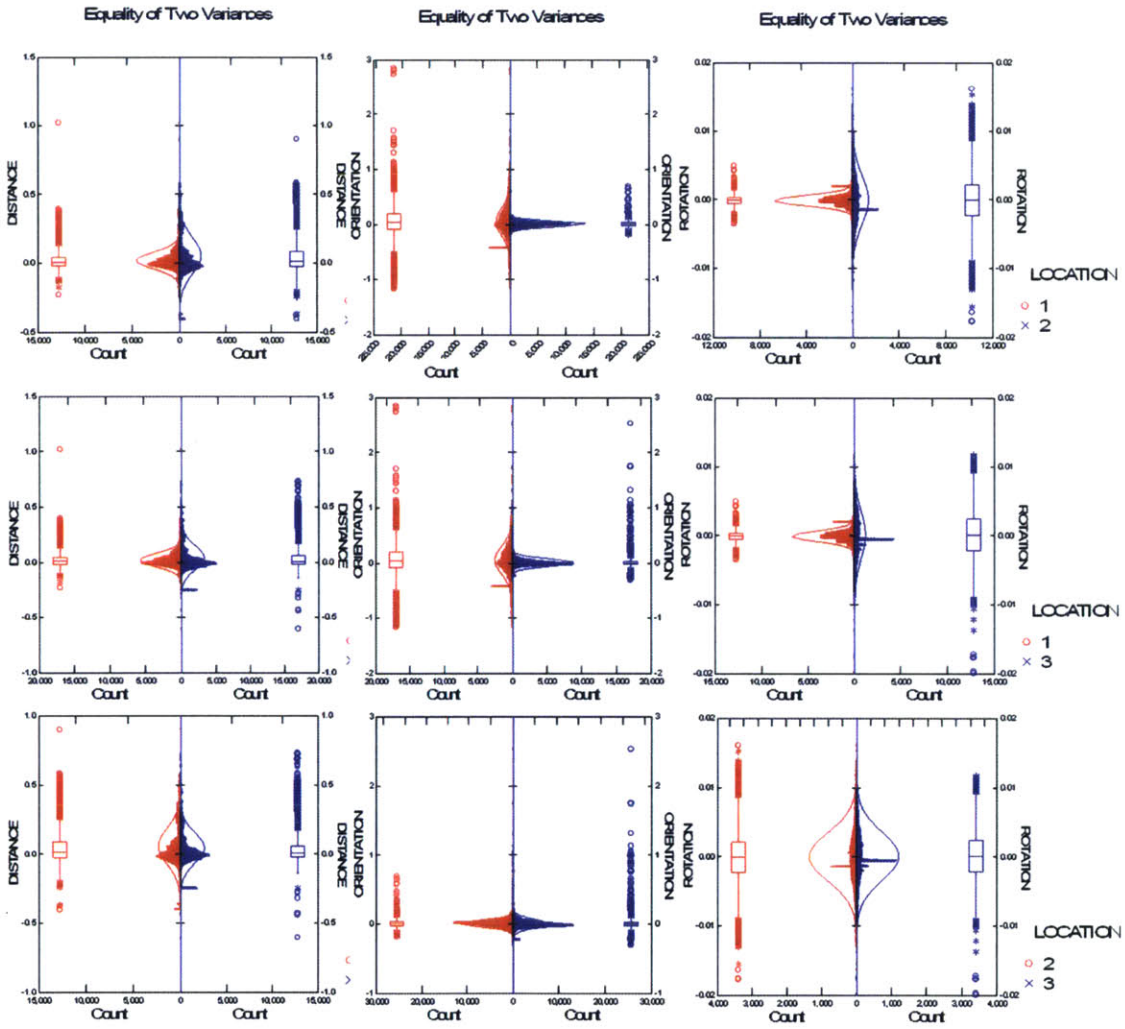

Figure D-1: Graphs showing comparisons of two variances for all combinations of IMU locations

Appendix E

Epochs, Strap Configuration Analysis

E.1 Conover-Inman Post-hoc tests for distance, orientation, and rotation for all motions

Table E.1: Motion A Conover-Inman post-hoc tests for distance. Red indicates p <0.0033

DISTANCE

IMU 1

0.0033	1	10	20	30	40	50	60	70	80	90	100
1											
10	0.418										
20	0.454	0.99									
30	0.007	0.035	0.042								
40	0.152	0.404	0.416	0.304							
50	0.996	0.566	0.585	0.031	0.249						
60	0.188	0.043	0.055	0	0.018	0.308					
70	0.885	0.359	0.393	0.006	0.132	0.911	0.252				
80	0.017	0.098	0.114	0.496	0.626	0.078	0.001	0.016			
90	0.922	0.507	0.539	0.011	0.191	0.946	0.178	0.817	0.03		
100	0.158	0.024	0.035	0	0.012	0.314	0.886	0.233	0	0.154	

IMU 2

0.0033	1	10	20	30	40	50	60	70	80	90	100
1											
10	0.304										
20	0.098	0.532									
30	0.045	0.316	0.695								
40	0.112	0.01	0.001	0							
50	0.388	0.065	0.014	0.006	0.489						
60	0.726	0.187	0.056	0.025	0.246	0.633					
70	0.715	0.506	0.196	0.098	0.051	0.224	0.487				
80	0.297	0.984	0.547	0.328	0.01	0.063	0.183	0.495			
90	0.019	0.182	0.473	0.751	0	0.002	0.01	0.046	0.191		
100	0	0	0.002	0.007	0	0	0	0	0	0.015	

IMU 3

0.0033	1	10	20	30	40	50	60	70	80	90	100
1											
10	0.297										
20	0.002	0.046									
30	0.002	0.053	0.845								
40	0.279	0.033	0	0							
50	0.095	0.573	0.126	0.151	0.005						
60	0	0.001	0.249	0.152	0	0.005					
70	0	0	0.001	0	0	0	0.037				
80	0	0	0.036	0.015	0	0	0.325	0.281			
90	0.539	0.684	0.018	0.02	0.094	0.326	0	0	0		
100	0	0	0	0	0.003	0	0	0	0	0	

Table E.2: Motion A Conover-Inman post-hoc tests for orientation. Red indicates p <0.0033

ORIENTATION

IMU 1

0.0033	1	10	20	30	40	50	60	70	80	90	100
1											
10	0.659										
20	0.112	0.043									
30	0	0	0.002								
40	0.001	0	0.042	0.413							
50	0	0	0.001	0.59	0.194						
60	0.001	0	0.085	0.172	0.645	0.066					
70	0.026	0.008	0.546	0.011	0.123	0.003	0.241				
80	0.936	0.624	0.159	0	0.002	0	0.003	0.046			
90	0.001	0	0.104	0.095	0.486	0.032	0.817	0.304	0.003		
100	0.004	0.012	0	0	0	0	0	0	0.005	0	

IMU 2

0.0033	1	10	20	30	40	50	60	70	80	90	100
1											
10	0.084										
20	0	0									
30	0	0	0.124								
40	0	0	0.58	0.038							
50	0	0	0.493	0.401	0.221						
60	0	0	0.724	0.068	0.858	0.315					
70	0	0.08	0.005	0	0.026	0.001	0.021				
80	0.599	0.236	0	0	0	0	0	0.003			
90	0	0	0	0	0	0	0	0	0		
100	0	0	0	0	0	0	0	0	0	0.025	

IMU 3

0.0033	1	10	20	30	40	50	60	70	80	90	100
1											
10	0.009										
20	0	0									
30	0	0	0								
40	0	0	0	0.41							
50	0	0	0	0.005	0						
60	0	0	0	0	0	0.276					
70	0	0	0	0.079	0.337	0	0				
80	0	0	0.03	0	0	0	0	0			
90	0	0.031	0	0	0	0	0	0	0.004		
100	0.188	0.238	0	0	0	0	0	0	0	0.001	

Table E.3: Motion A Conover-Inman post-hoc tests for rotation. Red indicates p <0.0033

ROTATION

IMU 1

0.0033	1	10	20	30	40	50	60	70	80	90	100
1											
10	0.391										
20	0.3	0.815									
30	0.059	0.216	0.315								
40	0	0	0	0.018							
50	0	0.001	0.002	0.054	0.73						
60	0	0.005	0.014	0.239	0.171	0.349					
70	0.036	0.192	0.312	0.871	0.004	0.021	0.121				
80	0.632	0.201	0.153	0.029	0	0	0	0.016			
90	0.001	0.009	0.025	0.382	0.068	0.18	0.679	0.216	0		
100	0.126	0.501	0.694	0.464	0	0.004	0.024	0.491	0.057	0.045	

IMU 2

0.0033	1	10	20	30	40	50	60	70	80	90	100
1											
10	0.734										
20	0	0									
30	0	0	0.002								
40	0	0	0	0.007							
50	0	0	0	0	0.006						
60	0	0	0	0	0.082	0.361					
70	0	0	0	0.78	0.011	0	0				
80	0.122	0.231	0.013	0	0	0	0	0			
90	0.001	0.004	0.467	0	0	0	0	0	0.086		
100	0	0.001	0.904	0.003	0	0	0	0.001	0.035	0.594	

IMU 3

0.0033	1	10	20	30	40	50	60	70	80	90	100
1											
10	0.982										
20	0.574	0.567									
30	0.005	0.005	0.032								
40	0.573	0.598	0.263	0							
50	0.003	0.004	0.023	0.877	0						
60	0.002	0.002	0.015	0.694	0	0.808					
70	0.094	0.097	0.29	0.28	0.022	0.223	0.158				
80	0.11	0.123	0.036	0	0.274	0	0	0.001			
90	0.729	0.75	0.379	0.002	0.853	0.001	0.001	0.05	0.228		
100	0.303	0.303	0.639	0.115	0.113	0.088	0.061	0.585	0.012	0.185	

Table E.4: Motion B Conover-Inman post-hoc tests for distance. Red indicates p <0.0033

DISTANCE

IMU 1

0.0033	1	10	20	30	40	50	60	70	80	90	100
1											
10	0.84										
20	0.195	0.271									
30	0.948	0.891	0.218								
40	0.655	0.806	0.392	0.703							
50	0.184	0.257	0.976	0.207	0.375						
60	0.846	0.693	0.14	0.796	0.525	0.132					
70	0.3	0.397	0.825	0.33	0.543	0.802	0.225				
80	0.637	0.785	0.415	0.684	0.976	0.397	0.51	0.567			
90	0.752	0.605	0.11	0.704	0.448	0.103	0.904	0.183	0.435		
100	0.754	0.608	0.113	0.706	0.452	0.106	0.905	0.186	0.439	1	

IMU 2

0.0033	1	10	20	30	40	50	60	70	80	90	100
1											
10	0.378										
20	0.1	0.45									
30	0.063	0.331	0.825								
40	0.679	0.206	0.045	0.027							
50	0.448	0.91	0.389	0.283	0.253						
60	0.001	0.013	0.076	0.121	0	0.01					
70	0.962	0.368	0.101	0.065	0.724	0.434	0.001				
80	0.68	0.637	0.217	0.148	0.416	0.724	0.003	0.655			
90	0.176	0.643	0.768	0.607	0.085	0.567	0.04	0.175	0.347		
100	0	0	0.001	0.002	0	0	0.145	0	0	0	

IMU 3

0.0033	1	10	20	30	40	50	60	70	80	90	100
1											
10	0.459										
20	0.38	0.103									
30	0.105	0.018	0.449								
40	0.002	0	0.022	0.122							
50	0	0	0	0.001	0.1						
60	0	0	0	0.003	0.13	0.94					
70	0.076	0.013	0.336	0.807	0.219	0.005	0.008				
80	0.328	0.087	0.902	0.537	0.034	0	0	0.409			
90	0.377	0.867	0.081	0.014	0	0	0	0.01	0.068		
100	0.005	0.034	0	0	0	0	0	0	0	0.057	

Table E.5: Motion B Conover-Inman post-hoc tests for orientation. Red indicates p <0.0033

ORIENTATION

IMU 1

0.0033	1	10	20	30	40	50	60	70	80	90	100
1											
10	0.117										
20	0.73	0.054									
30	0.459	0.409	0.276								
40	0.3	0.592	0.165	0.771							
50	0.003	0.144	0.001	0.023	0.046						
60	0.222	0.748	0.117	0.624	0.838	0.079					
70	0.096	0.884	0.045	0.345	0.506	0.205	0.649				
80	0.45	0.423	0.27	0.984	0.787	0.025	0.64	0.358			
90	0.207	0.778	0.108	0.596	0.807	0.086	0.968	0.677	0.612		
100	0	0	0	0	0	0	0	0	0	0	

IMU 2

0.0033	1	10	20	30	40	50	60	70	80	90	100
1											
10	0.447										
20	0.09	0.355									
30	0	0	0.001								
40	0	0	0.004	0.555							
50	0	0	0.002	0.689	0.848						
60	0	0	0	0.124	0.035	0.055					
70	0.005	0.044	0.275	0.02	0.08	0.053	0				
80	0.025	0.148	0.616	0.003	0.016	0.009	0	0.539			
90	0.004	0.04	0.263	0.019	0.078	0.051	0	0.991	0.526		
100	0	0	0.001	0.952	0.614	0.747	0.125	0.03	0.005	0.029	

IMU 3

0.0033	1	10	20	30	40	50	60	70	80	90	100
1											
10	0.007										
20	0.004	0.896									
30	0.092	0.296	0.234								
40	0.12	0.261	0.205	0.921							
50	0.359	0.086	0.062	0.475	0.545						
60	0.006	0.843	0.938	0.238	0.21	0.07					
70	0.283	0.13	0.097	0.596	0.67	0.867	0.105				
80	0.216	0	0	0.004	0.006	0.034	0	0.024			
90	0.026	0	0	0	0	0.002	0	0.001	0.312		
100	0.887	0.007	0.004	0.083	0.107	0.313	0.006	0.247	0.304	0.048	

Table E.6: Motion B Conover-Inman post-hoc tests for rotation. Red indicates p <0.0033

ROTATION

IMU 1

0.0033	1	10	20	30	40	50	60	70	80	90	100
1											
10	0.641										
20	0.53	0.871									
30	0.3	0.564	0.679								
40	0.37	0.665	0.788	0.884							
50	0.945	0.689	0.574	0.33	0.405						
60	0.208	0.42	0.518	0.813	0.703	0.231					
70	0.882	0.546	0.447	0.246	0.307	0.828	0.169				
80	0.052	0.135	0.184	0.36	0.287	0.059	0.504	0.041			
90	0.654	0.362	0.284	0.141	0.182	0.604	0.091	0.772	0.018		
100	0.503	0.829	0.954	0.729	0.838	0.544	0.566	0.424	0.214	0.27	

IMU 2

0.0033	1	10	20	30	40	50	60	70	80	90	100
1											
10	0.506										
20	0	0									
30	0	0	0								
40	0	0	0	0							
50	0	0	0	0	0.051						
60	0	0	0	0	0.843	0.102					
70	0	0	0.004	0.062	0	0	0				
80	0	0.001	0.362	0	0	0	0	0			
90	0.001	0.007	0.15	0	0	0	0	0	0.583		
100	0	0	0.014	0.037	0	0	0	0.769	0.001	0	

IMU 3

0.0033	1	10	20	30	40	50	60	70	80	90	100
1											
10	0										
20	0	0									
30	0	0	0								
40	0	0	0	0.407							
50	0	0	0	0.401	0.98						
60	0	0	0.479	0	0	0					
70	0	0.046	0.014	0	0	0	0.106				
80	0.002	0.115	0	0	0	0	0	0			
90	0.277	0	0	0	0	0	0	0	0.046		
100	0.426	0	0	0	0	0	0	0	0.027	0.799	

Table E.7: Motion C Conover-Inman post-hoc tests for distance. Red indicates p <0.0033

DISTANCE

IMU 1

0.0033	1	10	20	30	40	50	60	70	80	90	100
1											
10	0.399										
20	0.154	0.561									
30	0.17	0.58	0.995								
40	0.384	0.078	0.017	0.022							
50	0.891	0.48	0.197	0.215	0.31						
60	0.007	0.05	0.145	0.157	0	0.009					
70	0.525	0.866	0.471	0.489	0.134	0.614	0.043				
80	0.27	0.766	0.8	0.812	0.046	0.331	0.107	0.655			
90	0.262	0.774	0.774	0.787	0.041	0.323	0.091	0.659	0.983		
100	0.394	0.979	0.589	0.606	0.08	0.472	0.057	0.849	0.79	0.799	

IMU 2

0.0033	1	10	20	30	40	50	60	70	80	90	100
1											
10	0.26										
20	0.608	0.552									
30	0.948	0.301	0.661								
40	0.046	0.373	0.145	0.06							
50	0.002	0.053	0.013	0.004	0.307						
60	0	0	0	0	0.007	0.087					
70	0.003	0.058	0.015	0.004	0.315	0.995	0.095				
80	0.017	0.199	0.065	0.023	0.701	0.523	0.02	0.529			
90	0	0.003	0.001	0	0.044	0.309	0.479	0.323	0.1		
100	0	0	0	0	0	0	0.002	0	0	0	

IMU 3

0.0033	1	10	20	30	40	50	60	70	80	90	100
1											
10	0.989										
20	0	0									
30	0.027	0.023	0.102								
40	0.001	0.001	0.623	0.288							
50	0.233	0.226	0.01	0.333	0.049						
60	0.001	0.001	0.74	0.238	0.889	0.039					
70	0.025	0.022	0.132	0.939	0.337	0.309	0.282				
80	0.032	0.029	0.108	0.983	0.291	0.356	0.242	0.924			
90	0.254	0.247	0.011	0.327	0.05	0.976	0.04	0.304	0.349		
100	0.077	0.065	0	0	0	0.003	0	0	0	0.004	

Table E.8: Motion C Conover-Inman post-hoc tests for orientation. Red indicates p <0.0033

ORIENTATION

IMU 1

0.0033	1	10	20	30	40	50	60	70	80	90	100
1											
10	0.129										
20	0.881	0.08									
30	0.032	0.507	0.016								
40	0.814	0.187	0.688	0.049							
50	0.588	0.332	0.472	0.108	0.75						
60	0.598	0.347	0.485	0.119	0.756	0.998					
70	0.126	0.927	0.081	0.591	0.18	0.312	0.326				
80	0.006	0.192	0.003	0.514	0.01	0.027	0.032	0.25			
90	0.19	0.831	0.125	0.382	0.269	0.446	0.461	0.769	0.131		
100	0	0	0	0.001	0	0	0	0	0.009	0	

IMU 2

0.0033	1	10	20	30	40	50	60	70	80	90	100
1											
10	0.125										
20	0.761	0.068									
30	0.296	0.011	0.462								
40	0.911	0.1	0.847	0.351							
50	0.17	0.871	0.096	0.017	0.138						
60	0.564	0.352	0.383	0.11	0.492	0.441					
70	0.745	0.065	0.984	0.474	0.831	0.092	0.372				
80	0.918	0.151	0.684	0.251	0.83	0.203	0.632	0.669			
90	0.001	0.091	0.001	0	0.001	0.064	0.01	0	0.002		
100	0	0	0	0	0	0	0	0	0	0	

IMU 3

0.0033	1	10	20	30	40	50	60	70	80	90	100
1											
10	0.536										
20	0.024	0.003									
30	0.029	0.004	0.988								
40	0	0	0.136	0.155							
50	0.977	0.521	0.028	0.033	0.001						
60	0.116	0.026	0.59	0.594	0.06	0.127					
70	0.59	0.948	0.005	0.006	0	0.574	0.036				
80	0	0.001	0	0	0	0	0	0.001			
90	0	0	0	0	0	0	0	0	0.652		
100	0.545	0.198	0.076	0.087	0.002	0.571	0.281	0.238	0	0	

Table E.9: Motion C Conover-Inman post-hoc tests for rotation. Red indicates p <0.0033

ROTATION

IMU 1

0.0033	1	10	20	30	40	50	60	70	80	90	100
1											
10	0.811										
20	0.005	0.008									
30	0.06	0.029	0								
40	0.705	0.886	0.012	0.02							
50	0.945	0.756	0.004	0.068	0.652						
60	0.322	0.211	0	0.405	0.166	0.353					
70	0.93	0.747	0.005	0.081	0.647	0.983	0.378				
80	0.581	0.742	0.027	0.015	0.848	0.534	0.129	0.533			
90	0.493	0.646	0.029	0.009	0.752	0.447	0.092	0.449	0.91		
100	0.814	1	0.009	0.033	0.889	0.76	0.22	0.751	0.747	0.654	

IMU 2

0.0033	1	10	20	30	40	50	60	70	80	90	100
1											
10	0.323										
20	0	0									
30	0	0	0.136								
40	0	0	0.318	0.604							
50	0	0	0.624	0.045	0.13						
60	0.039	0.002	0.014	0	0.001	0.044					
70	0.038	0.002	0.014	0	0.001	0.044	0.993				
80	0.987	0.329	0	0	0	0	0.036	0.035			
90	0.115	0.548	0	0	0	0	0	0	0.117		
100	0	0.008	0	0	0	0	0	0	0	0.039	

IMU 3

0.0033	1	10	20	30	40	50	60	70	80	90	100
1											
10	0										
20	0	0									
30	0	0	0.403								
40	0	0	0.026	0.176							
50	0	0	0.011	0.091	0.723						
60	0	0	0	0.004	0.121	0.239					
70	0	0	0.422	0.993	0.185	0.098	0.005				
80	0	0.231	0	0	0	0	0	0			
90	0.224	0.012	0	0	0	0	0	0	0		
100	0	0.329	0	0	0	0	0	0	0.768	0	

Table E.10: Motion D Conover-Inman post-hoc tests for distance. Red indicates p <0.0033

DISTANCE

IMU 1

0.0033	1	10	20	30	40	50	60	70	80	90	100
1											
10	0.335										
20	0.127	0.013									
30	0	0	0.029								
40	0	0	0	0.003							
50	0	0	0	0	0.179						
60	0	0	0	0	0.008	0.245					
70	0	0	0	0	0.405	0.504	0.037				
80	0	0	0	0.164	0.055	0.001	0	0.001			
90	0.128	0.013	0.99	0.027	0	0	0	0	0		
100	0.291	0.045	0.64	0.009	0	0	0	0	0	0.647	

IMU 2

0.0033	1	10	20	30	40	50	60	70	80	90	100
1											
10	0										
20	0	0									
30	0	0	0								
40	0	0	0	0							
50	0	0	0	0	0.883						
60	0	0	0	0.54	0	0					
70	0	0	0.242	0	0	0	0.002				
80	0	0	0.752	0	0	0	0	0.173			
90	0	0.417	0	0	0	0	0	0	0.002		
100	1	0	0	0	0	0	0	0	0	0	

IMU 3

0.0033	1	10	20	30	40	50	60	70	80	90	100
1											
10	0										
20	0.022	0									
30	0.055	0	0.644								
40	0	0.093	0	0							
50	0	0.287	0	0	0.55						
60	0.363	0	0	0.001	0	0					
70	0	0.32	0	0	0.467	0.915	0				
80	0	0	0	0	0.033	0.009	0	0.006			
90	0	0.813	0.007	0.003	0.086	0.239	0	0.265	0.001		
100	0.04	0.004	0.928	0.656	0	0	0.001	0	0	0.021	

Table E.11: Motion D Conover-Inman post-hoc tests for orientation. Red indicates p <0.0033

ORIENTATION

IMU 1

0.0033	1	10	20	30	40	50	60	70	80	90	100
1											
10	0.775										
20	0	0									
30	0	0	0.698								
40	0.062	0.038	0.129	0.077							
50	0.001	0	0.979	0.787	0.205						
60	0	0	0.002	0.008	0	0.015					
70	0	0	0	0	0	0	0.107				
80	0	0	0.063	0.17	0.003	0.173	0.137	0.001			
90	0.001	0	0.229	0.128	0.551	0.359	0	0	0.002		
100	0.034	0.017	0.022	0.011	0.809	0.085	0	0	0	0.274	

IMU 2

0.0033	1	10	20	30	40	50	60	70	80	90	100
1											
10	0.02										
20	0	0									
30	0	0	0								
40	0	0	0	0.005							
50	0	0	0	0	0.39						
60	0	0	0	0.026	0	0					
70	0.003	0.093	0	0	0	0	0				
80	0.706	0.075	0	0	0	0	0	0.008			
90	0.001	0	0.203	0	0	0	0	0	0		
100	0	0	1	0	0	0	0	0	0	0.17	

IMU 3

0.0033	1	10	20	30	40	50	60	70	80	90	100
1											
10	0.28										
20	0.393	0.653									
30	0.509	0.036	0.029								
40	0.073	0.446	0.169	0.003							
50	0.472	0.7	0.987	0.103	0.251						
60	0.422	0.037	0.038	0.791	0.004	0.094					
70	0	0.003	0	0	0.023	0.001	0				
80	0.168	0.632	0.371	0.028	0.876	0.423	0.027	0.043			
90	0.004	0	0	0.004	0	0	0.015	0	0		
100	0.915	0.195	0.267	0.543	0.038	0.368	0.445	0	0.117	0.003	

Table E.12: Motion D Conover-Inman post-hoc tests for rotation. Red indicates p <0.0033

ROTATION

IMU 1

0.0033	1	10	20	30	40	50	60	70	80	90	100
1											
10	0.573										
20	0.435	0.825									
30	0.109	0.283	0.39								
40	0	0	0	0							
50	0	0	0	0	0.32						
60	0	0	0	0	0.72	0.479					
70	0	0	0	0	0.008	0	0.001				
80	0.808	0.43	0.317	0.073	0	0	0	0			
90	0.776	0.782	0.62	0.183	0	0	0	0	0.605		
100	0.163	0.405	0.544	0.772	0	0	0	0	0.11	0.268	

IMU 2

0.0033	1	10	20	30	40	50	60	70	80	90	100
1											
10	0.164										
20	0	0									
30	0.001	0	0.001								
40	0.022	0	0	0.234							
50	0.094	0.001	0	0.053	0.472						
60	0.006	0	0.001	0.724	0.473	0.171					
70	0.644	0.694	0	0.005	0.042	0.113	0.015				
80	0.049	0.373	0	0	0	0	0	0.358			
90	0	0	0	0	0	0	0	0.007	0.014		
100	0.01	0	0	0.222	0.941	0.384	0.482	0.031	0	0	

IMU 3

0.0033	1	10	20	30	40	50	60	70	80	90	100
1											
10	0										
20	0	0.037									
30	0	0.484	0.079								
40	0	0	0	0							
50	0	0	0	0	0.188						
60	0	0.63	0.005	0.189	0	0					
70	0	0.219	0.492	0.467	0	0	0.075				
80	0	0.168	0.929	0.329	0	0.004	0.069	0.698			
90	0	0.79	0.038	0.371	0	0	0.883	0.176	0.136		
100	0.105	0.001	0	0	0	0	0.003	0	0	0.008	

Table E.13: Motion E Conover-Inman post-hoc tests for distance. Red indicates p <0.0033

DISTANCE

IMU 1

0.0033	1	10	20	30	40	50	60	70	80	90	100
1											
10	0.02										
20	0	0									
30	0	0	0.147								
40	0	0	0.14	0.996							
50	0	0	0.048	0.614	0.603						
60	0	0	0.187	0.857	0.858	0.48					
70	0	0.018	0.109	0.001	0.001	0	0.002				
80	0.23	0.247	0	0	0	0	0	0			
90	0.14	0.382	0	0	0	0	0	0.001	0.776		
100	0.349	0.16	0	0	0	0	0	0	0.796	0.589	

IMU 2

0.0033	1	10	20	30	40	50	60	70	80	90	100
1											
10	0.175										
20	0	0									
30	0	0	0								
40	0	0	0	0.906							
50	0	0	0	0	0						
60	0	0	0.003	0.359	0.377	0.091					
70	0	0	0.193	0.027	0.024	0	0.047				
80	0	0.002	0	0	0	0	0	0			
90	0.021	0	0	0	0	0	0	0	0		
100	0	0	0	0	0	0	0	0	0	0	

IMU 3

0.0033	1	10	20	30	40	50	60	70	80	90	100
1											
10	0.6										
20	0.093	0.027									
30	0	0	0								
40	0	0	0	0.001							
50	0	0	0	0	0.005						
60	0	0	0	0	0	0.462					
70	0.001	0	0.042	0.07	0	0	0				
80	0	0	0	0	0	0	0	0			
90	0	0	0	0	0	0	0	0	0.277		
100	0	0.001	0	0	0	0	0	0	0.003	0.043	

Table E.14: Motion E Conover-Inman post-hoc tests for orientation. Red indicates p <0.0033

ORIENTATION

IMU 1

0.0033	1	10	20	30	40	50	60	70	80	90	100
1											
10	0.124										
20	0.056	0.645									
30	0.001	0.094	0.258								
40	0	0.008	0.041	0.361							
50	0	0	0	0	0.001						
60	0	0	0	0	0	0.07					
70	0	0	0	0	0	0.543	0.222				
80	0	0.004	0.025	0.281	0.892	0.001	0	0			
90	0	0.032	0.124	0.719	0.551	0	0	0	0.447		
100	0.02	0.451	0.812	0.329	0.05	0	0	0	0.029	0.157	

IMU 2

0.0033	1	10	20	30	40	50	60	70	80	90	100
1											
10	0										
20	0	0									
30	0	0	0								
40	0	0	0	0.001							
50	0	0	0.02	0.007	0.441						
60	0	0	0	0.005	0	0					
70	0.024	0.078	0	0	0	0	0				
80	0.023	0.002	0	0	0	0	0	0.613			
90	0.027	0	0	0	0	0	0	0.415	0.718		
100	0.002	0.001	0	0	0	0	0	0.703	0.818	0.479	

IMU 3

0.0033	1	10	20	30	40	50	60	70	80	90	100
1											
10	0.04										
20	0	0.023									
30	0.001	0.4	0.043								
40	0.006	0.818	0.008	0.411							
50	0.001	0.295	0.21	0.681	0.298						
60	0.548	0.115	0	0.003	0.027	0.004					
70	0	0	0	0	0	0	0				
80	0.002	0	0	0	0	0	0	0.703			
90	0	0.102	0.775	0.233	0.088	0.457	0.001	0	0		
100	0.197	0.48	0.003	0.093	0.289	0.076	0.434	0	0	0.022	

Table E.15: Motion E Conover-Inman post-hoc tests for rotation. Red indicates p <0.0033

ROTATION

IMU 1

0.0033	1	10	20	30	40	50	60	70	80	90	100
1											
10	0										
20	0	0.417									
30	0	0	0								
40	0	0	0.001	0.478							
50	0	0.015	0.136	0.012	0.066						
60	0	0.006	0.074	0.026	0.123	0.761					
70	0	0.636	0.209	0	0	0.004	0.001				
80	0.001	0.312	0.076	0	0	0	0	0.596			
90	0	0.763	0.268	0	0	0.005	0.002	0.858	0.47		
100	0.535	0	0	0	0	0	0	0	0	0	

IMU 2

0.0033	1	10	20	30	40	50	60	70	80	90	100
1											
10	0										
20	0.003	0									
30	0	0	0								
40	0	0	0	0							
50	0	0	0	0.015	0.942						
60	0.341	0.001	0.043	0.417	0.051	0.064					
70	0	0	0	0.27	0.426	0.473	0.193				
80	0.241	0	0.254	0	0	0	0.148	0			
90	0	0.201	0	0	0	0	0	0	0		
100	0	0.35	0	0	0	0	0	0	0	0.681	

IMU 3

0.0033	1	10	20	30	40	50	60	70	80	90	100
1											
10	0.484										
20	0	0									
30	0	0	0.012								
40	0	0	0	0.001							
50	0	0	0	0	0.157						
60	0	0	0	0.081	0.402	0.048					
70	0	0	0	0	0.007	0.23	0.002				
80	0	0	0	0	0.048	0.431	0.016	0.811			
90	0.011	0.002	0.022	0	0	0	0	0	0		
100	0	0	0.829	0.031	0	0	0.001	0	0	0.073	

Table E.16: Motion F Conover-Inman post-hoc tests for distance. Red indicates p <0.0033

DISTANCE

IMU 1

0.0033	1	10	20	30	40	50	60	70	80	90	100
1											
10	0.752										
20	0.876	0.632									
30	0.028	0.055	0.018								
40	0	0	0	0							
50	0	0	0	0	0.459						
60	0	0	0	0.004	0.21	0.041					
70	0.001	0.003	0.001	0.38	0.001	0	0.037				
80	0.027	0.055	0.017	0.913	0	0	0.002	0.296			
90	0.716	0.961	0.598	0.061	0	0	0	0.004	0.061		
100	0.133	0.064	0.174	0	0	0	0	0	0	0.057	

IMU 2

0.0033	1	10	20	30	40	50	60	70	80	90	100
1											
10	0.036										
20	0	0.039									
30	0	0	0								
40	0	0	0.16	0.002							
50	0	0	0.016	0.049	0.2						
60	0	0	0	0.69	0.008	0.13					
70	0.344	0.386	0.009	0	0	0	0				
80	0.476	0.273	0.005	0	0	0	0	0.836			
90	0.043	0.927	0.032	0	0	0	0	0.427	0.305		
100	0.006	0.587	0.093	0	0	0	0	0.173	0.109	0.52	

IMU 3

0.0033	1	10	20	30	40	50	60	70	80	90	100
1											
10	0										
20	0	0.016									
30	0.019	0	0.028								
40	0.019	0	0	0							
50	0.01	0	0	0	0.796						
60	0.722	0	0	0.019	0.001	0					
70	0.008	0	0.035	0.825	0	0	0.007				
80	0	0.221	0.286	0.002	0	0	0	0.002			
90	0	0.383	0.002	0	0	0	0	0	0.05		
100	0	0.106	0.644	0.019	0	0	0	0.023	0.627	0.023	

Table E.17: Motion F Conover-Inman post-hoc tests for orientation. Red indicates p <0.0033

ORIENTATION

IMU 1

0.0033	1	10	20	30	40	50	60	70	80	90	100
1											
10	0.995										
20	0.044	0.041									
30	0	0	0.009								
40	0	0	0.012	0.991							
50	0	0	0.078	0.455	0.474						
60	0	0	0	0.021	0.024	0.002					
70	0	0	0	0	0	0	0.012				
80	0	0	0	0.141	0.15	0.026	0.354	0			
90	0	0	0.003	0.873	0.867	0.342	0.021	0	0.159		
100	0.013	0.012	0.684	0.021	0.026	0.148	0	0	0	0.007	

IMU 2

0.0033	1	10	20	30	40	50	60	70	80	90	100
1											
10	0.93										
20	0.758	0.709									
30	0	0	0								
40	0	0	0	0							
50	0	0	0	0	0.357						
60	0	0	0	0	0	0					
70	0.69	0.751	0.543	0	0	0	0				
80	0.001	0.001	0.01	0	0	0	0	0.001			
90	0	0	0.01	0	0	0	0	0	0.771		
100	0.971	0.901	0.777	0	0	0	0	0.664	0.001	0	

IMU 3

0.0033	1	10	20	30	40	50	60	70	80	90	100
1											
10	0										
20	0	0									
30	0	0	0.742								
40	0	0.027	0	0							
50	0	0.001	0	0	0.243						
60	0	0.034	0.063	0.128	0	0					
70	0	0	0.386	0.226	0	0	0.005				
80	0	0	0.285	0.169	0	0	0.005	0.756			
90	0	0.378	0	0	0.27	0.033	0.005	0	0		
100	0	0.387	0	0	0.309	0.047	0.007	0	0	0.979	

Table E.18: Motion F Conover-Inman post-hoc tests for rotation. Red indicates p <0.0033

ROTATION

IMU 1

0.0033	1	10	20	30	40	50	60	70	80	90	100
1											
10	0.407										
20	0	0.003									
30	0.002	0.021	0.676								
40	0.004	0.031	0.627	0.94							
50	0	0.002	0.646	0.415	0.385						
60	0.039	0.2	0.126	0.305	0.358	0.065					
70	0.73	0.241	0	0.001	0.001	0	0.017				
80	0.606	0.759	0.001	0.01	0.016	0.001	0.119	0.391			
90	0.674	0.206	0	0.001	0.001	0	0.013	0.945	0.346		
100	0.004	0.04	0.328	0.636	0.708	0.176	0.519	0.001	0.019	0.001	

IMU 2

0.0033	1	10	20	30	40	50	60	70	80	90	100
1											
10	0.855										
20	0.571	0.678									
30	0	0	0								
40	0	0	0	0							
50	0	0	0	0	0.689						
60	0	0	0	0	0.379	0.221					
70	0	0	0	0	0	0	0				
80	0	0	0.006	0	0	0	0	0.081			
90	0.183	0.261	0.629	0	0	0	0	0	0.005		
100	0.22	0.31	0.704	0	0	0	0	0	0.003	0.887	

IMU 3

0.0033	1	10	20	30	40	50	60	70	80	90	100
1											
10	0.116										
20	0	0									
30	0	0	0								
40	0	0	0.415	0							
50	0	0	0.002	0.001	0.022						
60	0	0	0	0.173	0	0					
70	0	0	0	0.75	0	0.001	0.077				
80	0	0	0.318	0	0.073	0	0	0			
90	0.752	0.192	0	0	0	0	0	0	0		
100	0	0	0.913	0	0.559	0.013	0	0	0.33	0	

Appendix F

Effect size

F.1 Dependent variable and IMU individual subject ranges by location

Table F.1: Dependent variable individual subject ranges

	IMU 1			IMU 2			IMU 3		
Subject	distance (mm)	orientation (deg)	rotation (deg)	distance (mm)	orientation (deg)	rotation (deg)	distance (mm)	orientation (deg)	rotation (deg)
1	17.05	28.15	48.15	33.17	11.98	36.28	28.60	119.85	55.05
2	4.36	2.44	42.68	92.79	49.20	24.69	48.56	17.40	2.98
3	64.97	44.81	122.88	149.27	25.57	65.22	73.21	20.77	52.84
4	4.50	13.42	28.66	5.13	9.22	14.59	7.01	21.92	22.85
5	0.00	0.00	0.00	0.00	0.00	0.00	0.00	0.00	0.00
6	22.51	7.93	19.92	53.58	14.30	9.15	49.03	5.17	15.91
7	3.93	7.03	11.37	75.73	8.22	6.00	52.03	2.08	1.06
8	29.02	1.44	44.76	87.60	2.11	37.08	86.62	0.44	16.71
9	45.64	0.53	90.72	194.31	9.92	10.60	114.68	13.17	16.50
10	28.28	3.38	58.72	125.98	7.67	41.20	86.46	2.55	22.89
11	14.33	24.24	25.33	10.09	9.97	26.67	6.39	8.69	49.03
12	12.95	15.06	1.48	85.40	0.76	4.04	68.03	0.41	19.88
13	25.98	8.05	65.73	157.95	10.20	61.89	143.00	7.69	35.77
14	12.90	11.60	6.52	27.03	5.63	50.87	12.96	83.18	99.57
15	44.53	8.38	88.94	118.06	3.66	45.71	67.69	6.00	51.03
16	15.99	6.42	116.15	210.48	20.17	52.01	112.01	5.22	31.37
17	35.65	11.11	73.62	200.46	21.21	7.07	132.40	2.46	30.73
18	15.61	2.97	33.17	81.11	10.09	3.01	33.86	2.84	1.10
19	5.72	10.63	18.49	166.86	17.15	26.05	109.20	4.51	33.46
20	9.26	10.64	73.13	129.70	9.49	8.57	87.94	23.64	26.73
21	77.87	22.02	93.37	116.71	28.31	73.97	77.99	19.44	69.66
22	4.16	13.21	16.68	22.79	6.61	19.33	66.97	17.33	45.89

Table F.2: Euler angle individual subject ranges

	IMU1			IMU2			IMU 3		
Subject	Roll (deg)	Pitch (deg)	Yaw (deg)	Roll (deg)	Pitch(deg)	Yaw(deg)	Roll (deg)	Pitch(deg)	Yaw(deg)
1	128.95	10.01	347.60	144.71	69.30	166.51	121.47	86.14	292.39
2	35.78	41.31	359.42	289.36	99.98	275.92	142.31	113.36	352.53
3	63.07	27.84	111.96	276.62	96.08	355.31	211.33	119.39	358.31
4	359.25	24.52	330.39	219.99	144.88	324.36	347.48	175.75	343.60
5	19.97	41.21	47.21	179.10	134.16	261.86	113.40	90.89	301.45
6	359.13	23.37	359.86	249.62	99.85	242.86	346.03	104.65	358.25
7	48.40	48.27	359.74	242.61	106.82	358.92	357.75	112.17	290.53
8	92.51	29.89	358.73	202.81	97.71	175.72	120.04	91.29	349.36
9	55.60	45.51	359.41	225.42	117.22	186.85	111.82	119.79	355.27
10	356.10	21.35	358.14	229.39	101.60	206.23	204.83	108.31	340.20
11	80.02	35.37	358.19	207.79	86.99	358.77	132.62	142.94	358.93
12	42.05	47.52	351.13	220.07	88.75	153.42	144.89	101.83	329.54
13	352.33	27.34	341.87	238.46	107.12	233.75	342.51	134.76	305.82
14	355.06	45.43	357.26	248.29	97.98	337.85	202.10	98.62	350.61
15	42.10	47.97	356.96	178.07	94.64	197.85	141.83	93.25	357.00
16	45.73	52.97	348.17	344.93	98.61	353.77	154.06	109.91	308.64
17	314.28	59.53	351.91	275.79	106.24	224.10	357.18	108.77	358.11
18	233.19	57.39	359.05	345.29	94.04	354.10	149.68	114.70	326.98
19	258.09	21.36	352.77	319.24	90.87	359.42	168.24	97.76	356.62
20	343.63	22.54	354.26	216.00	98.13	187.04	218.01	87.79	333.74
21	338.74	58.45	353.43	184.96	108.39	246.77	346.63	125.02	357.56
22	66.95	24.56	356.40	350.53	94.24	349.81	155.54	98.01	347.76

Table F.3: Mean and standard deviation of ranges of values for roll, pitch, and yaw of all subjects within each IMU location grouped by motion

Motion	IMU	Roll (X)		Pitch (Y)		Yaw (Z)	
		Mean	SD	Mean	SD	Mean	SD
A	1	9.08	7.13	5.40	3.29	48.55	41.31
	2	29.06	35.44	12.18	6.23	22.28	17.66
	3	4.36	7.04	29.98	28.56	3.89	3.81
B	1	8.29	2.97	5.82	1.36	32.04	17.41
	2	20.02	22.31	10.26	6.63	25.29	23.78
	3	20.69	23.48	19.24	24.86	21.64	13.96
C	1	7.68	1.87	8.15	4.59	14.33	16.98
	2	20.40	26.35	9.20	6.68	13.73	6.34
	3	21.79	23.92	8.86	4.27	13.73	10.66
D	1	13.38	13.73	6.36	6.16	24.09	25.14
	2	43.34	7.60	26.61	21.28	7.49	4.55
	3	55.70	41.67	26.55	36.15	26.35	15.26
E	1	10.35	8.31	6.17	5.60	21.97	18.17
	2	98.64	45.11	28.35	29.74	99.66	25.72
	3	20.53	13.01	30.86	30.80	15.64	24.07
F	1	30.07	33.78	9.30	2.42	44.19	29.78
	2	23.52	13.64	16.67	8.59	6.27	8.19
	3	29.51	20.60	29.02	25.20	63.63	40.66

Appendix G

Mean and standard deviation Values for Euler Axes

Figure G-1: Euler axes (Yaw, Pitch, Roll) mean and standard deviation values for IMU 1 for multiple donnings of Motion A.

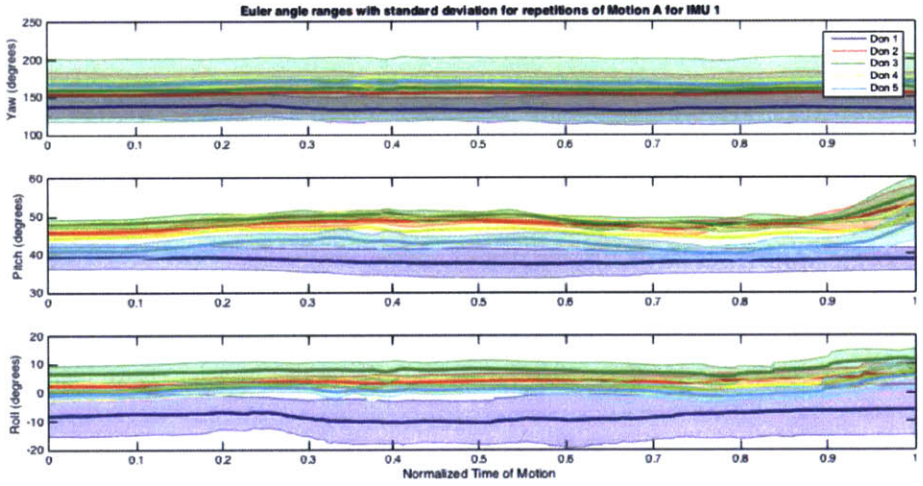

Figure G-2: Euler axes (Yaw, Pitch, Roll) mean and standard deviation values for IMU 2 for multiple donnings of Motion A.

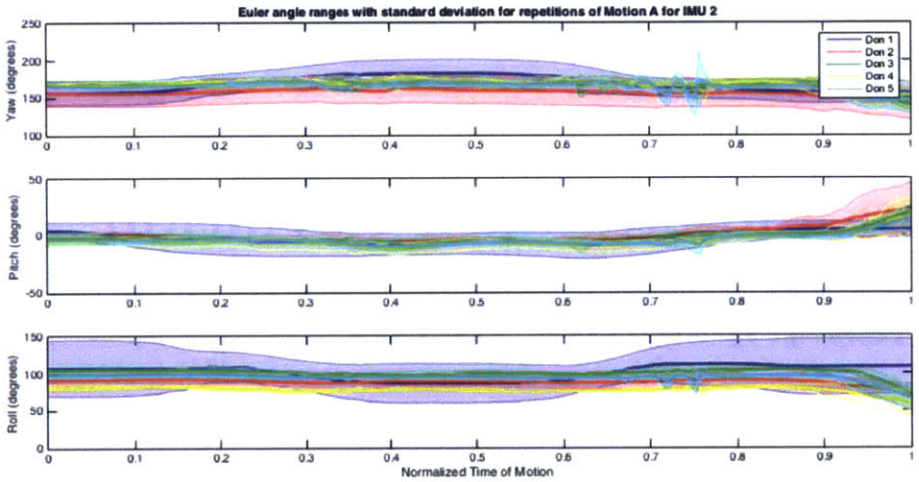

Figure G-3: Euler axes (Yaw, Pitch, Roll) mean and standard deviation values for IMU 3 for multiple donnings of Motion A.

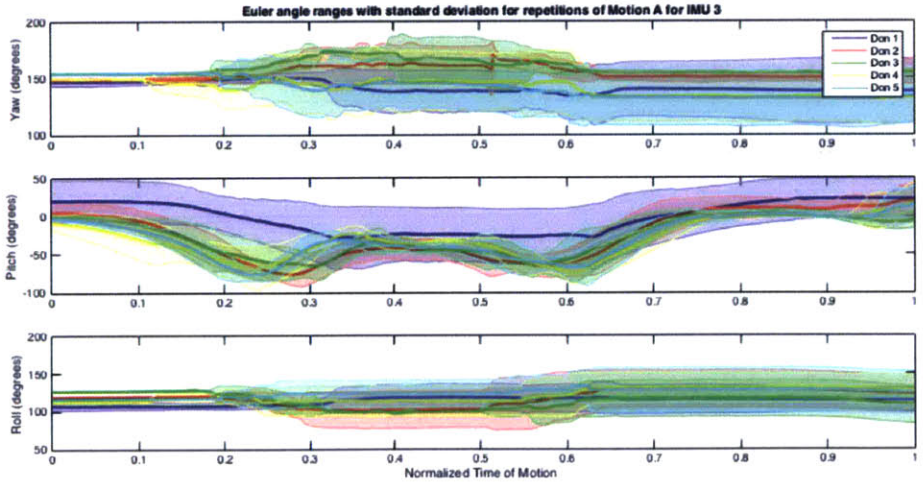

Figure G-4: Euler axes (Yaw, Pitch, Roll) mean and standard deviation values for IMU 1 for multiple donnings of Motion B.

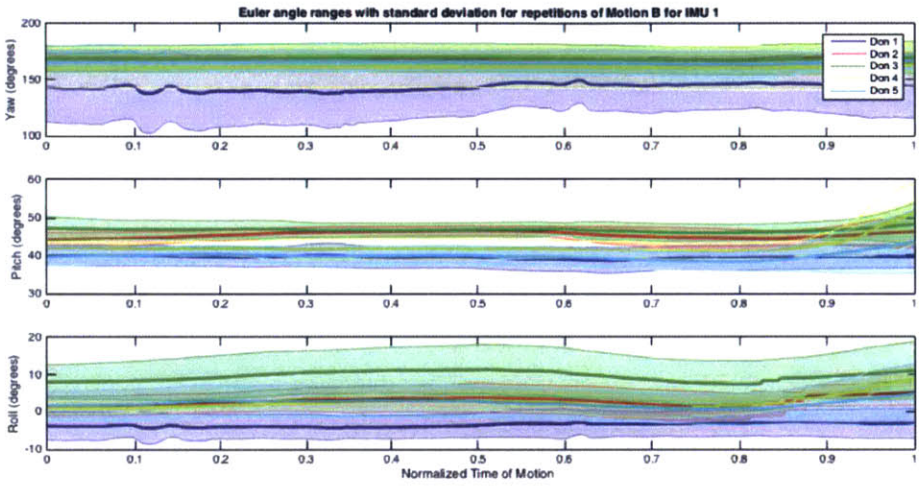

Figure G-5: Euler axes (Yaw, Pitch, Roll) mean and standard deviation values for IMU 2 for multiple donnings of Motion B.

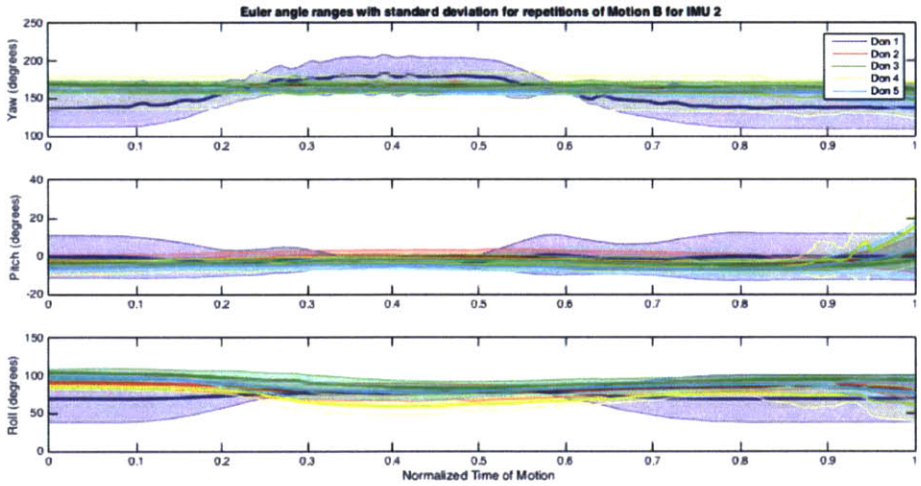

Figure G-6: Euler axes (Yaw, Pitch, Roll) mean and standard deviation values for IMU 3 for multiple donnings of Motion B.

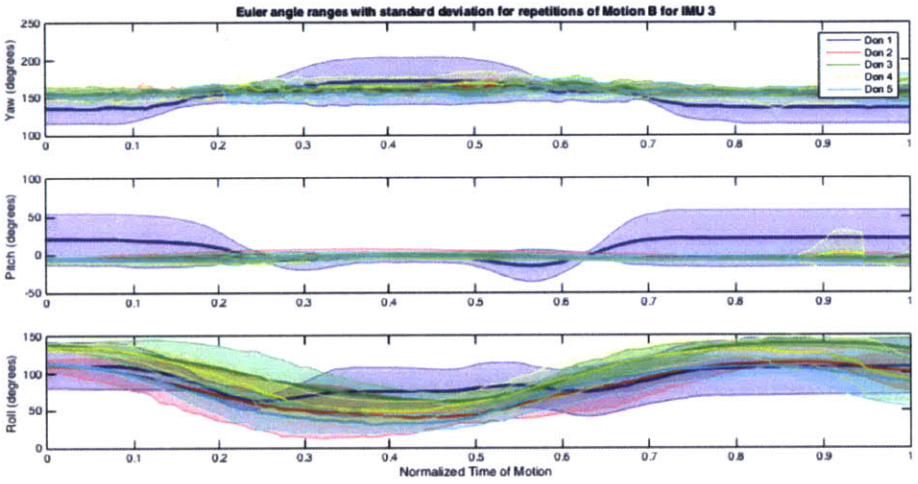

Figure G-7: Euler axes (Yaw, Pitch, Roll) mean and standard deviation values for IMU 1 for multiple donnings of Motion C.

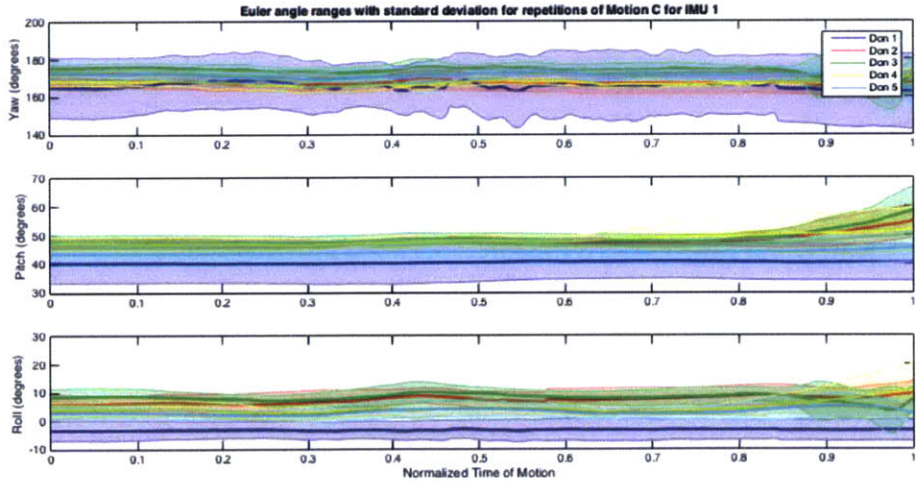

Figure G-8: Euler axes (Yaw, Pitch, Roll) mean and standard deviation values for IMU 2 for multiple donnings of Motion C.

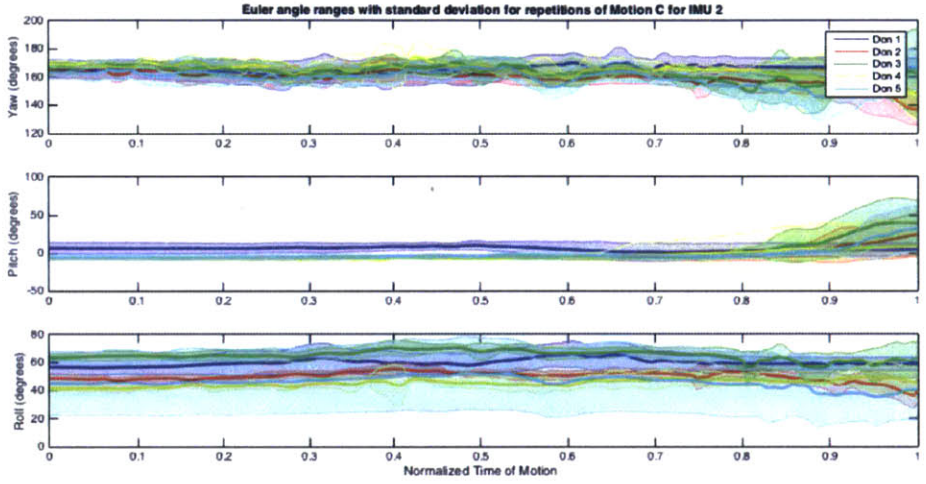

Figure G-9: Euler axes (Yaw, Pitch, Roll) mean and standard deviation values for IMU 3 for multiple donnings of Motion C.

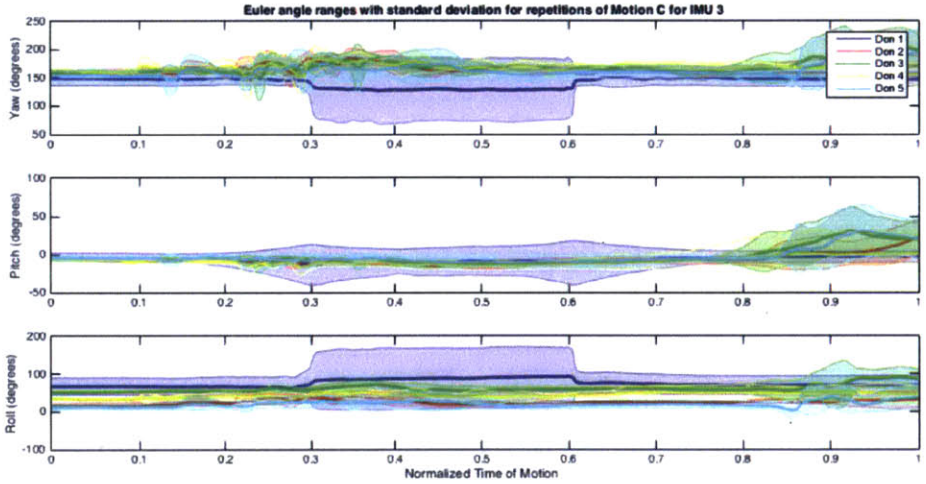

Figure G-10: Euler axes (Yaw, Pitch, Roll) mean and standard deviation values for IMU 1 for multiple donnings of Motion D.

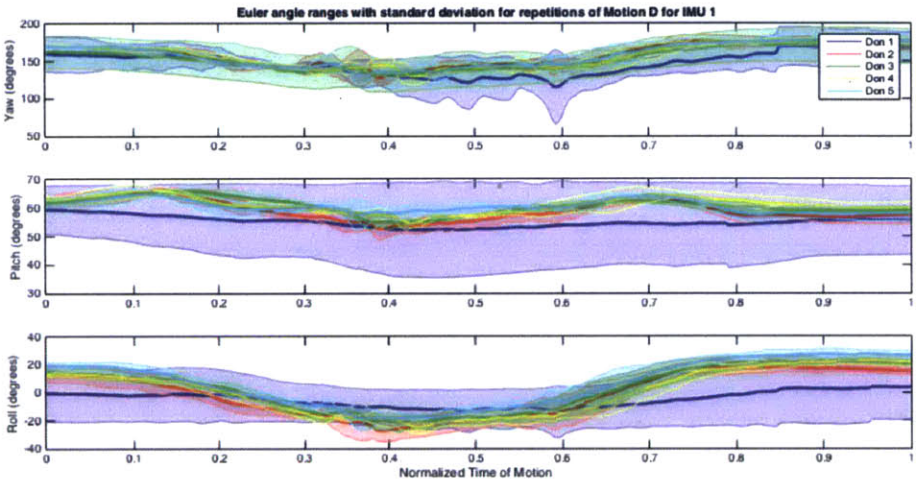

Figure G-11: Euler axes (Yaw, Pitch, Roll) mean and standard deviation values for IMU 2 for multiple donnings of Motion D.

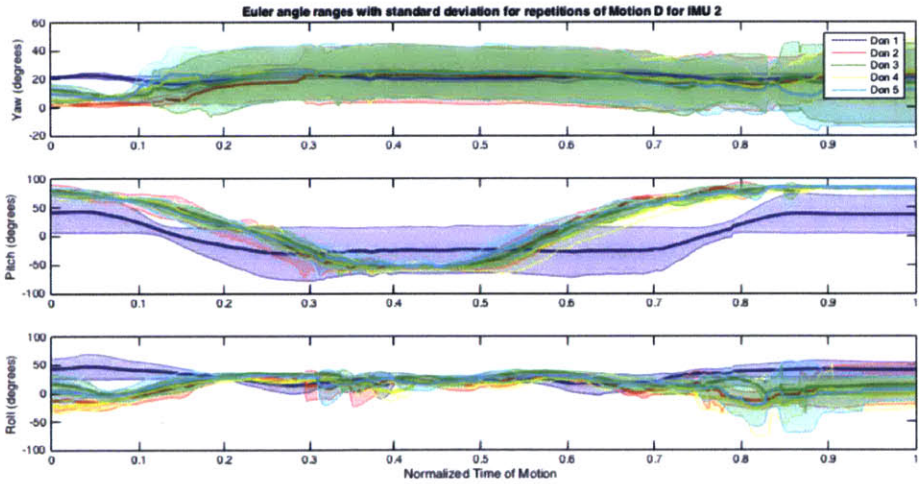

Figure G-12: Euler axes (Yaw, Pitch, Roll) mean and standard deviation values for IMU 3 for multiple donnings of Motion D.

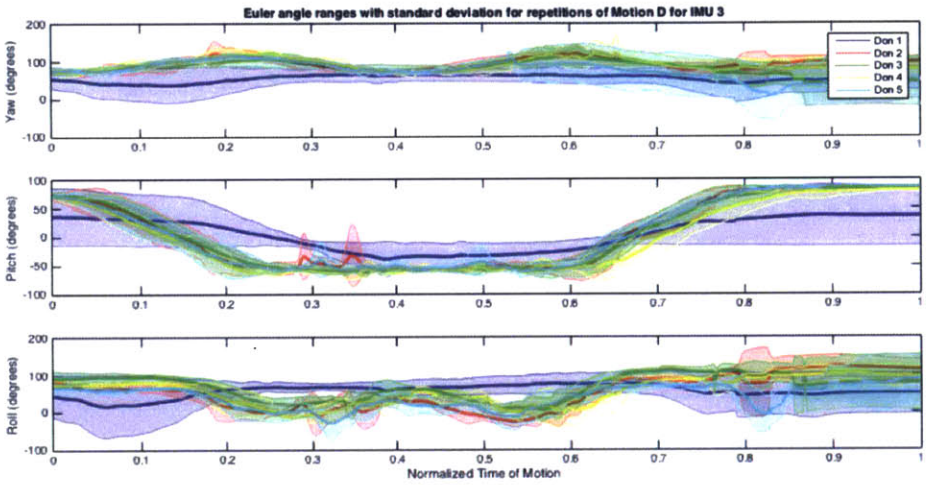

Figure G-13: Euler axes (Yaw, Pitch, Roll) mean and standard deviation values for IMU 1 for multiple donnings of Motion E.

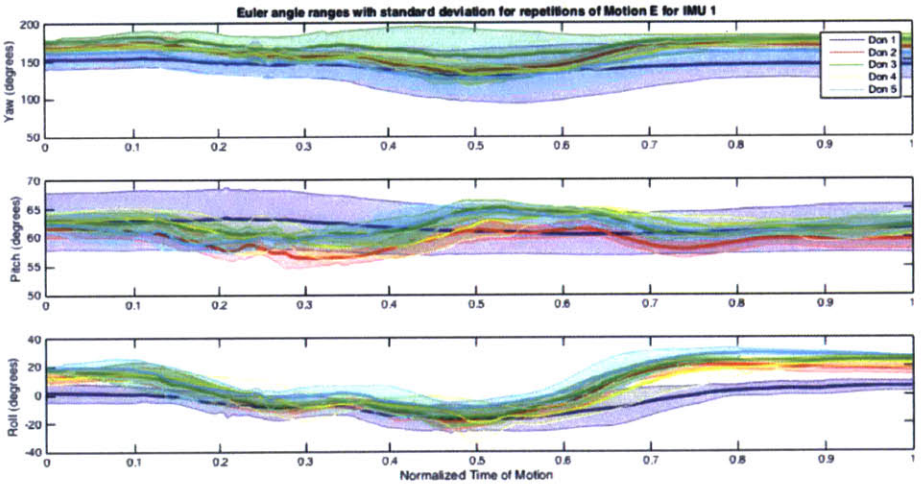

Figure G-14: Euler axes (Yaw, Pitch, Roll) mean and standard deviation values for IMU 2 for multiple donnings of Motion E.

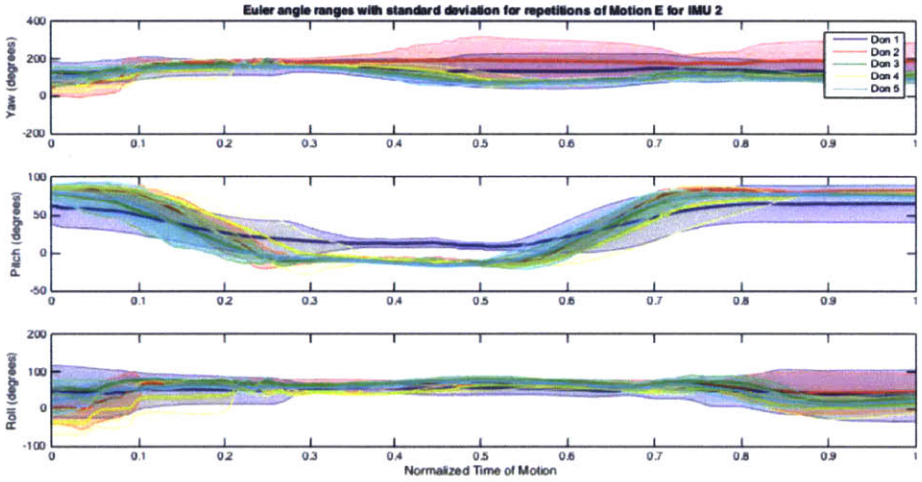

Figure G-15: Euler axes (Yaw, Pitch, Roll) mean and standard deviation values for IMU 3 for multiple donnings of Motion E.

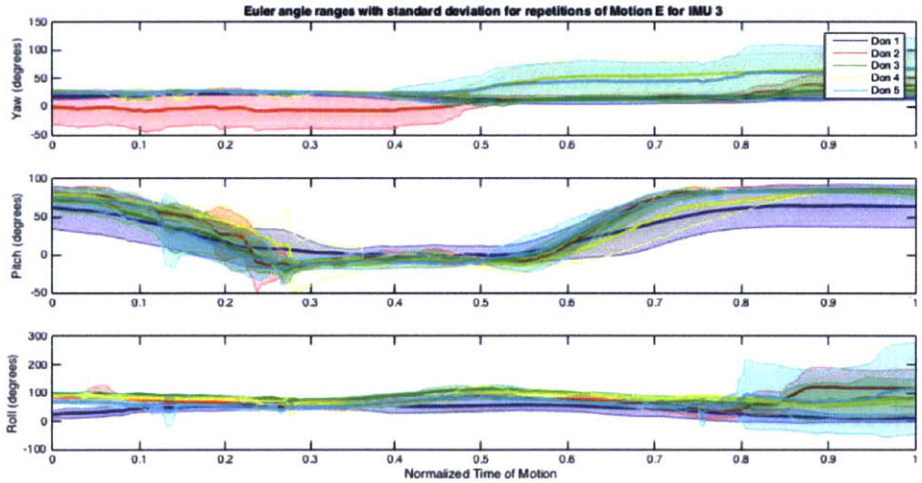

Figure G-16: Euler axes (Yaw, Pitch, Roll) mean and standard deviation values for IMU 1 for multiple donnings of Motion F.

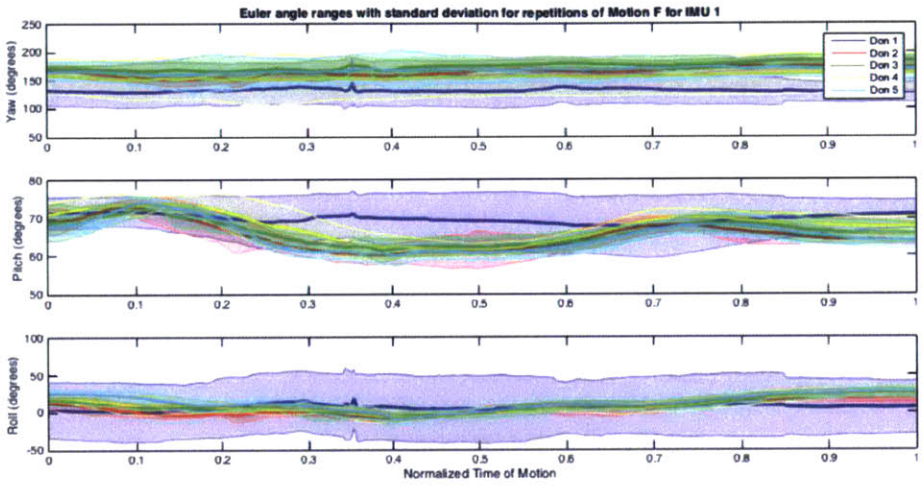

Figure G-17: Euler axes (Yaw, Pitch, Roll) mean and standard deviation values for IMU 2 for multiple donnings of Motion F.

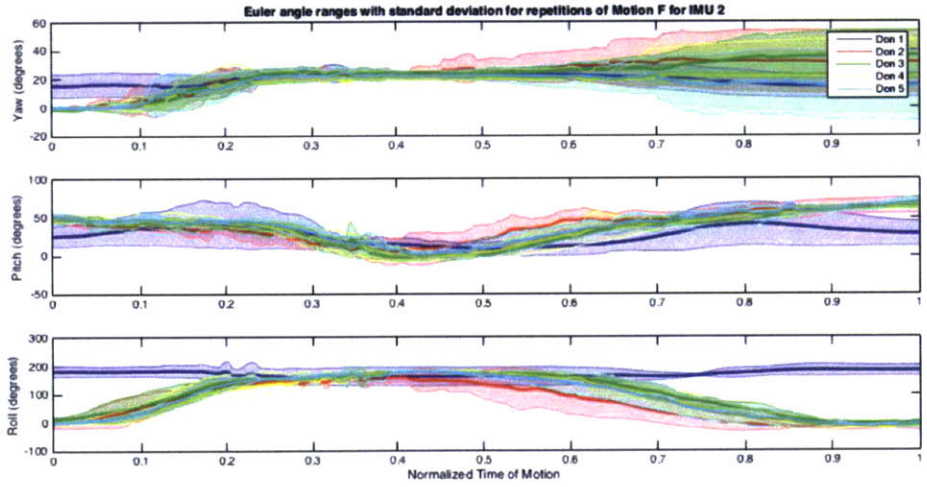

Figure G-18: Euler axes (Yaw, Pitch, Roll) mean and standard deviation values for IMU 3 for multiple donnings of Motion F.

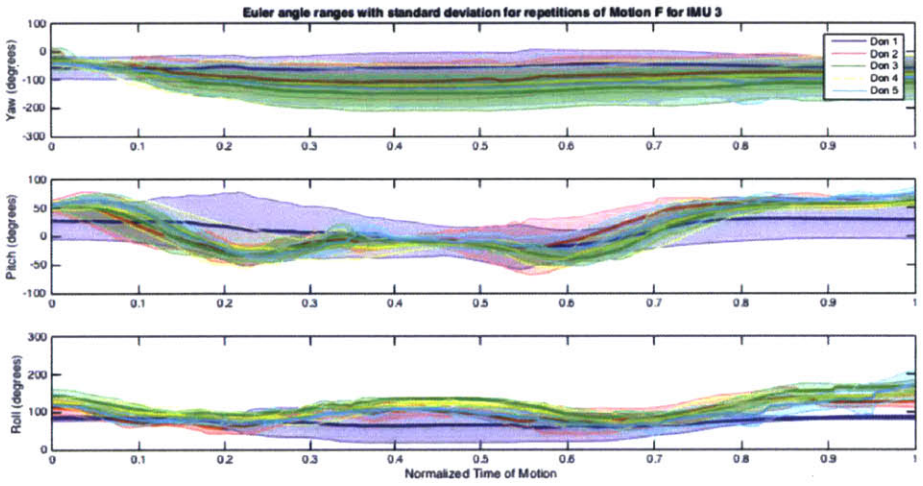

Bibliography

[1] BioDigital. The biodigital human. http://human.biodigital.com.

[2] Seppo Nissilä, Jérémie Bouchaud, and Marwan Boustany. MEMS & Sensors for Wearables Report - 2014. *IHS Technology Technical Report*, 2014.

[3] Kathryn Hurlbert, Bob Bagdigian, Carol Carroll, Antony Jeevarajan, Mark Kliss, and Bhim Singh. Human Health, Life Support and Habitation Systems. Technical report, NASA, Washington, DC, 2012.

[4] Yoshihiko Nakamura. Somatosensory Computation for Man Machine Interface From Motion-Capture Data and. *IEEE*, 21(1):58–66, 2005.

[5] Yisheng Chen and Rick Parent. Markerless Monocular Motion Capture Using Image Features and Physical Constraints. *IEEE*, pages 36–43, 2005.

[6] David E Difranco, Tat-Jen Cham, and James M Rehg. Reconstruction of 3-D Figure Motion from 2-D Correspondences. *IEEE*, pages 307–314, 2001.

[7] J. Klein, S. J. Spencer, J. Allington, K. Minakata, E. T. Wolbrecht, R. Smith, J. E. Bobrow, and D. J. Reinkensmeyer. Biomimetic orthosis for the neurorehabilitation of the elbow and shoulder (BONES). In *Proceedings of the 2nd Biennial IEEE/RAS-EMBS International Conference on Biomedical Robotics and Biomechatronics, BioRob 2008*, pages 535–541, 2008.

[8] CJ Walsh, Ken Endo, and Hugh Herr. A quasi-passive leg exoskeleton for load-carrying augmentation. *International Journal of Humanoid ...*, 04(03):487–506, September 2007.

[9] Daniel Vlasic and Rolf Adelsberger. Practical motion capture in everyday surroundings. *ACM Transactions on Graphics (TOG) - Proceedings of ACM SIGGRAPH 2007*, 26(3):35, July 2007.

[10] Angelo Sabatini. Quaternion-based extended Kalman filter for determining orientation by inertial and magnetic sensing. *IEEE transactions on Biomedical Engineering*, 53(7):1346–56, July 2006.

[11] Hassen Fourati, Noureddine Manamanni, Lissan Afilal, and Yves Handrich. Complementary observer for Body Segments Motion Capturing by Inertial and Magnetic Sensors. *IEEE Transactions on Mechatronics*, 19(1):149–157, 2014.

[12] David Fontaine, Dominique David, and Yanis Caritu. Sourceless human body motion capture. Département systèmes pour l'information et la sant LETI, CEA Grenoble.

[13] Henk J Luinge and Peter H Veltink. Inclination Measurement of Human Movement Using a 3-D Accelerometer With Autocalibration. *IEEE Transactions on Neural Systems and Rehabilitation Engineering*, 12(1):112–121, 2004.

[14] Claudia C Meruane Naranjo. Analysis and Modeling of MEMS based Inertial Sensors. *IEEE Transactions on Instrumentation and Measurement*, 57(1):140–149, 2008.

[15] Iman Prayudi and D Kim. Design and implementation of IMU-based human arm motion capture system. *IEEE International Conference on Mechatronics and Automation*, pages 670–675, 2012.

[16] Hao Yang and Juntao Ye. A calibration process for tracking upper limb motion with inertial sensors. *2011 IEEE International Conference on Mechatronics and Automation*, 1:618–623, August 2011.

[17] Xiaoxu Wu, Yan Wang, Chieh Chien, and Greg Pottie. Self-calibration of sensor misplacement based on motion signatures. *IEEE Body Sensor Networks*, 1, 2013.

[18] John Bortz. Mathematical Formulation for Strapdown Inertial Navigation New. *IEEE Transactions on Aerospace and Electronic Systems*, 7(1):61–66, 1970.

[19] Rong Zhu and Zhaoying Zhou. A Real-Time Articulated Human Motion Tracking Using Tri-Axis Inertial / Magnetic Sensors Package. *IEEE Transactions on Neural Systems and Rehabilitation Engineering*, 12(2):295–302, 2004.

[20] Daniel Roetenberg, Henk J Luinge, Chris T M Baten, and Peter H Veltink. Compensation of Magnetic Disturbances Improves Inertial and Magnetic Sensing of Human Body Segment Orientation. *IEEE transactions on Biomedical Engineering*, 13(3):395–405, 2005.

[21] Xiaoping Yun and Eric R Bachmann. Design, Implementation, and Experimental Results of a Quaternion-Based Kalman Filter for Human Body Motion Tracking. *IEEE Transactions on Robotics*, 22(6):1216–1227, 2006.

[22] Peng Cheng and Bengt Oelmann. Joint-angle measurement using accelerometers and gyroscopesA survey. *IEEE Transactions on Instrumentation and Measurement*, 59(2):404–414, 2010.

[23] H J Luinge, P H Veltink, and C T M Baten. Ambulatory measurement of arm orientation. *Journal of biomechanics*, 40(1):78–85, January 2007.

[24] Katherine R S Holzbaur, Wendy M. Murray, and Scott L. Delp. A model of the upper extremity for simulating musculoskeletal surgery and analyzing neuromuscular control. *Annals of Biomedical Engineering*, 33(6):829–840, 2005.

[25] Xu Xu, Jia Hua Lin, and Raymond W. McGorry. A regression-based 3-D shoulder rhythm. *Journal of Biomechanics*, 47(5):1206–1210, 2014.

[26] Nicholas Stergiou, Regina T Harbourne, and James T Cavanaugh. Optimal Movement Variability : A New Theoretical Perspective for Neurologic Physical Therapy. *Journal of Neurologic Physical Therapy*, 30(3):120–129, 2006.

[27] Huiying Yu, Jody Riskowski, Richard Brower, and Thompson Sarkodie-gyan. Gait Variability while Walking with Three Different Speeds. *IEEE International Conference on Rehabilitation Robotics*, pages 823–827, 2009.

[28] P A Fransson S Gomez and M Patel L Johansson. Changes in multi-segmented body movements and EMG activity while standing on firm and foam support surfaces. *European Journal of Applied Physiology*, 101:81–89, 2007.

[29] Jeffery J Summers and J Greg Anson. Human Movement Science Current status of the motor program : Revisited. *Human Movement Science*, 28(5):566–577, 2009.

[30] David E Sherwood and Timothy D Lee. Schema Theory : Critical Review and Implications for the Role of Cognition in a New Theory of Motor Learning. *Research Quarterly for Exercise and Sport*, 74(December):376–382, 2003.

[31] Mark L Latash, John P Scholz, and Gregor Schöner. Motor Control Strategies Revealed in the Structure of Motor Variability. *Exercise and Sport Science*, 30(1):26–31, 2002.

[32] Jane E Clark and Sally J Phillips. A Longitudinal Study of Intralimb Coordination in the First Year of Independent Walking : A Dynamical Systems Analysis. *Child Development*, 64:1143–1157, 1993.

[33] G.J.P Savelsberch and Simone R Caljouw. (Re)Discovery of Motor Development: A tribute to Esther Thelen. *The Behavior Analyst Today*, 6(4):243–249, 2005.

[34] Jeffrey M Hausdorff. Gait variability : methods , modeling and meaning Example of Increased Stride Time Variability in Elderly Fallers Quantification of Stride-to-Stride Fluctuations. *Journal of NeuroEngineering and Rehabilitation*, 2:1–10, 2005.

[35] Jeffrey M. Hausdorff, Dean a. Rios, and Helen K. Edelberg. Gait variability and fall risk in community-living older adults: A 1-year prospective study. *Archives of Physical Medicine and Rehabilitation*, 82(8):1050–1056, 2001.

[36] Hyun G. Kang and Jonathan B. Dingwell. Separating the effects of age and walking speed on gait variability. *Gait and Posture*, 27(4):572–577, 2008.

[37] M. Costa, C. K. Peng, Ary L. Goldberger, and Jeffrey M. Hausdorff. Multiscale entropy analysis of human gait dynamics. *Physica A: Statistical Mechanics and its Applications*, 330(1-2):53–60, 2003.

[38] Madalena Costa, Ary L. Goldberger, and C. K. Peng. Multiscale entropy analysis of biological signals. *Physical Review E - Statistical, Nonlinear, and Soft Matter Physics*, 71(2):1–18, 2005.

[39] APDM. Opal 425. http://www.apdm.com/wearable-sensors/.

[40] Vicon. 10-camera bonita system. http://www.vicon.com/System/Bonita.

[41] Jeffrey Hoffman. Informal interview discussing motions in space. not published, October 2013. Informal interview with Jeff discussing motions in space.

[42] Stephanie Armand and Arnaud Barre. b-tk: Biomechanical toolkit. http://code.google.com/p/b-tk/.

[43] Delsys. DELSYS Technical Note 101: EMG Sensor Placement.